[American Journal of Science, Vol. 317, June, 2017, P. 707–753, DOI 10.2475/06.2017.03]

PALEOPROTEROZOIC EVOLUTION OF THE ARC–BACK-ARC SYSTEM IN THE EAST SARMATIAN OROGEN (EAST EUROPEAN CRATON): ZIRCON SHRIMP GEOCHRONOLOGY AND GEOCHEMISTRY OF THE LOSEVO VOLCANIC SUITE

ROMAN A. TERENTIEV*,†, KONSTANTIN A. SAVKO*, and M. SANTOSH**,***,§

ABSTRACT. The East European Craton has a thick sequence of volcano-sedimentary rocks preserved in the Losevo belt that developed along the junction between Sarmatian and Volgo-Uralian microcontinents. The major lithologies of the Losevo terrain (LT) are a dominant bimodal volcanic suite and basalt–andesite–dacite–rhyolite assemblages (BADR). The LT rocks have been divided from lower to upper sequences into the Terrigene, Strelitsa and Podgornoye Formations, but the stratigraphic subdivisions have not been geochronologically tested. Here we present geochemistry and SHRIMP zircon geochronology of volcanic rocks from the LT. The volcanic suite from the Terrigene Formation has tholeiitic and calc-alkaline affinites, significant enrichment in LILE and LREE and strong depletion in HFSE with $\varepsilon Nd(t) = +2.6$, whereas the felsic dikes display an A-type affinity, with typical enrichment in Zr, Nb, Y, and depletion in Sr and Ti, fractionated REE patterns, and strong negative Eu anomalies with $\varepsilon Nd(t)$ in the range of -0.5 to 2.6. The bimodal volcanic suite of the Strelitsa Formation is composed of tholeiites displaying minor depletion in LREE, slight enrichment of LILE, no or weak depletion of Nb resembling transition MORB with $\varepsilon Nd(t) = +3.0$ to $+3.6$) and rhyolites with high LREE/HREE, high Sr/Y, no Eu anomaly, and strong depletion in Nb and Ti ($\varepsilon Nd(t) = +1.8$ to $+2.9$) resembling slab-derived high pressure adakitic melts. The volcanic rocks of the Podgornoye Formation are bimodal with tholeiitic chemistry, lack enrichment in LILE and LREE and have a slight depletion in HFSE ($\varepsilon Nd(t) = +3.7$) together with rhyolites having high LREE/HREE, moderate Sr/Y, no Eu anomaly, and strong depletion in Nb and Ti ($\varepsilon Nd(t) = +2.1$ to $+2.6$) resembling slab derived relatively low-pressure adakite-like melts. The BADR assemblage has significant enrichment in LILE and LREE and strong depletion in HFSE, similar to arc-like volcanics. Geochronological data indicate that the early LT volcanic rocks were formed during the early (Terrigene Formation) stage of intra-continental arc with a continental basement whereas the Strelitsa bimodal volcanic rocks were formed during a middle stage of back-arc extension and the Podgornoye bimodal volcanic rocks and BADR were formed during a later stage intra-oceanic arc. The identification of a 2170 to 2120 Ma back-arc basin in the East Sarmatian Orogen together with broadly coeval arcs indicate that the eastern margin of the Sarmatia was active with an arc–back-arc environment. Our new data suggest that the initial melts of the bimodal suite were adakitic derived by slab melting, followed by mantle metasomatism, whereas the basaltic magmas formed in an island arc setting. The LT and similar-aged volcanic belts in other terrains are considered to represent the initial (2.1–2.0 Ga), subduction-related growth of the Paleoproterozoic Columbia supercontinent.

Key words: East European Craton, Continental margin, bimodal volcanic rocks, zircon geochronology, petrogenesis

* Department of Geology, Voronezh State University, Russia
** Centre for Tectonics, Resources and Exploration, Department Earth Sciences, University of Adelaide, SA 5005, Australia
*** School of Earth Sciences and Resources, China University of Geosciences Beijing, 29 Xueyuan Road, Beijing 100083, China
§ Division of Interdisciplinary Science, Faculty of Science, Kochi University, Kochi 780-8520, Japan
† Corresponding author: Terentiev Roman Anatolievich, Russia, Voronezh, Kholzunova street, 72b, apartment 172, postcode 394016; mobile phone +7-906-580-99-18, office phone/fax +7-4732-22-73-63; E-mail address: terentiev@geol.vsu.ru

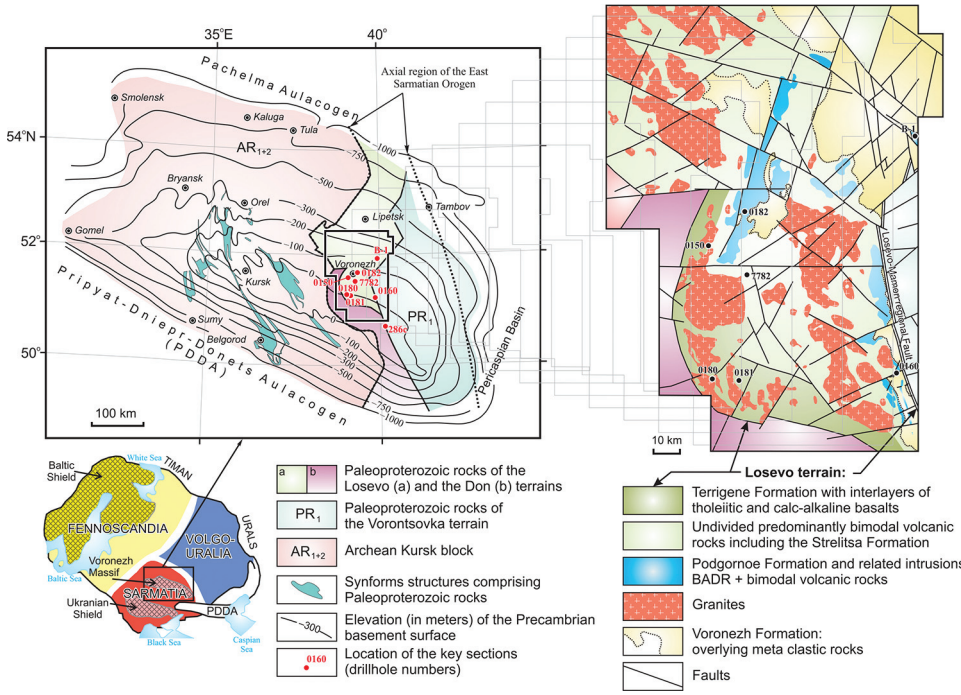

Fig. 1. Tectonic framework of the Precambrian basement of the Voronezh crystalline massif (VCM) and simplified geological framework of the Precambrian basement of the Losevo terrain.

INTRODUCTION

The global Paleoproterozoic (2.1–1.8 Ga) orogenic events leading to the formation of the supercontinent Columbia (Zhao and others, 2002; Rogers and Santosh, 2002; Santosh, 2010; Meert, 2014; Nance and others, 2014; Yang and Santosh, 2015, among others) have been a topic of wide interest in recent studies, particularly related to crustal evolution and formation of Earth's first coherent supercontinent assembly. The East European Craton (EEC) is considered an integral component of the Columbia supercontinent and has been divided into three segments: the Fennoscandia, Sarmatia and Volgo-Uralia (fig. 1, Bogdanova, 1993). The East Sarmatian Orogen (ESO, Shchipansky and others, 2007) is located along the junction between Sarmatia and Volgo-Uralia and is a key belt for investigating the Paleoproterozoic tectonic evolution of the EEC. The central part of the ESO is represented by a major volcanic belt and is traditionally named the Losevo belt (terrain). This belt has a width of up to 150 km and a lateral extent of nearly 450 km. It is bounded by Vorontsovka terrain, separated by the Losevo–Mamon Fault in the east, and by the Paleoproterozoic–Neoarchean (?) Don terrain or the Archean Sarmatia core in the west. The major lithologies of the Losevo terrain (LT) are dominantly components of a bimodal volcanic suite and rocks forming basalt–andesite–dacite–rhyolite assemblages (BADR) with interlayers including terrigenous rocks and volcanic tuffs (Terentiev, 2014). The tectonic nature of the Losevo belt has remained controversial, particularly in terms of whether the LT is a fragment that broke away from the Columbia supercontinent, or represents the margin of one of the EEC megablocks. Ever since Zaytsev (1966) reported the lithology of this terrain, the origin and significance of the LT volcanics has been debated. The bimodal character of the LT volcanics were not previously

recognized (Chernyshov and others, 1997) until the first detailed petrological work on these rocks was published (Terentiev, 2002, 2014; Terentiev and Chuvashina, 2003). Earlier studies (for example, Chernyshov and others, 1997) suggested intracontinental rifting (also Mints and others, 2015) as the main mechanism for the formation of the Losevo belt volcanic rocks. On the other hand, lithological assemblages, as well as the geochemical and isotopic data on these volcanic rocks suggest that they formed under a tectonic setting similar to either an Eastern-Pacific (Cordillera) type (Shchipansky and Bogdanova, 1996; Shchipansky and others, 2007) or a Western-Pacific type (Terentiev, 2014; Terentiev and others, 2014) continental margin.

The major lines of evidence supporting an active continental margin model include (1) the presence of BADR assemblages, (2) geochemical data indicating that these volcanic rocks have affinities to magmatic/island arcs with different contributions of subduction components to their magma genesis, and (3) juvenile isotope-geochemical compositions of the volcanic rocks. However, precise ages of these volcanic rocks have not been well constrained and this limits our understanding on the initiation of the orogenic process and its evolution. Furthermore, recent studies have identified the Losevo rock series as a complex stratigraphic unit with a lower Strelitsa Formation/Fm. (with bimodal volcanics) and an upper Podgornoye Fm. (with BADR)* (Terentiev, 2014), which are underlain by a clastic unit (Terrigene Fm.) interbedded with volcanic rocks (Terentiev, 2013). However, this stratigraphic subdivision has not been geochronologically tested.

In this study, we have applied U-Pb SHRIMP zircon dating techniques to determine the ages of different units of the Losevo terrain. We also present new geochemical data on the LT volcanic rocks and discuss their tectonic environment of formation and petrogenesis. Our results provide insights into the Paleoproterozoic history of the zone of amalgamation between Sarmatia and Volgo-Uralia and may aid in reconstructing the Columbia/Nuna supercontinent.

GEOLOGICAL BACKGROUND

The Losevo, Vorontsovka and Don terrains form part of the Paleoproterozoic East Sarmatian Orogen (ESO, fig. 1), which divides the Archean cores of the Sarmatian and Volgo-Uralia segments of the East European Craton (Bogdanova and others, 2016). The eastern part of the Vorontsovka terrain is bordered by Paleoproterozoic structures of Volgo-Uralia (Bibikova and others, 2009), while the Losevo terrain borders the western Sarmatia. The Losevo series (fig. 2) is composed of a metamorphosed sequence including: (1) terrigenous rocks, volcanic tuffs, basalts and rhyolites (bimodal suite 1, BS-1) belonging to the Strelitsa Fm.; (2) polymodal basalt–andesite–dacite–rhyodacite (BADR) and bimodal suite 2 (BS-2) association belonging to the Podgornoye Fm. (Terentiev, 2014); and (3) the underlying Terrigene Fm. are considered to have derived from mafic and intermediate volcanic source rocks and are different in geochemistry from those in the Strelitsa and Podgornoye Fms. (Terentiev, 2013). The Terrigene and Strelitsa Fms. are intruded by metagabbros belonging to the Rozhdestvenskoe complex (~2120 Ma) (Terentiev, 2014), calc-alkaline intrusions ranging from gabbro-diorites to trondhjemites and trondhjemite–granodiorites and monzogranites (~2065–2080 Ma) of the Usman and Devitsa complexes (Terentiev, 2014; Terentiev and others, 2016). The Losevo series are overlain by low grade metamorphosed coarse terrigenous rocks and phyllites of the Voronezh Formation,

* Herein after we use the following stratigraphic units from the early to the late, which include (in brackets) volcanic rocks: Terrigene Fm. (BBA, calc-alkaline basalts, basaltic andesites; tholeiites; FR+R, Fe-rhyolites plus rhyolites), Strelitsa Fm. (BS-1, Bimodal suite 1 = tholeiites plus adakitic rhyolites); Podgornoye Fm. (BADR, calc-alkaline basalts, andesites, dacites and ±rhyolites; BS-2, Bimodal suite 2 = tholeiites plus adakite-like rhyolites).

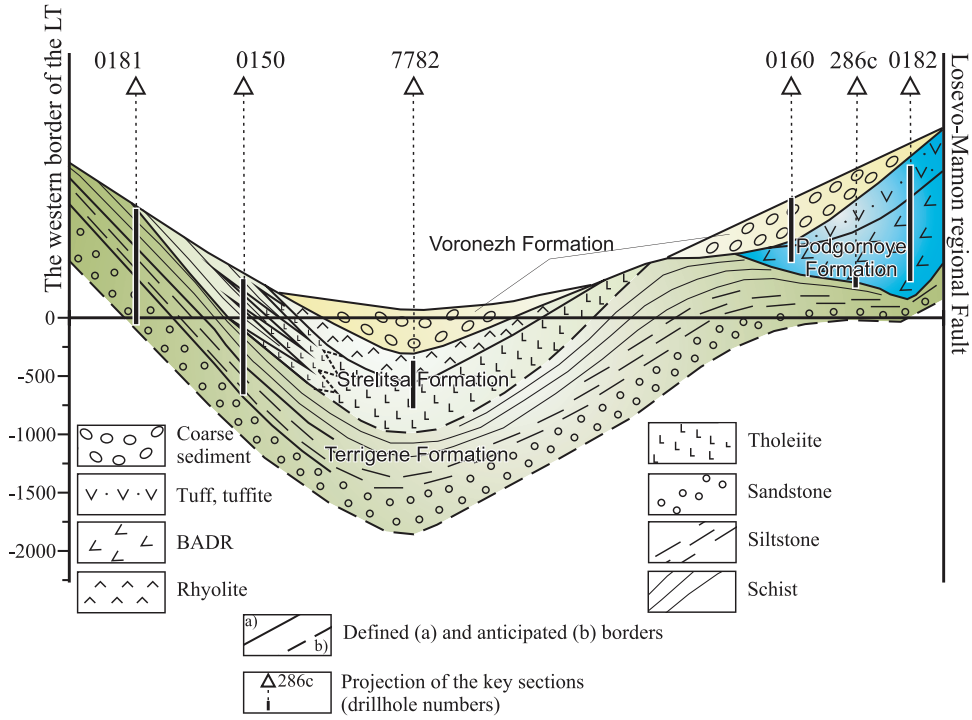

Fig. 2. Idealized section of the Losevo terrain.

which fill the graben-synclinal structures and represent the upper molasse sequence (Zaitsev, 1979; Terentiev and Skryabin, 2014).

The Terrigene Fm. is exposed as a N-NW trending belt in the western region of the LT (inset of fig. 1). It is predominantly composed of metamorphosed psammites and pelites intercalated with minor metamorphosed basalts (amphibolites) (fig. 3, DH 0181). Thin felsic meta-dikes also occur. All these rocks experienced greenschist to amphibolite facies metamorphism. Our P–T calculations indicate that peak metamorphism took place at temperatures of 750 °C [refers to Holland and Blundy (1994) Hbl-Pl thermometry] and pressures of 5 to 6 kbar (Terentiev and others, 2016). Intensive migmatization (fig. 3, DH 0180) along the western border of this Formation makes it difficult to establish the protolith nature. The Terrigene Formation and migmatites were intruded by monzogranites of the Paleoproterozoic Devitsa complex and tonalite dikes of the Usman complex.

The Strelitsa Fm. occupies mainly the central part of the LT and comprises a dominant bimodal association of metamorphosed tholeiites and rhyolites. The lower part of the Formation is composed of mafic rocks whereas the upper part is characterized by an alternation of felsic and mafic rocks including meta-tuffs (the first type of stratigraphic section, fig. 3, DH 7782; Terentiev, 2005). The second type is represented by felsic and mafic subvolcanic rocks (fig. 3, DH 0150) which also intrude the graywackes and arkose units of the Terrigene Fm. Peak metamorphic temperatures of 600 °C and pressures of ~5 to 6 kbar were estimated from mineral thermobarometry of these rocks (Savko and Gerasimov, 2002). The Strelitsa Fm. was intruded by the granite batholiths of the Usman complex (fig. 1) and rocks belonging to the Rozdestvenskoe mafic complex.

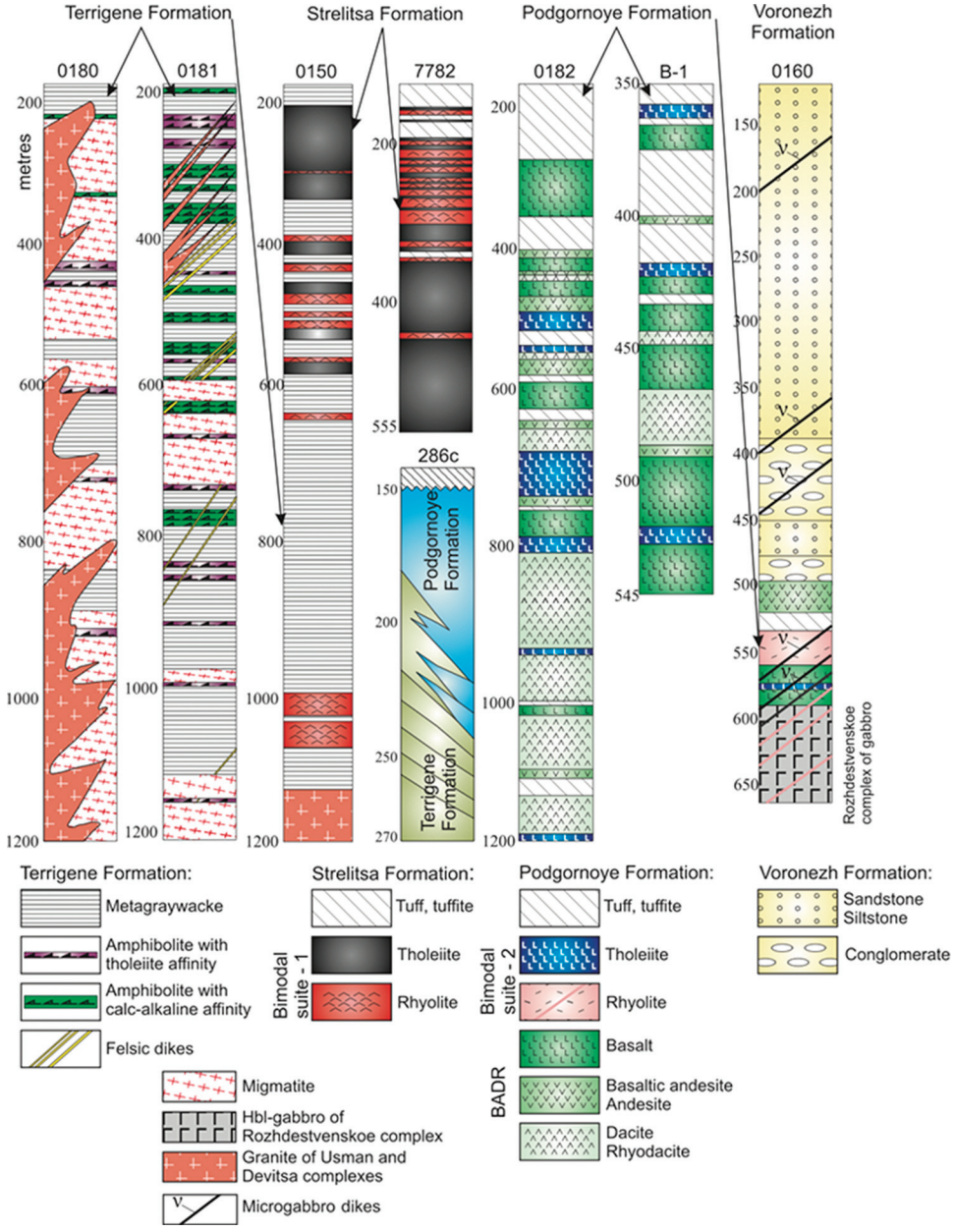

Fig. 3. Representative stratigraphic sections of the Losevo terrain volcanic rocks from drill core data. Locations of the samples used for geochronological studies are shown in the figure.

The Podgornoye Fm. occurs as narrow discontinuous zones along the eastern border and in the central part of the LT. One of the complete sections represented in borehole 0182 (fig. 3) shows that the lower part is composed of alternating metamorphosed basalts, basaltic andesites, andesites, tuffs, volcanic-sedimentary rocks and paleoflows (7–30 m) of Fe-basalts–basaltic andesites and tuffs (tholeiites of the BS-2).

The upper part of this section is composed of meta-sedimentary volcanic units interbedded with layers (up to 20 m) of basalts, basaltic andesites and tuffs. The rhyolites of the second bimodal association represents either subvolcanic bodies or thin dikes (fig. 3, DH 0160). The Podgornoye Fm. is distinguished from the Strelitsa Fm. by the amygdaloidal texture, lower grade of metamorphism and preservation of relict volcanic textures in both felsic and mafic rocks (Terentiev, 2005, 2014). The Podgornoye Fm. volcanic rocks are spatially associated with subvolcanic bodies of metamorphosed microgabbro (which are coeval with the tholeiites), as well as with poorly studied intrusions of differentiated gabbro/diorite to trondhjemitic calc-alkaline rocks.

The gradual transition through the alternation of the underlying Terrigene Fm. and overlying Podgornoye Fm. can be observed in the southern part of the LT (fig. 3, DH 286c).

IGNEOUS SAMPLES DESCRIPTION AND EFFECTS OF METAMORPHISM

The samples in this study were collected from the volcanic rocks of all three formations (fig. 3).

Volcanic Rocks Alternating with the Terrigene Fm. Meta-graywackes (Samples from DH 0180, 0181)

(1) Meta-felsic rocks are inferred to be dike rocks based on their fine grain size, narrow width of units and cross-cutting relationship with the foliation of host rocks. The mineral assemblages of the felsic dikes include 5 percent phenocrysts (plagioclase up to 0.5 mm) and 90 to 95 percent quartz-albite granoblastic matrix. Minor minerals are 3 to 5 percent chloritized biotite, sericite near areas of tectonic deformation, and <1 percent garnet. The appearance of fine-grained magnetite (2–3%) allows the distinction among the various types of ferroan felsic dikes. Zircon grains in these rocks are too small (5–10 μm) and not suitable for geochronological studies.

(2) Amphibolites and greenstones (metamorphosed mafic volcanic rock) have compositional variation from epidote-chlorite and actinolite schist to fine-grained hornblende amphibolites. This rock group is different from the sub-volcanic basalts (the next group) in their cryptocrystalline structure, almost azonal morphology and sinuous contacts with the underlying rocks. The mineral assemblages of the metamorphosed tholeiites include scarce actinolite porphyroblast and fine grained matrix of up to 70 percent amphibole, 10 to 25 percent saussuritizated plagioclase/epidote, and minor quartz, biotite, titanite and relics of metamorphic clinopyroxene. The texture of the amphibolite varies from fine- (0.1 mm) to medium-grained (0.2–0.5 mm). The weakly metamorphosed greenstone rocks show alternating albite-chlorite-epidote-actinolite composition and retain their original porphyritic texture in some areas.

(3) Plagioclase-rich amphibolites (calc-alkaline microgabbro and sub-volcanic basalt) are mostly composed of zoned bodies with thickness of 5 to 30 m. The core of the calc-alkaline mafic body is composed of rocks with the relic gabbro-ophitic texture whereas the margins gradually change into microgabbro with the endocontact represented by basalt porphyrites, which transformed into schistose amphibolites. The phenocrysts are represented by albitized plagioclase and mafic minerals that show alteration to amphibole. Thin plagioclase amphibolite bodies have lost their original igneous texture. The metamorphosed calc-alkaline rocks differ from the tholeiites in their high contents of quartz (up to 10%) and plagioclase (up to 40%), and less amphibole (50%).

The Strelitsa Fm. (Bimodal suite 1, Samples from DH 7782, 0150)

(1) Basaltic rocks from the Strelitsa Fm. can be divided into two groups based on their mineral assemblage: quartz actinolite-rich and carbonate-chlorite-rich rocks.

These metabasite types contain epidote. Original igneous textures of the mafic rocks are completely lost, with the exception of metamorphosed sub-volcanic rocks, in which hornblende porphyroblasts are observed. The metabasites are divided into massive, schistose and banded based on texture, representing the effusive→pyroclast→volcanic-sedimentary volcanic facies (Terentiev, 2002).

(2) The felsic rocks of Strelitsa Fm. are rhyolite to dacite based on chemistry. The mineral assemblages of the metarhyolites include 5 to 20 percent phenocrysts of zoned plagioclase, and matrix containing fine grained plagioclase, quartz, sericite and minor chlorite and epidote. Quartz phenocrysrs are minor or absent.

The Podgornoye Fm. (BADR Plus Bimodal Suite 2, Samples from DH 0182, 0160, B-1)

(1) Tholeiites are confined to the middle and lower part of the Podgornoye Fm. The rocks of this formation are predominantly metamorphosed volcanics, and pyroclastics of basalt and basaltic andesite composition. The tholeiites are characterized by amygdaloidal relic textures. The amygdales are filled with quartz, and rare epidote/chlorite. The rock matrix consists of acicular actinolite, chlorite, epidote, laths of plagioclase and minor quartz, carbonates, and opaque minerals. Rarely, phenocrystic aggregates of secondary epidote, chlorite, and actinolite occur replacing the original mafic minerals.

(2) Rhyolites occur in bimodal association with tholeiites. They show similar mineral composition with those of the Strelitsa Fm. felsic rocks, but differ in their geochemical characteristics and extensive development of quartz phenocrysts.

(3) Calc-alkaline volcanic rocks vary in composition from basalts, basaltic andesites, and andesites to rhyodacite (BADR) of different facies types including subvolcanic, effusive, and pyroclastic. Relict phenocrysts in the mafic and intermediate rocks are plagioclase, rare pseudomorphs of epidote, actinolite and chlorite after original mafic minerals. Relic phenocrysts of quartz also occur. The BADR rock series have a relict amygdaloidal texture, but in contrast to the tholeiites, they are dominated by amygdales composed of epidote, chlorite, and carbonate. The rock matrix consists of quartz, epidote, albite, chlorite, carbonates and minor actinolite.

All volcanic rocks analyzed have been subjected to regional metamorphism, and some also to a later event of thermal metamorphism and migmatization. To minimize the effects of alteration, all samples were carefully selected to exclude veining and quartz amygdales or xenocrysts. Metamorphic recrystallization and alteration of the felsic volcanics is very limited, and when present is represented by minor muscovite. Metabasalts are relatively altered during metamorphism. The most obvious effects being high modal proportions of metamorphic chlorite and/or epidote, amphibole, biotite; elevated (>2%) loss-on-ignition (LOI) values. Their K_2O, CaO, Rb, Sr and Cs concentrations are highly variable. In addition, sea water alteration of basalts would result in a significant enrichment of K, Rb, Sr, U and Cs (Hart, 1969). Relatively mobile (Winchester and Floyd, 1986; Polat and others, 1999) elements like Si, Na, K and Ca, as well as a number of trace elements (Cs, Rb, Ba and Sr), can undergo redistribution and therefore may not reflect the original composition. Such samples with high loss on ignition and with highly variable mobile elements were excluded. Only screened data as described above are considered for interpretation in the following sections. Even in the screened data, some large ion lithophile elements (Rb, Ba and K) show a high degree of scatter, suggesting mobility during metamorphism and their concentrations must be treated with caution. However, the HFSE and HREE were immobile and can represent the primary composition (Ludden and Thompson, 1978; Bienvenu and others, 1990; MacLean and Barrett, 1993; Roser and Nathan, 1997). The HFSE and REE are therefore used for evaluating the petrogenesis and geodynamic setting of the rocks.

ANALYTICAL PROCEDURES

Zircon U–Pb Dating

Samples weighing 0.5 to 2 kg were taken from the core of the least altered volcanic rocks, crushed to 0.5 mm, and washed and separated in tribromomethane. Zircon crystals were handpicked under a binocular microscope. The selected zircon grains together with 91500 (1065.4±0.3 Ma, Wiedenbeck and others, 1995) and Temora (416.75±0.24 Ma, Black and others, 2003) reference materials were mounted using epoxy resin on a 25-mm plate, which was polished until the crystals appeared on the surface. Cathodoluminescence images were produced by a CamScan MX2500 electronic scanning microscope (SEM), which enabled the selection of appropriate domains for U–Pb analysis. The zircons were analyzed using a SHRIMPII multicollector secondary-ion high-resolution mass spectrometer at the Centre of Isotopic Research at A.P. Karpinsky Russian Geological Research Institute (VSEGEI), following procedures described in Larionov and others (2004).

The U/Pb ratios were calibrated against a 1065 Ma reference zircon (Wiedenbeck and others, 1995), which was analyzed repeatedly during each session. CL-dark areas of the "unknown" zircons were chosen for analysis. The results were then processed with ISOPLOT/Ex3.6 (Ludwig, 2008) software, with decay constants of Steiger and Jäger (1977). The common lead correction was applied on the basis of measured $^{204}Pb/^{206}Pb$ and modem (that is 0 Ma) Pb isotope composition, according to the model of Stacey and Kramers (1975). Calculations were performed using previously reported decay constants (Steiger and Jäger, 1977).

Major and Trace Element Analyses

Powdered samples were digested in an acid mixture following standard procedures described by Karandashev and others (2008). Bulk-rock major element oxides (SiO_2, TiO_2, Al_2O_3, Fe_2O_3total, MnO, MgO, CaO, Na_2O, K_2O, and P_2O_5) were analyzed using a Perkin Elmer Optima 3300 inductively coupled plasma-optical emission spectrometer (ICP-OES) at the Institute of Mineralogy, Geochemistry and Crystal Chemistry of Rare Elements, Moscow (Russia). FeO and CO_2 contents were measured by the titrimetric and spectrophotometric dichromate method; H_2O^- and H_2O^+ were measured by the gravimetric standard method; and the contents of F, CI, and S were measured by X-ray fluorescence using an Axios Advanced device. Precisions (1σ) for most elements based on rock standards GSO (granite, diorite), OSO (basalts) (National Geological Standard Reference Materials of Russia) and GSP-2, AGV-2, BHVO-2 (US Geological Survey) are better than 1.0 percent with the exception of TiO_2 ($_2O_5$ (1.0–1.5%). For precision check several samples were analyzed on S8 Tiger sequential spectrometer (manufactured by Bruker AXS GmbH, Germany) at the Voronezh State University using XRF method.

Trace and rare earth elements were analyzed by inductively coupled plasma method (ICP-MS) at the IMGRE. Rock samples were decomposed, depending on their composition, with acid in open or closed systems. Detection limits for REE, Hf, Ta, Th and U were up 0.02 to 0.03 ppm, for Nb, Be and Co - 0.03 to 0.05 ppm, for Li, Ni, Ga and Y - 0.1 ppm, for Zr - 0.2 ppm, for Rb , Sr and Ba - 0.3 ppm, for Cu, Zn, V and Cr – 1 to 2 ppm. Accuracy of the analysis was controlled by means of measuring Russian and international standard samples GSP-2, AGV-2, BHVO-2, BM and SGD-1A CT-1. Errors of determining concentrations range from 3 to 5 percent for the most part of the elements.

Trace Element Contents of Zircons

The REE and other elements in zircons were determined by secondary-ion mass-spectrometry (SIMS) method in Yaroslavl branch of the Institute of Physics and Technology, Russian Academy of Sciences by using CAMECA IMS-4F secondary-ion

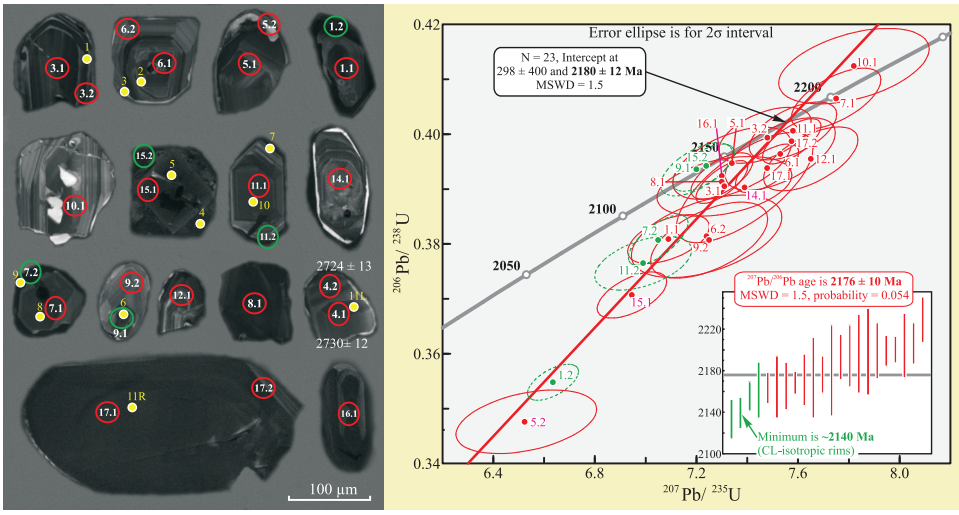

Fig. 4. Cathodoluminescence images of zircon grains and zircon U–Pb concordia diagram for the metarhyolite from the Strelitsa Formation of the central part of the LT. Numbers of analytical points correspond to those in the table 1.

microprobe. Measurement procedures followed those outlined in Nosova and others (2002).

Sm–Nd Isotopes of Whole Rocks

Samarium–Nd isotopic analyses were performed on a TRITON thermal ionization magnetic sector mass spectrometer at the Centre of Isotopic Research at A.P. Karpinsky Russian Geological Research Institute (VSEGEI), St. Petersburg. The Sm and Nd concentrations were determined according to the method of double isotopic dilution with the use of mixed ^{149}Sm–^{150}Nd spikes. About 100 mg of powdered sample was dissolved in Teflon beakers with a HF+HNO_3 mixture acid. The separation of Sm and Nd was performed via ion-exchange chromatography during two stages. At the first stage, the rare earth elements were separated on chromatographic columns with AG50W-X8 resin. Further separation of Sm and Nd was performed on columns with a fluoroplastic carrier coated with HDEHP cationite. Analyses of the La Jolla standard yield an average ^{143}Nd/^{144}Nd ratio of 0.511842±4. Mass fractionation corrections for Nd isotopic ratio was based on values of ^{146}Nd/^{144}Nd = 0.7219. Uncertainties in Sm/Nd ratios are less than ±0.5 percent (relative).

RESULTS

U-Pb Isotopic Age

Sample 7782/188.5–193.0 is a metarhyolite collected from the Strelitsa Fm. in the western part of the LT. It is composed mainly of plagioclase phenocryst (~15%) with microgranular quartz-albite–oligoclase groundmass (~85%). The zircons extracted from the ~800-g sample (about 20 grains) are represented by translucent crystals and crystal fragments, predominantly with abrasion tracks. The presence of abrasion tracks, together with the variety of shapes (prismatic, short-prismatic, and isometric crystals), suggests the xenocrystic/inherited nature of the zircons. In terms of their internal structure, the grains are characterized by fine oscillatory zoning (fig. 4) suggesting their magmatic origin. Five zircon grains contain repeated growth rims,

which are isotropic in cathode luminescent images. The boundaries between the isotropic rims and zonal parts of the grains are sharp with resorption tracks in the central parts. SHRIMP U-Pb analyses were made on 15 zircon grains, and their U–Pb isotopic results are listed in table 1 and plotted in figure 4. These grains have low to moderate U (55–444 ppm) and Th (21–246 ppm) contents, with Th/U ratios ranging from 0.15 to 0.99. Among the 20 analyses on the inherited/xenocrystic zircons, except one grain (spots 4.1 and 4.2) that gives a discordant age at 2756±190 Ma and $^{207}Pb/^{206}Pb$ age at 2485±15 and 2532±15 Ma (see table 1), which is the oldest age still found in the ESO, all others have $^{207}Pb/^{206}Pb$ apparent ages scattering between 2163±15 Ma and 2229±22 Ma, interpreted as the crystallization ages of xenocrystic/inherited zircons. As shown in figure 4, one concordant population of inherited zircons yields a weighted mean $^{207}Pb/^{206}Pb$ age of 2176±10 Ma (MSWD = 1.5). Five isotropic rims give $^{207}Pb/^{206}Pb$ apparent ages younger than those of the inherited/xenocrystic zircons, and yield a weighted mean $^{207}Pb/^{206}Pb$ age of 2146±17 Ma (MSWD = 0.47, probability = 0.70).

Sample 0150/471.9–472.8 is a metarhyolite collected from the Strelitsa Fm. in the eastern part of the LT. It shows porphyritic texture with plagioclase (25%) occurring as phenocrysts. The groundmass consists of fine-grained plagioclase, quartz, muscovite and Mg–Fe oxides. Fifty two zircon grains were separated from this rock which are represented by transparent euhedral crystals of various habit or isometric crystals with a size of range of 105 to 225 μm length and 55 to 90 μm width, and length. Oscillatory growth zoning is well manifested in all the zircon crystals under CL (fig. 5). Some of these zircons show core-rim textures. The magmatic zircons in the sample are dark in CL images. Chemically, these grains are characterized by higher U (322–1246 ppm) and Th (116–551 ppm) contents and Th/U (0.20–0.57) ratios than those of the core zircons that contain U contents ranging from 66 ppm to 526 ppm, Th contents from 26 ppm to 360 ppm, and Th/U ratios between 0.09 to 0.84. We dated eight zircon cores and seven magmatic zircon rims, the results from which are listed in table 1. The co-magmatic zircon rims and cores have $^{207}Pb/^{206}Pb$ indistinguishable ages. On a concordia plot (fig. 5), most of the analyses on the zircons are discordant but define an upper intercept age of 2141±7.9 Ma. The thirteen most concordant data points yielded a weighted mean $^{207}Pb/^{206}Pb$ age of 2140±9.5 Ma (MSWD = 0.55, probability = 0.82), which is interpreted as the best estimate of the eruption age of the rock.

Sample 0160/535–538.0 is a metarhyolite collected from the Podgornoye Fm. in the eastern part of the LT, and contains phenocrysts of corroded quartz (~15%) and plagioclase (~5%) in a fine-grained groundmass. Sixty zircon grains were separated from this sample and most grains are colorless and euhedral to subhedral prismatic with highly luminescent oscillatory zoning in CL images, typical of igneous zircons (fig. 6). The zircon Th/U ratios are relatively high and range from 0.40 to 1.19, suggesting magmatic origin. The 15 analyses yielded a weighted mean $^{207}Pb/^{206}Pb$ age of 2122±7 Ma (MSWD = 0.35, probability = 0.99), interpreted as the crystallization age of the rock (fig. 6). The 12 analyses gave a concordant U-Pb age of 2120±9 Ma (MSWD = 0.0066, probability = 0.94).

Trace Element Contents in Zircons

The concentrations of trace elements in zircons determined by secondary-ion microprobe are given in table 2. Distribution of rare earth element (REE) relatively to chondrite for zircons is shown in figure 7. The REE analyses were performed on zircon cores and rims for three samples. The Hf content ranges from 6207 to 12502 ppm. The Y content of cores and rims overlaps, although higher values are seen in the inherited/xenocrystic zircons in sample 7782/188.5–193.0. The highest REE contents are recorded in rims of sample 0150/471.9–472.8. In a chondrite-normalized diagram, the

TABLE 1

SHRIMP-II zircon U–Pb isotopic analyses from the LT rhyolites

Spot Name	$^{206}Pb_c$, %	U, ppm	Th, ppm	$^{232}Th/^{238}U$	$^{206}Pb^*$, ppm	(1) Age $^{206}Pb/^{238}U$ Ma	±	(1) Age $^{207}Pb/^{206}Pb$ Ma	±	D, %	(1) $^{238}U/^{206}Pb^*$	±, %	(1) $^{207}Pb^*/^{206}Pb^*$	±, %	(1) $^{207}Pb^*/^{235}U$	±, %	(1) $^{206}Pb^*/^{238}U$	±, %	Rho
Metarhyolite (Sample 7782/188.5–193.0)																			
Azonal parts (spot 9.1 is in the center, the rest are in rims)																			
9.1	0.16	171	163	0.99	57.9	2140	±15	2133	± 19	-0.3	2.539	0.81	2.539	0.81	0.1327	1.10	7.200	1.3	0.3936
15.2	0.15	267	49	0.19	90.6	2141	±13	2139	± 15	-0.1	2.538	0.72	2.538	0.72	0.1331	0.87	7.228	1.1	0.3939
7.2	0.21	444	85	0.20	146.0	2080	±14	2155	± 14	3.6	2.625	0.79	2.625	0.79	0.1343	0.81	7.049	1.1	0.3807
11.2	0.83	236	50	0.22	77.3	2060	±15	2161	± 27	4.9	2.650	0.86	2.650	0.86	0.1347	1.50	6.990	1.8	0.3765
1.2	0.38	291	42	0.15	89.2	1958	±10	2172	± 14	11.0	2.815	0.61	2.815	0.61	0.1356	0.81	6.635	1.0	0.3548
Zonal parts (central parts of grains and rims)																			
10.1	0.53	67	43	0.66	23.9	2226	±21	2196	± 38	-1.3	2.421	1.10	2.421	1.10	0.1375	2.20	7.820	2.5	0.4124
3.2	1.26	153	104	0.70	53.5	2168	±15	2171	± 25	0.1	2.493	0.84	2.493	0.84	0.1355	1.40	7.470	1.6	0.3998
7.1	--	133	68	0.53	46.5	2199	±17	2206	± 20	0.3	2.460	0.90	2.460	0.90	0.1383	1.10	7.750	1.5	0.4065
5.1	0.29	64	28	0.45	21.9	2144	±20	2164	± 30	0.9	2.532	1.10	2.532	1.10	0.1350	1.70	7.340	2.1	0.3947
11.1	0.13	135	72	0.55	46.6	2172	±16	2193	± 22	1.0	2.495	0.87	2.495	0.87	0.1372	1.20	7.580	1.5	0.4006
16.1	0.23	243	94	0.40	82.1	2134	±13	2163	± 15	1.4	2.547	0.71	2.547	0.71	0.1349	0.88	7.300	1.1	0.3924
17.2	0.02	291	66	0.23	99.7	2163	±13	2200	± 13	1.7	2.508	0.68	2.508	0.68	0.1378	0.73	7.575	1.0	0.3987
8.1	--	409	246	0.62	138.0	2129	±12	2168	± 11	1.9	2.556	0.66	2.556	0.66	0.1353	0.64	7.300	0.9	0.3913
6.1	0.03	72	44	0.63	24.5	2152	±20	2199	± 27	2.1	2.523	1.10	2.523	1.10	0.1377	1.50	7.530	1.9	0.3964
3.1	2.57	85	58	0.71	29.5	2125	±17	2173	± 39	2.3	2.543	0.92	2.543	0.92	0.1357	2.30	7.310	2.4	0.3905
17.1	0.02	200	32	0.16	67.7	2140	±14	2199	± 15	2.7	2.539	0.74	2.539	0.74	0.1377	0.85	7.478	1.1	0.3938
14.1	0.14	71	24	0.35	23.9	2124	±30	2194	± 30	3.3	2.561	1.70	2.561	1.70	0.1374	1.70	7.390	2.4	0.3903
1.1	0.22	109	72	0.68	35.8	2080	±14	2165	± 23	4.1	2.624	0.77	2.624	0.77	0.1351	1.30	7.090	1.5	0.3809
6.2	0.81	55	22	0.42	18.1	2083	±23	2198	± 42	5.5	2.616	1.30	2.616	1.30	0.1376	2.40	7.240	2.7	0.3814
9.2	0.20	55	21	0.39	18.1	2079	±21	2204	± 31	6.0	2.626	1.20	2.626	1.20	0.1381	1.80	7.250	2.1	0.3807
15.1	0.41	220	92	0.43	70.3	2033	±13	2176	± 18	7.0	2.695	0.75	2.695	0.75	0.1359	1.00	6.946	1.3	0.3707
5.2	1.93	132	66	0.52	40.3	1923	±18	2180	± 44	13.4	2.862	1.10	2.862	1.10	0.1362	2.50	6.530	2.8	0.3476
12.1	--	87	53	0.62	29.7	2148	±18	2229	± 22	3.8	2.528	0.97	2.528	0.97	0.1402	1.30	7.650	1.6	0.3955
Archean clast																			
4.1	0.05	200	187	0.96	82.8	2532	±15	2730	± 12	7.8	2.078	0.72	2.078	0.72	0.1886	0.71	12.510	1.0	0.4811
4.2	0.07	249	133	0.55	101.0	2486	±15	2724	± 13	9.6	2.125	0.71	2.125	0.71	0.1880	0.79	12.190	1.1	0.4705

TABLE 1
(continued)

Spot Name	$^{206}Pb_c$, %	U, ppm	Th, ppm	$^{232}Th/^{238}U$	$^{206}Pb^*$, ppm	(1) Age $^{206}Pb/^{238}U$ Ma	±	(1) Age $^{207}Pb/^{206}Pb$ Ma	±	D, %	(1) $^{228}U/^{206}Pb^*$	±, %	(1) $^{207}Pb^*/^{206}Pb^*$	±, %	(1) $^{207}Pb^*/^{235}U$	±, %	(1) $^{206}Pb^*/^{238}U$	±, %	Rho
Metarhyolite porphyry (Sample 0150/471.9–472.8)																			
Cores																			
1.1	0.27	66	26	0.41	19.3	1893	±17	2117	±31	12	2.928	1.00	0.1314	1.70	6.180	2.00	0.3413	1.00	0.500
9.1	0.11	526	74	0.14	162	1976.4	± 8.1	2144.8	± 9.7	9	2.787	0.48	0.13352	0.55	6.605	0.73	0.3588	0.48	0.652
4.1	0.16	188	68	0.37	58.3	1986	±11	2127	±16	7	2.770	0.64	0.1321	0.92	6.576	1.10	0.3609	0.64	0.571
10.1	0.28	138	42	0.31	43.8	2024	±13	2129	±20	5	2.710	0.75	0.1323	1.20	6.728	1.40	0.3688	0.75	0.544
6.1	0.13	441	360	0.84	144	2073.2	± 7.9	2150	±10	4	2.635	0.45	0.13393	0.60	7.005	0.74	0.3793	0.45	0.598
7.1	0.25	165	51	0.32	54.1	2082	±12	2151	±18	3	2.622	0.69	0.1340	1.00	7.040	1.20	0.3812	0.69	0.559
3.1	0.39	131	70	0.56	45.1	2166	±14	2140	±20	-1	2.501	0.77	0.1331	1.20	7.330	1.40	0.3994	0.77	0.555
5.1	0.15	274	23	0.09	96	2204	±10	2143	±13	-3	2.452	0.54	0.1334	0.73	7.497	0.91	0.4076	0.54	0.594
Rims																			
4.2	0.09	994	551	0.57	255	1684.9	± 5.1	2085.7	± 8.3	24	3.347	0.35	0.12909	0.47	5.317	0.59	0.2987	0.35	0.593
13.1	0.07	1050	390	0.38	290	1793.6	± 5.2	2091.7	± 7.7	17	3.117	0.33	0.12954	0.44	5.730	0.55	0.3208	0.33	0.609
12.1	0.04	615	293	0.49	199	2056.7	± 6.8	2146	±11	4	2.661	0.39	0.13362	0.64	6.924	0.75	0.3758	0.39	0.515
11.1	0.01	518	242	0.48	169	2070.5	± 7.4	2133.6	± 9.3	3	2.640	0.42	0.13267	0.53	6.928	0.68	0.3788	0.42	0.615
2.1	0.02	740	234	0.33	241	2074.5	± 6.4	2137.2	± 7.9	3	2.634	0.36	0.13294	0.45	6.958	0.58	0.3796	0.36	0.625
3.2	0.01	1246	247	0.20	407	2078.3	± 5.6	2121.8	± 6.3	2	2.629	0.31	0.13178	0.36	6.913	0.48	0.3804	0.31	0.655
8.1	0.11	322	116	0.37	108	2129.3	± 9.2	2127	±12	-0.09	2.554	0.51	0.13218	0.71	7.133	0.87	0.3914	0.51	0.581
Metarhyolite (Sample 0160/535–538.0)																			
10.2	0.05	562	412	0.76	176	2005	±16	2119	±12	6	2.740	0.93	0.1316	0.66	6.619	1.10	0.3649	0.93	0.814
6.2	0.05	936	1082	1.19	298	2033	±14	2114.9	± 7.5	4	2.696	0.79	0.1313	0.43	6.711	0.90	0.3708	0.79	0.878
5.2	0.02	1096	1011	0.95	353	2051	±13	2132.9	± 7.6	4	2.669	0.76	0.1326	0.43	6.850	0.88	0.3746	0.76	0.869
1.2	0.05	684	383	0.58	225	2087	±15	2118	±10	1.5	2.615	0.86	0.1315	0.58	6.932	1.00	0.3824	0.86	0.832
3.1	0.18	73	28	0.40	24.4	2108	±27	2126	±29	0.8	2.584	1.5	0.1321	1.70	7.040	2.20	0.3869	1.50	0.671
2.1	0.22	77	34	0.46	25.7	2108	±27	2117	±30	0.4	2.584	1.5	0.1314	1.70	7.010	2.30	0.3869	1.50	0.654
10.1	0.08	145	98	0.70	48.5	2114	±22	2120	±21	0.3	2.576	1.2	0.1317	1.20	7.040	1.70	0.3881	1.20	0.724
9.1	0.00	92	44	0.49	30.9	2125	±29	2132	±24	0.3	2.560	1.6	0.1325	1.40	7.140	2.10	0.3906	1.60	0.763
6.1	0.15	217	161	0.77	73.2	2132	±18	2133	±15	0.05	2.549	0.98	0.1327	0.85	7.172	1.30	0.3921	0.98	0.753
8.1	0.16	162	88	0.56	54.1	2112	±19	2112	±19	0.01	2.579	1.1	0.1310	1.10	7.000	1.50	0.3876	1.10	0.710
7.1	0.07	152	79	0.53	51.1	2125	±20	2119	±17	-0.3	2.560	1.1	0.1316	0.97	7.090	1.50	0.3906	1.10	0.746
3.2	0.07	153	66	0.45	51.7	2136	±22	2118	±20	-0.9	2.545	1.2	0.1315	1.10	7.120	1.60	0.3928	1.20	0.731
5.1	0.00	90	36	0.41	30.7	2153	±30	2128	±24	-1.2	2.522	1.6	0.1322	1.40	7.230	2.10	0.3965	1.60	0.761
1.1	0.33	120	60	0.52	40.7	2144	±23	2117	±29	-1.3	2.532	1.3	0.1314	1.70	7.150	2.10	0.3946	1.30	0.598

Errors are ±1σ; Pb_c and Pb* indicate the common and radiogenic portions, respectively. (1) Correction for common Pb made using that measured $^{204}Pb/^{206}Pb$ ratio. D, % is the individual discordance = 100 × [(age $^{207}Pb/^{206}Pb$)/(age $^{206}Pb/^{238}U$) – 1]. Rho is error correlation for $^{207}Pb/^{235}U$ vs. $^{206}Pb/^{238}U$ ratios. Error in standard calibration for spots were 0.29 (Sample 7782/188.5–193.0), 0.36 (Sample 0150/471.9–472.8) and 0.71 (Sample 0160/535–538.0).

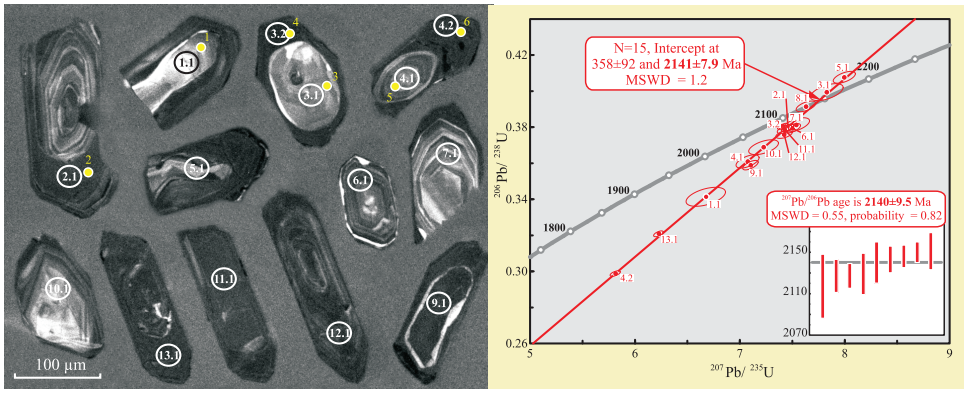

Fig. 5. Cathodoluminescence images of zircon grains and zircon U–Pb concordia diagram for the metarhyolite porphyrite from the Strelitsa Formation of the western part of the LT. Numbers of analytical points correspond to those in the table 1.

data define distinct REE patterns. The zircons of sample 7782/188.5–193.0 are characterized by heavy rare earth element (HREE) moderate enrichment ($952 \leq Yb_N \leq 8730$; $13 \leq (Lu/La)_N \leq 13628$), positive Ce e anomaly ($Ce/Ce^* = 1.32–32.9$) and negative Eu anomaly ($Eu/Eu^* = 0.09–0.44$) (fig. 7). The zircons of sample 0150/471.9–472.8 show almost flat patterns of REE ($1561 \leq Yb_N \leq 4363$; $2 \leq (Lu/La)_N \leq 85$) with a negative to positive Eu anomaly ($Eu/Eu^* = 0.12–1.25$) and a weak positive Ce anomaly ($Ce/Ce^* = 1.24–1.60$). The zircons of sample 0160/535–538.0 are characterized by HREE enrichment ($1600 \leq Yb_N \leq 4287$; $848 \leq (Lu/La)_N \leq 6278$), highly positive Ce anomaly ($Ce/Ce^* = 3.54–18.1$) and negative Eu anomaly ($Eu/Eu^* = 0.29–0.36$) (fig. 7).

Whole-Rock Chemistry

The representative chemical compositions of the Losevo terrain samples are given in table 3 and Supplementary data (http://earth.geology.yale.edu/%7eajs/Supplemen-

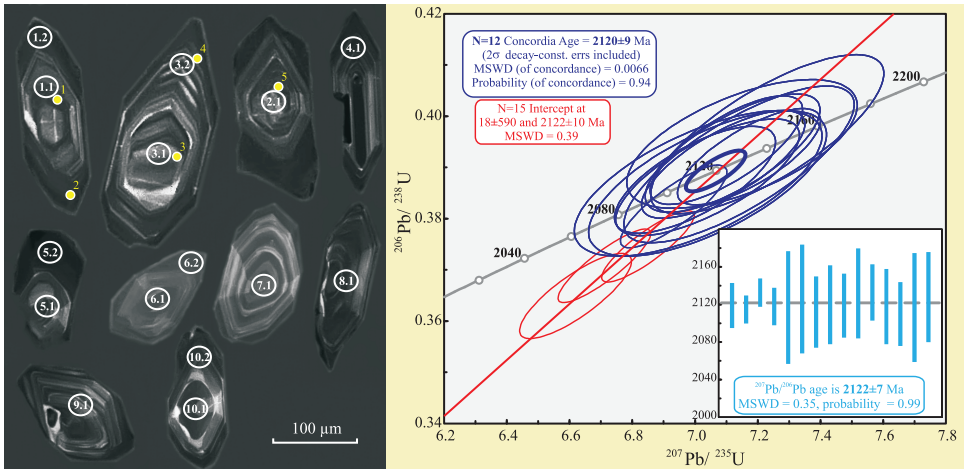

Fig. 6. Cathodoluminescence images of zircon grains and zircon U–Pb concordia diagram for the metarhyolite from the Podgornoe Formation of the eastern part of the LT. Numbers of analytical points correspond to those in the table 1.

TABLE 2

Trace and rare earth element analyses (ppm) of zircons from the LT rhyolites

	Metarhyolite (Sample 7782/188.5–193.0)											
Spot name	1	2	3	5	7	8	10	11R	11L	4	6	9
Location	rim	center	rim	center	rim	center	center	center	center	rim	center	rim
Age spot	3.2	6.1	6.2	15.1	11.2	7.1	11.1	17.1	4.1	15.2	9.1	7.2
P	382	3334	583	596	396	475	357	282	73.9	392	198	288
Ca	32.2	5693	909	715	10.0	21.9	21.2	16.5	8.64	29.9	28.2	586
Rb				4.59	2.21	2.78	3.52	0.793	0.939		0.964	1.84
Ba	3.46	21.8	1.66							3.95		
Th	114	35.4	27.5	238	90.8	79.6	80.1	45.9	114	35.8	24.6	136
U	223	79.9	91.9	470	215	216	214	330	189	322	77.1	486
Nb	31.6	13.6	12.2							115		
La	0.919	11.6	2.19	87.2	0.517	4.24	0.173	1.62	0.240	2.72	1.35	88.4
Ce	33.0	43.1	18.6	847	26.0	70.1	21.6	36.0	25.0	61.6	20.6	1183
Sr	1.05	11.6	1.54	32.3	1.14	2.68	1.22	1.08	0.342	2.32	0.740	43.5
Pr	2.98	5.29	1.52	138	0.798	9.7	0.692	6.59	0.134	5.85	4.12	181
Nd	29.1	30.8	13.5	741	6.25	46.7	9.48	52.5	0.896	40.6	26.5	817
Hf	7725	6207	7997	7778	7968	8395	8737	11078	9171	12502	7227	12492
Sm	21.6	15.7	7.43	135	7.10	13.9	14.8	17.4	1.51	12.5	5.46	128
Eu	2.91	1.87	0.916	16.9	0.66	1.90	1.42	2.87	0.202	1.64	1.20	18.3
Ti	7.75	9.25	8.57	86.8	6.02	7.69	4.89	5.85	14.5	8.71	11.8	58.3
Gd	86.6	57.3	31.0	224	46.6	66.4	88.2	23.3	7.97	22.5	20.2	136
Dy	349	191	139	551	230	279	409	62.8	35.7	113	81.7	209
Y	4012	2202	1774	6144	2885	3488	5013	935	476	1536	1128	2153
Er	737	416	333	1112	541	643	917	167	86.8	367	206	369
Yb	1280	730	653	1824	923	1119	1508	451	199	1270	401	707
Lu	201	116	109	278	148	181	245	91.8	34.8	230	70.2	119
T(°C)*	750	766	759	1024	728	749	710	725	809	761	789	969
T(°C)**	756	773	765	1054	732	755	713	729	819	767	798	993

Table 2

(continued)

Sample	Metarhyolite porphyry (Sample 0150/471.9–472.8)						Metarhyolite (Sample 0160/535–538.0)				
Spot name	1	3	5	2	4	6	1	2	3	4	5
Location	center	center	center	rim	rim	rim	center	rim	center	rim	center
Age spot	1.1	3.1	4.1	2.1	3.2	4.2	1.1	1.2	3.1	3.2	2.1
P	67.2	3001	204	411	168	164	189	346	219	217	236
Ca							7.46	10.8	0.362	3.11	0.673
Rb	0.898	1.13	0.937	2.15	1.03	2.24					
Ba	2.82	2.24	1.66	2.64	8.96	32.6					
Th	19.4	65.1	70.2	208	216	539	37.6	259	24.4	54.4	48.8
U	123	159	282	864	1555	1146	122	696	93.0	165	150
Nb	41.1	4.57	9.81	41.8	15.0	19.9	82.6	45.2	32.1	30.7	26.2
La	13.7	11.6	8.99	17.3	50.4	396	0.684	1.29	0.094	0.125	0.132
Ce	79.2	42.1	60.3	128	323	2304	10.0	45.9	5.34	8.89	8.47
Sr	3.17	5.51	1.96	5.23	22.7	105	0.589	1.66	0.539	0.652	0.581
Pr	11.5	4.75	7.88	17.5	55.2	407	0.588	1.42	0.079	0.099	0.103
Nd	102	25.6	76.1	153	482	3484	5.31	9.72	0.872	1.23	1.17
Hf	8066	7096	7747	8414	9933	7941	7160	9092	7189	6593	6287
Sm	55.4	12.4	42.5	61.8	213	1613	5.85	11.9	1.86	2.75	2.73
Eu	25.0	0.990	13.3	8.91	55.1	312	1.57	3.40	0.753	1.17	1.12
Ti	9.26	9.75	10.3	16.8	22.1	130	9.85	9.10	6.05	10.9	9.20
Gd	67.3	42.5	57.9	85.0	196	1487	22.2	66.8	12.2	21.9	18.3
Dy	97.2	136	89.5	201	179	725	73.4	268	51.1	95.4	82.7
Y	1101	1954	1210	2654	1341	2911	887	3124	679	1276	1089
Er	193	320	187	467	203	306	157	531	132	233	201
Yb	363	574	394	912	334	326	334	896	290	466	403
Lu	56.8	89.6	74.4	153	55.7	74.2	60.2	143	55.3	81.7	71.1
T(°C)*	766	771	777	824	853	1085	772	765	728	781	766
T(°C)**	773	778	784	835	867	1121	779	771	732	789	772

T(°C)* = temperature calculated using Ti-in-zircon geothermometer of Watson and others (2006).
T(°C)** = temperature calculated using Ti-in-zircon geothermometer of Ferry and Watson (2007).

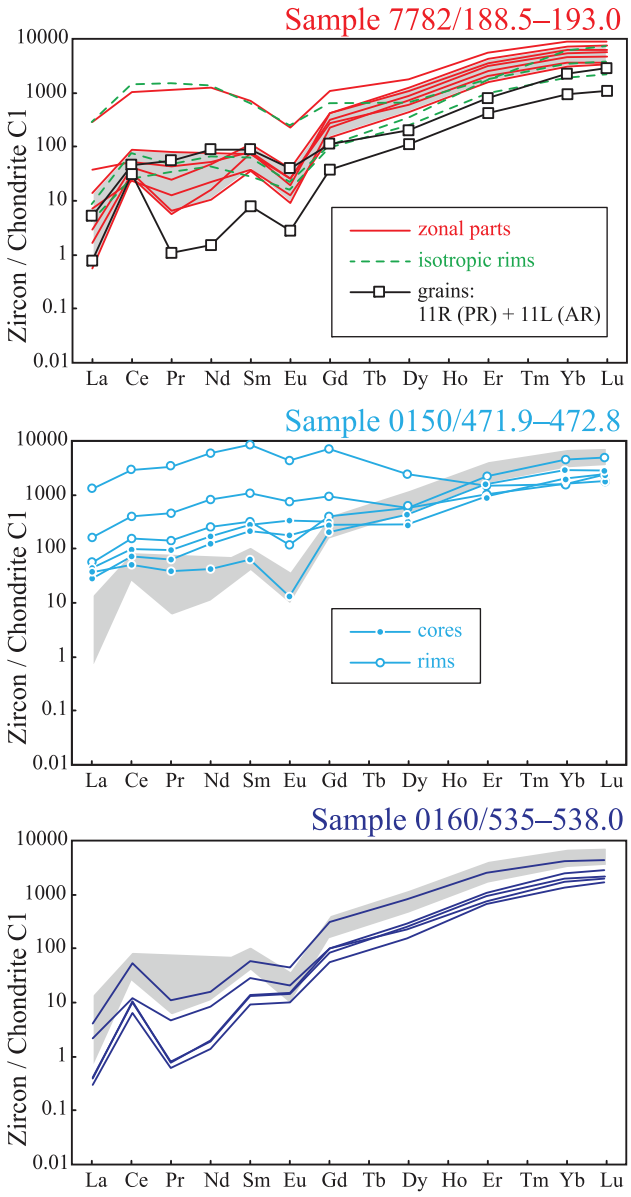

Fig. 7. Chondrite-normalized (after Sun and McDonough, 1989) REE patterns for zircons from the felsic rocks of the LT.

taryData/2017/Terentiev). Because of high LOI contents in some samples, totals for major oxides of the mafic to felsic rocks are recalculated to 100 percent (volatile free) for presentation in plots. On the classification diagram after Winchester and Floyd (1976) (figs. 8A and 8B), the mafic rocks of the bimodal suites classify as basalts and andesites, the felsic rocks as rhyolites, and the BBA plus FR+R plus BADR series as basalts, andesites, dacites and rhyodacites. The samples plot within low-K, calc-alkaline and high-K calc-alkaline rocks (fig. 8C). The AFM diagram is used to provide key

TABLE 3

Representative major (wt% oxide) and trace (ppm) element contents of the LT rocks

	Volcanics in Terrigene Formation:										
	Amphibolite with tholeiite affinity			Amphibolite with calc-alkaline affinity					Felsic dikes		
Drillhole	0181	0181	0180	0181	0181	0181	0181	0181	0181	0181	0181
Depth, m	242.0	841.2	438.3	499.5	341.5	389.2	625.5	415.5	439.5	578.8	595.3
SiO_2	51.60	50.30	46.0	48.60	54.70	56.10	50.70	75.90	75.20	74.80	74.50
TiO_2	0.714	0.605	2.37	1.050	1.470	0.668	0.762	0.215	0.200	0.237	0.207
Al_2O_3	12.50	7.99	14.9	15.00	16.90	15.20	12.00	11.60	11.60	13.70	12.80
$Fe_2O_{3(total)}$	10.50	11.40	17.4	9.86	10.90	8.07	9.81	4.20	4.53	2.56	2.53
$Fe_2O_{3(wet)}$	–	–	–	–	–	–	–	–	–	–	–
MnO	0.169	0.218	0.340	0.143	0.130	0.123	0.176	0.113	0.096	0.017	0.027
MgO	10.30	12.90	5.07	8.37	2.93	5.19	9.18	0.42	0.33	0.36	0.34
CaO	8.77	10.80	6.81	10.50	6.55	7.34	9.41	1.44	0.95	0.59	1.37
Na_2O	1.73	0.89	4.27	2.78	3.60	4.00	1.67	5.10	5.21	4.91	6.03
K_2O	0.616	1.780	1.11	0.990	1.620	0.976	2.770	0.910	1.010	2.180	0.815
P_2O_5	0.191	0.155	0.898	0.487	0.561	0.201	0.199	0.042	0.023	0.066	0.028
S	–	–	–	–	–	–	–	–	–	–	–
LOI	2.17	2.35	1.37	2.03	0.66	1.19	2.64	0.78	0.43	1.05	1.01
H_2O^+	–	–	–	–	–	–	–	–	–	–	–
H_2O^-	–	–	–	–	–	–	–	–	–	–	–
CO_2	–	–	–	–	–	–	–	–	–	–	–
F	–	–	–	–	–	–	–	–	–	–	–
Cl	–	–	–	–	–	–	–	–	–	–	–
LOI	2.17	2.35	1.37	2.03	0.66	1.19	2.64	0.78	0.43	1.05	1.01
Total	99.26	99.38	100.54	99.89	100.05	99.17	99.32	100.72	99.58	100.47	99.66
FeO	6.62	7.98	–	6.35	5.77	5.12	6.28	2.01	2.37	1.35	1.69
Be	1.13	1.41	1.40	1.43	2.03	0.995	1.14	2.74	2.71	1.72	1.35
Sc	–	–	–	30.08	–	–	–	–	–	–	–
Ti	4957	4188	15769	5949	9842	4706	6394	1494	1605	5991	1472
V	250	294	221	180	265	197	300	9.04	11.30	205.00	31.80
Cr	677	1183	436	436	76.9	665	402	78.5	76.3	77.9	31.9
Co	48.3	51.6	33.9	39.6	30.4	42.0	44.8	3.31	2.37	4.40	5.22
Ni	142	161	45.5	194	66.2	295	242	23.4	29.5	26.7	18.2
Cu	67.2	216	138	44.7	170	89.3	103	76.8	110.0	43.1	68.4
Zn	94.5	161	168	81.4	143	92.9	109	120	187	116	31
Ga	17.4	11.8	31.9	17.4	26.8	21.9	21.4	28.6	43.9	17.5	15.8
Rb	22.5	45.7	48.2	42.4	56.7	20	69.2	15.7	23.6	50.5	73.8
Sr	268	197	340	514	724	674	619	158	143	149	151
Y	18.0	15.4	41.7	16.8	33	15.1	24.9	94.2	110.0	20.9	9.3
Zr	79.5	57.5	118	133	251	108	106	466	550	137	178
Nb	4.21	3.09	6.33	12.6	15.3	6.01	5.42	21.2	22.0	10.6	10.2
Mo	3.97	2.72	16.1	4.73	4.22	5.64	2.86	63.3	3.9	3.3	7.8
Sn	1.00	0.784	1.06	0.986	1.76	0.896	0.973	4.03	3.41	1.40	0.93
Cs	2.27	1.29	1.36	2.79	3.34	1.75	2.57	0.520	0.351	2.520	2.630
Ba	152	438	222	256	620	282	639	540	450	318	523
La	9.63	6.60	14.1	20.3	54.1	24.2	23.4	34.9	32.1	36.4	29.7
Ce	25.9	15.9	38.0	51.3	127	53.5	54.0	87.7	76.9	85.3	57.3
Pr	3.72	2.33	6.15	6.92	16.4	6.86	7.46	12.2	10.4	11.7	5.8
Nd	16.5	10.6	30.6	29.7	66.1	27.9	32.2	53.4	40.9	49.1	18.9
Sm	4.02	2.71	8.16	5.75	11.5	4.84	6.72	13.0	9.9	8.8	2.8
Eu	1.03	0.696	3.49	1.47	2.44	1.14	1.77	2.25	1.95	2.02	0.45
Gd	3.98	2.93	9.30	4.72	9.35	3.92	6.13	14.6	9.6	6.9	2.2
Tb	0.589	0.484	1.51	0.653	1.25	0.554	0.880	2.58	1.57	0.88	0.30
Dy	3.42	2.96	8.51	3.54	6.44	2.85	4.75	16.4	9.7	4.3	1.6
Ho	0.640	0.603	1.74	0.676	1.21	0.552	0.951	3.47	2.02	0.77	0.31
Er	1.87	1.70	4.57	1.87	3.43	1.6	2.67	10.3	6.0	2.1	1.0
Tm	0.243	0.241	0.614	0.254	0.451	0.211	0.371	1.51	0.86	0.26	0.14
Yb	1.53	1.56	3.80	1.55	2.91	1.37	2.43	9.63	5.56	1.63	0.98
Lu	0.232	0.245	0.585	0.236	0.452	0.207	0.373	1.47	0.86	0.24	0.16
Hf	2.13	1.68	3.36	3.10	5.95	2.68	2.82	12.7	7.4	3.0	4.4
Ta	0.354	0.244	0.924	0.673	0.85	0.719	0.481	1.26	0.69	0.53	0.81
Th	2.45	1.97	2.23	2.09	6.78	3.85	3.98	5.26	3.60	7.64	8.55
U	0.670	0.254	0.249	0.693	1.74	0.976	0.768	1.43	0.82	1.66	2.36

Table 3
(continued)

	Strelitsa Formation (BS-1):										
	Roof tholeiite		Basal tholeiite		Subvolcanic tholeiite			Rhyolite		Subvolcanic rhyolite	
Drillhole	7782	7782	7782	7782	0150	0150	0150	7782	7782	0150	0150
Depth, m	215.0	237.9	395.0	546.0-549.6	290.5	402.8	511.1	189.0	416.3	442.5	615.8
SiO_2	49.00	46.86	48.30	47.80	48.20	50.10	52.60	70.50	73.30	69.30	69.80
TiO_2	2.10	1.58	0.99	1.13	1.15	0.71	0.81	0.23	0.07	0.23	0.31
Al_2O_3	13.40	13.83	14.30	13.50	15.20	16.80	15.50	15.20	13.10	15.00	15.80
$Fe_2O_{3(total)}$	17.2	15.92	14.2	15.4	12.6	11.2	11.0	3.54	2.83	3.61	2.48
$Fe_2O_{3(wet)}$	–	–	–	–	–	–	–	–	–	–	–
MnO	0.149	0.250	0.212	0.213	0.191	0.168	0.153	0.034	0.030	0.041	0.031
MgO	3.70	5.52	7.01	6.32	7.49	6.45	6.43	0.52	0.10	0.52	0.89
CaO	4.22	8.76	10.90	11.40	9.81	7.17	7.82	2.91	1.93	2.62	3.34
Na_2O	2.56	1.17	1.28	1.38	2.44	4.49	3.14	5.05	5.01	4.91	5.20
K_2O	0.711	0.005	0.093	0.026	0.657	0.465	0.325	1.000	1.490	2.160	1.090
P_2O_5	0.252	0.005	0.092	0.100	0.009	0.005	0.117	0.015	0.008	0.040	0.077
S	0.009	0.018	0.064	0.026	0.022	0.022	0.014	0.006	0.075	0.019	0.020
LOI	–	–	–	–	–	–	–	–	–	–	–
H_2O^+	4.31	3.86	2.46	2.04	1.58	1.85	1.78	0.73	0.83	0.95	0.65
H_2O^-	0.44	0.07	0.20	0.28	0.09	0.21	0.14	0.07	0.13	0.14	0.07
CO_2	1.60	1.99	0.10	0.44	0.56	0.55	0.12	0.20	1.23	0.50	0.22
F	0.091	0.097	0.079	0.083	0.067	0.055	0.061	0.008	0.004	0.011	0.020
Cl	0.0020	0.003	0.0010	0.004	0.005	0.005	0.003	0.002	0.003	0.002	0.002
LOI	6.45	6.04	2.90	2.87	2.32	2.69	2.12	1.02	2.27	1.62	0.98
Total	99.74	99.94	100.28	100.14	100.07	100.25	100.02	100.02	100.14	100.05	100.00
FeO	8.90	9.31	8.07	8.57	8.56	8.35	7.62	2.14	2.16	2.91	1.68
Be	0.788	0.760	0.352	0.403	0.592	0.464	0.495	0.805	0.664	0.992	1.220
Sc	35.4	53.5	50.4	49.8	54.9	51.2	27.4	13.1	17.6	10.3	53.5
Ti	12201	10813	5602	6885	8190	5530	4371	1408	475	1255	2381
V	250	479	298	327	357	310	197	62.3	40.0	58	144
Cr	10.6	41.2	228	190	250	137	287	49.7	40.3	40.9	111
Co	33.0	55.6	49.1	51.8	56.4	55.8	38.2	5.74	6.39	6.13	7.61
Ni	–	44.7	73.6	78.0	151	146	97.0	17.2	–	1.28	20.7
Cu	37.9	99.0	57.2	76.5	237	164	60.9	6.6	–	25.5	54.3
Zn	114	134	93.0	79.3	146	81.1	42.3	42.2	27.5	24.7	50.4
Ga	22.8	26.8	16.8	17.0	22.1	23.3	17.0	17.3	15.6	16.4	24.7
Rb	23.0	0.5	3.16	1.57	26.3	16.1	13.8	26.3	39.7	45.9	31.6
Sr	150	460	140	223	215	271	290	348	204	326	466
Y	31.4	35.4	20.29	21.4	23.2	18.9	12.8	3.01	3.03	5.35	5.51
Zr	168	112	64.5	73.2	90.0	69.9	84.5	106	51.4	116	135
Nb	5.02	4.20	2.94	2.98	6.78	3.59	3.20	2.72	2.66	3.82	4.82
Mo	2.19	3.24	2.52	2.72	3.77	2.95	2.72	6.84	7.57	4.59	8.19
Sn	1.42	0.744	0.709	0.715	5.55	0.848	0.615	0.762	0.729	0.789	0.809
Cs	0.528	0.306	0.215	0.159	0.608	1.627	0.284	0.719	0.664	0.574	0.775
Ba	156	56.9	47.5	32.2	226	87.4	92.3	288	296	582	635
La	6.02	7.71	3.26	3.85	5.89	4.63	4.53	8.47	9.23	10.6	15.4
Ce	15.8	20.0	8.85	10.0	15.5	10.4	11.4	16.9	17.5	22.7	31.1
Pr	2.36	3.13	1.33	1.50	2.37	1.45	1.64	1.79	1.87	2.56	3.57
Nd	11.5	15.7	6.80	7.78	11.6	6.93	7.95	6.49	6.82	9.28	13.3
Sm	3.60	4.91	2.27	2.50	3.16	1.97	2.25	1.20	1.23	1.67	2.34
Eu	1.36	1.70	0.874	0.911	1.17	0.770	0.755	0.441	0.338	0.505	0.611
Gd	4.39	5.93	3.00	3.34	3.69	2.55	2.46	0.894	0.932	1.44	1.62
Tb	0.860	1.040	0.546	0.585	0.631	0.467	0.404	0.122	0.114	0.192	0.208
Dy	6.16	6.78	3.73	4.04	4.11	3.17	2.51	0.639	0.565	1.06	1.05
Ho	1.36	1.41	0.858	0.888	0.859	0.708	0.520	0.114	0.100	0.202	0.197
Er	3.97	4.15	2.45	2.55	2.47	2.09	1.44	0.287	0.255	0.539	0.485
Tm	0.587	0.581	0.354	0.380	0.351	0.306	0.213	0.045	0.033	0.082	0.071
Yb	3.79	3.72	2.27	2.51	2.25	2.02	1.35	0.269	0.222	0.547	0.425
Lu	0.551	0.578	0.355	0.379	0.354	0.317	0.204	0.038	0.035	0.084	0.070
Hf	5.16	3.31	2.07	2.17	2.50	1.88	2.43	3.05	1.53	3.49	3.39
Ta	0.451	0.486	0.243	0.269	0.504	0.336	0.295	0.325	0.340	0.549	0.779
Th	1.55	1.38	1.14	0.962	1.35	1.26	1.03	2.39	2.39	3.61	4.68
U	0.304	0.330	0.089	0.129	0.129	0.138	0.211	0.401	0.476	1.72	1.26

Table 3

(continued)

	Podgornoye Formation (BS-2 + BADR):											
	Tholeiite of the BS-2				Rhyolite of the BS-2		Basalt–andesite–dacite–rhyolite (BADR)					
Drillhole	0182	0182	B-1	0160	0160	0160	0182	0182	0182	0182	0182	0160
Depth, m	806.0	809.1	358.0	588.5	537.0	653.0	287.0	647.9	1149.2	671.0	854.0	562.5
SiO_2	52.43	47.81	49.00	54.3	76.2	68.0	48.85	51.00	55.28	60.60	67.90	58.6
TiO_2	1.30	1.48	1.59	0.598	0.076	0.377	0.52	0.64	0.62	0.65	0.34	0.695
Al_2O_3	13.40	15.40	14.40	13.6	11.9	15.2	10.85	12.90	15.48	16.70	17.10	16.9
$Fe_2O_{3(total)}$	–	–	17.2	8.27	1.34	4.07	9.16	7.63	–	4.94	4.17	7.16
$Fe_2O_{3(wet)}$	4.13	3.50	–	–	–	–	–	–	1.86	–	–	–
MnO	0.270	0.150	0.263	0.121	0.022	0.053	0.140	0.108	0.090	0.071	0.025	0.131
MgO	4.73	4.67	4.92	5.27	0.585	1.29	13.63	9.25	4.91	1.45	0.54	3.32
CaO	7.42	4.90	6.71	5.51	1.87	3.49	7.30	5.98	8.90	8.88	1.54	5.72
Na_2O	3.34	3.37	1.60	3.68	3.19	4.93	1.14	2.34	2.58	2.89	4.43	3.83
K_2O	0.060	0.040	0.401	0.329	2.16	0.618	0.090	0.120	0.790	0.993	1.990	0.947
P_2O_5	0.140	0.160	0.258	0.163	0.033	0.118	0.170	0.295	0.170	0.027	0.005	0.202
S	0.080	0.080	0.056	–	–	–	0.011	0.060	0.060	0.036	0.071	–
LOI	–	–	–	7.83	2.62	1.60	–	–	–	–	–	2.51
H_2O^+	2.82	4.49	3.35	–	–	–	4.45	3.69	2.14	1.15	1.79	–
H_2O^-	0.04	0.08	0.11	–	–	–	0.08	0.08	0.04	0.03	0.22	–
CO_2	1.53	2.28	0.02	–	–	–	3.27	5.51	3.42	1.70	0.01	–
F	0.040	0.046	0.091	–	–	–	0.075	0.067	0.005	0.025	0.011	–
Cl	0.023	0.027	0.008	–	–	–	0.002	0.003	0.019	0.002	0.003	–
LOI	4.53	7.00	3.64	7.83	2.62	1.60	7.89	9.41	5.68	2.94	2.11	2.51
Total	100.35	99.70	99.98	99.67	100.00	99.75	99.74	99.68	99.97	100.14	100.14	100.02
FeO	8.60	11.22	7.42	5.55	0.80	2.60	6.62	5.47	3.61	2.29	2.48	4.84
Be	0.901	0.778	0.567	0.371	0.724	0.702	0.854	0.936	19.6	1.060	0.804	0.716
Sc	32.6	36.9	46.1	20.0	3.59	5.49	24.6	17.3	23.0	35.7	8.9	13.8
Ti	7307	8904	8929	3578	480	2341	3185	3851	3374	4572	2070	3936
V	359.7	347.6	382	175	8.29	62.1	153	126	117	119	66.2	145
Cr	14.3	11.9	56.2	199	29.5	23.8	1246	686	54.6	58.8	26.6	79.4
Co	33.9	40.7	41.0	26.0	2.00	8.90	52.8	37.7	19.3	13.8	9.23	19.9
Ni	20.06	22.02	28.5	86.1	13.2	33.8	364	196	56.7	38.0	–	54.4
Cu	92.38	98.13	61.1	86.9	25.6	62.3	47.7	36.7	36.5	44.1	10.8	93.0
Zn	106.1	120.4	148	75.7	26.9	45.8	73.1	84.0	49.4	56.1	58.6	74.3
Ga	17.2	22.1	17.3	16.5	13.2	18.4	12.8	15.3	13.6	24.4	18.5	20.3
Rb	0.97	0.81	9.24	4.62	63.0	12.0	2.70	7.20	16	25.8	58.7	23.6
Sr	203	157	189	272	75.2	308	223	459	181	201	400	553
Y	27.41	34.53	18.0	15.4	5.17	7.74	11.3	10.1	10.1	25.5	4.68	16.9
Zr	79	100	88	119	62.8	108	94	126	76.8	278	100	127
Nb	4.54	5.97	5.87	5.60	3.48	4.08	5.27	4.40	3.55	13.1	2.38	6.70
Mo	1.7	0.7	3.84	2.73	2.70	4.06	3.43	3.22	0.711	5.84	7.18	3.51
Sn	–	–	0.944	0.845	0.748	0.693	0.686	1.58	–	0.464	0.559	1.09
Cs	2.8	3.3	0.294	0.900	3.13	1.21	0.838	1.25	3.33	0.702	1.37	1.94
Ba	30	34	127	95.1	600	206	83.8	276	53.4	138	389	386
La	5.0	6.8	5.53	11.9	11.8	14.5	13.5	18.9	8.49	23.1	4.95	17.9
Ce	12.8	17.6	14.2	25.6	24.3	27.3	31.9	40.0	19.5	48.6	11.7	39.0
Pr	1.89	2.65	1.94	3.32	2.64	3.07	4.12	4.78	2.61	6.10	1.48	5.05
Nd	9.4	13.4	8.3	13.5	10.1	11.0	17.2	18.9	11	25.0	5.92	20.8
Sm	3.01	4.10	2.29	2.79	1.66	1.95	3.62	3.44	2.3	5.15	1.15	4.11
Eu	1.254	1.857	0.880	0.774	0.411	0.586	1.07	1.03	0.726	1.37	0.219	1.16
Gd	3.91	5.31	2.75	2.80	1.33	1.75	3.00	2.68	2.23	4.79	1.02	3.74
Tb	0.679	0.925	0.512	0.432	0.179	0.251	0.432	0.363	0.328	0.737	0.159	0.555
Dy	4.49	6.13	3.31	2.63	0.961	1.37	2.31	2.03	2.05	4.53	0.926	3.19
Ho	1.009	1.368	0.745	0.527	0.176	0.266	0.472	0.398	0.407	0.914	0.197	0.639
Er	2.918	3.982	2.14	1.57	0.538	0.767	1.26	1.09	1.15	2.64	0.539	1.86
Tm	0.425	0.567	0.336	0.232	0.073	0.109	0.182	0.159	0.166	0.385	0.081	0.262
Yb	2.810	3.822	2.21	1.52	0.517	0.724	1.13	1.01	1.07	2.52	0.544	1.67
Lu	0.414	0.568	0.340	0.240	0.074	0.115	0.171	0.149	0.162	0.388	0.083	0.262
Hf	1.87	2.67	2.57	2.87	2.30	2.65	2.60	3.32	1.82	6.88	3.14	3.24
Ta	0.28	0.37	0.413	0.390	0.387	0.390	0.403	0.286	0.247	1.19	0.183	0.524
Th	0.5	0.6	1.59	1.28	3.59	2.39	2.42	3.35	0.753	3.68	1.45	2.31
U	0.17	0.20	0.201	0.604	1.08	0.785	0.646	0.846	0.242	0.889	0.308	0.809

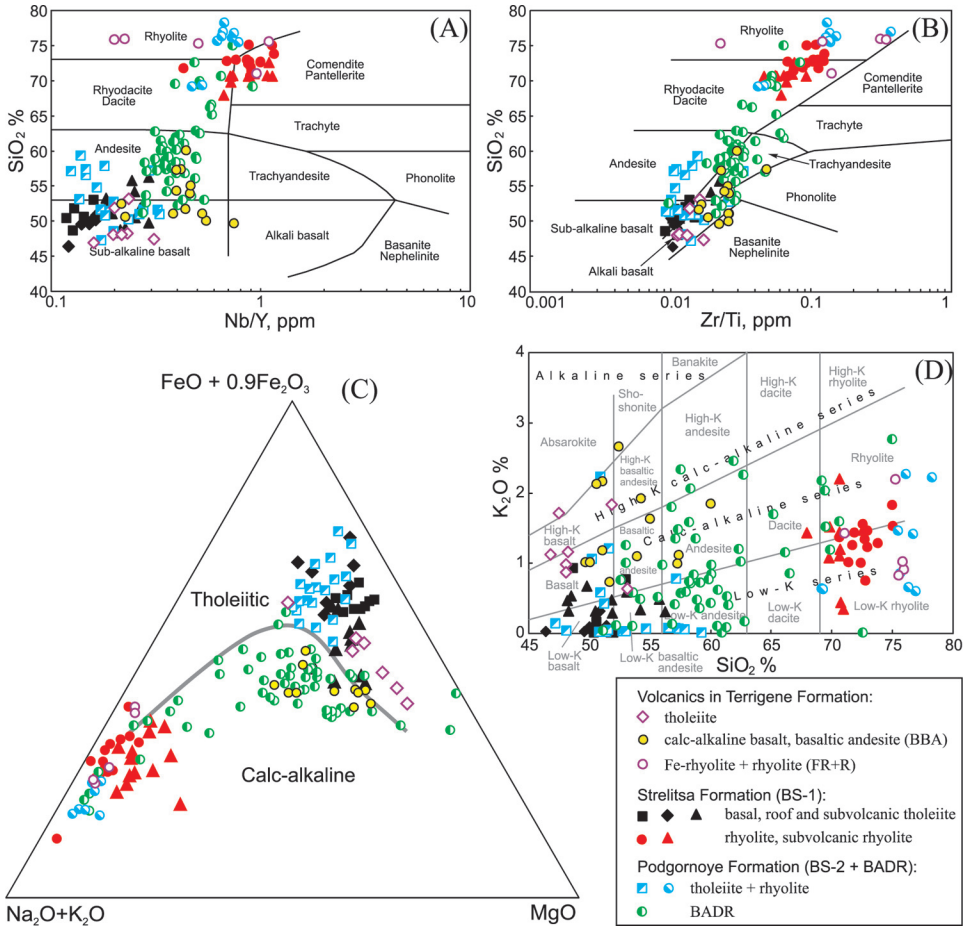

Fig. 8. (A and B) Nb/Y vs. SiO_2 and Ti/Zr vs. SiO_2 diagram (Winchester and Floyd, 1976); (C) K_2O vs. SiO_2 diagram (Ewart, 1982) and (D) AFM diagram (Irvine and Baragar, 1971) for classification of the Losevo terrain volcanic rocks.

discriminations (fig. 8D). The amphibolites in the Terrigene Fm. show a tholeiitic and calc-alkaline affinity, whereas the felsic rocks of the Formation have a calc-alkaline trend for three samples (rhyolites) and high Fe contents for two samples (Fe-rhyolites). Some of the amphibolites in the Terrigene Fm. are enriched in MgO (5.2–10.7 wt.%), which is typical of high-Mg andesites and basalts. The high Mg composition is also confirmed by Mg # ($Mg/(Mg + Fe^{2+})$ molar %) values, which range from 0.48 up to 0.69 (Supplementary data, http://earth.geology.yale.edu/%7eajs/SupplementaryData/2017/Terentiev). The chemical composition of the Strelitsa Fm. bimodal volcanic rocks (bimodal suite -1, BS-1) mainly belong to low-K tholeiites and low-K rhyolites with SiO_2 ranging from 46.4 to 54.2 weight percent and from 67.9 to 75.0 weight percent, respectively (Supplementary data, http://earth.geology.yale.edu/%7eajs/SupplementaryData/2017/Terentiev). The majority of the Strelitsa volcanic rocks are enriched in Na_2O (up to 4.6 wt.% in tholeiites and up to 6.3 wt.% in rhyolites). The Podgornoye extrusive and subvolcanic rocks are classified as: (1) tholeiitic basalts, tholeiitic basaltic andesites and rhyolites of bimodal association (bimodal suite 2, BS-2); (2) calc-alkaline

BADR association of low-K and moderate-K content with SiO_2 in the range of 51.1 up to 69.5 weight percent (Supplementary data, http://earth.geology.yale.edu/%7eajs/SupplementaryData/2017/Terentiev). The majority of intermediate rocks of the BADR are characterized by moderate contents of MgO (1.5–6.8 wt.%), which is typical of 'normal' moderate-Mg andesites. Only part of the basaltic andesite and andesite samples is comparable with high-Mg andesites. Their Mg# values ranges from 0.57 to 0.77 (Supplementary data, http://earth.geology.yale.edu/%7eajs/SupplementaryData/2017/Terentiev).

The tholeiites of the Terrigene Fm. exhibit weakly fractionated LREE patterns (La/Sm_N = 1.49–2.11), weakly fractionated HREE patterns (Gd/Yb_N = 1.16–2.1) and moderately negative Eu anomalies (Eu/Eu* = 0.67–0.89) on chondrite-normalized REE diagrams (fig. 9A). Primitive mantle normalized spidergrams show strong enrichments in some LILE (for example, Rb, Ba and U), but show low to moderate degrees of depletion in HFSE (Nb and Ti) (fig. 9B). On the chondrite-normalized REE diagram (fig. 9A), the BBA of the Terrigene Fm. are enriched in light rare-earth elements (LREE) (La/Sm_N = 2.11–3.15), with moderately negative or absent Eu anomalies (Eu/Eu* = 0.7–1.0). These calc-alkaline rocks are characterized by extreme enrichments in most incompatible elements such as Rb, Ba, Th and U, but are depleted in Nb, Zr and Ti relative to their neighboring elements. All samples of the FR+R are enriched in LREE (La/Sm_N = 1.69–6.77), but show different fractionated REE patterns (La/Yb_N = 2.4–3.9 for Fe-rhyolites, La/Yb_N = 15.1–20.5 for rhyolites) with prominent Eu anomalies (Eu/Eu* = 0.42–0.77). They (fig. 9B) are relatively enriched in the primitive mantle in Rb, Ba, Th and U, depleted by Nb, Sr and Ti and are characterized by low Sr/Y = 1−26 ratio.

Chondrite-normalized REE concentrations of BM-1 tholeiites (Strelitsa Fm.) show N-,E-MORB-like, LREE depleted patterns (La/Yb_N = 0.97–1.30) (fig. 9C) similar to those of enriched and depleted back-arc basin basalts (D-BABB and E-BABB, Pearce and Stern, 2006) from East Scotia Ridge basin (for example, Leat and others, 2000; Fretzdorff and others, 2002). The tholeiites exhibit up to 10×primitive mantle values of Sun and McDonough (1989) in LILE (for example, Rb, Ba and U) and REE, but show variable degrees of depletion in Th, Sr and Zr (fig. 9D). Overall, the tholeiites have both MORB- and arc-like trace-element distribution patterns. All the rhyolite samples of the BS-1 are enriched in LREE (La/Sm_N = 2.99–5.93, La/Yb_N = 13.1–28.0). The REE patterns show strongly fractionated nature, in the absence of any significant europium anomalies (Eu/Eu* = 0.78–1.25). The rhyolites (fig. 9D) are enriched in Rb, Ba, Th, U, Zr and Sr relative to the primitive mantle, and are depleted in Nb and Ti, with high Sr/Y ratio (46−116).

Chondrite-normalized REE concentrations of BM-2 tholeiites (Podgornoye Fm.) show N-, E-MORB-like, LREE depleted patterns (La/Yb_N = 1.06–2.42) (fig. 9E) similar to those arc basalts. The tholeiites exhibit up to 10×primitive mantle values of Sun and McDonough (1989) in trace elements, but show variable degrees of depletion in Rb, Ba and Nb and enrichment in Th and Sr (fig. 9F). Overall, the tholeiites have arc-like trace-element distribution patterns. The rhyolite samples of the BS-2 are enriched in LREE (La/Sm_N = 4.3–7.0, La/Yb_N = 13.0–26.5). The REE patterns show strongly fractionated nature, in the absence of any significant europium anomalies (Eu/Eu* = 0.81–1.0). The rhyolites (fig. 9F) are enriched in Rb, Ba, Th, U and Zr relative to the primitive mantle, and are depleted in Nb, Sr and Ti, with low to moderate Sr/Y ratio (15−52). The BADR of Podgornoye Fm. exhibit fractionated LREE patterns (La/Sm_N = 1.93–3.99), generally flat HREE patterns (Gd/Yb_N = 1.3–2.1) and variable Eu anomalies (Eu/Eu* = 0.50–1.28) on chondrite-normalized REE diagrams (fig. 9G). Primitive mantle normalized spidergrams show strong enrichments in LILE (for example, Rb, Ba, Th and U), but show depletion in HFSE (Nb and Ti) (fig. 9H).

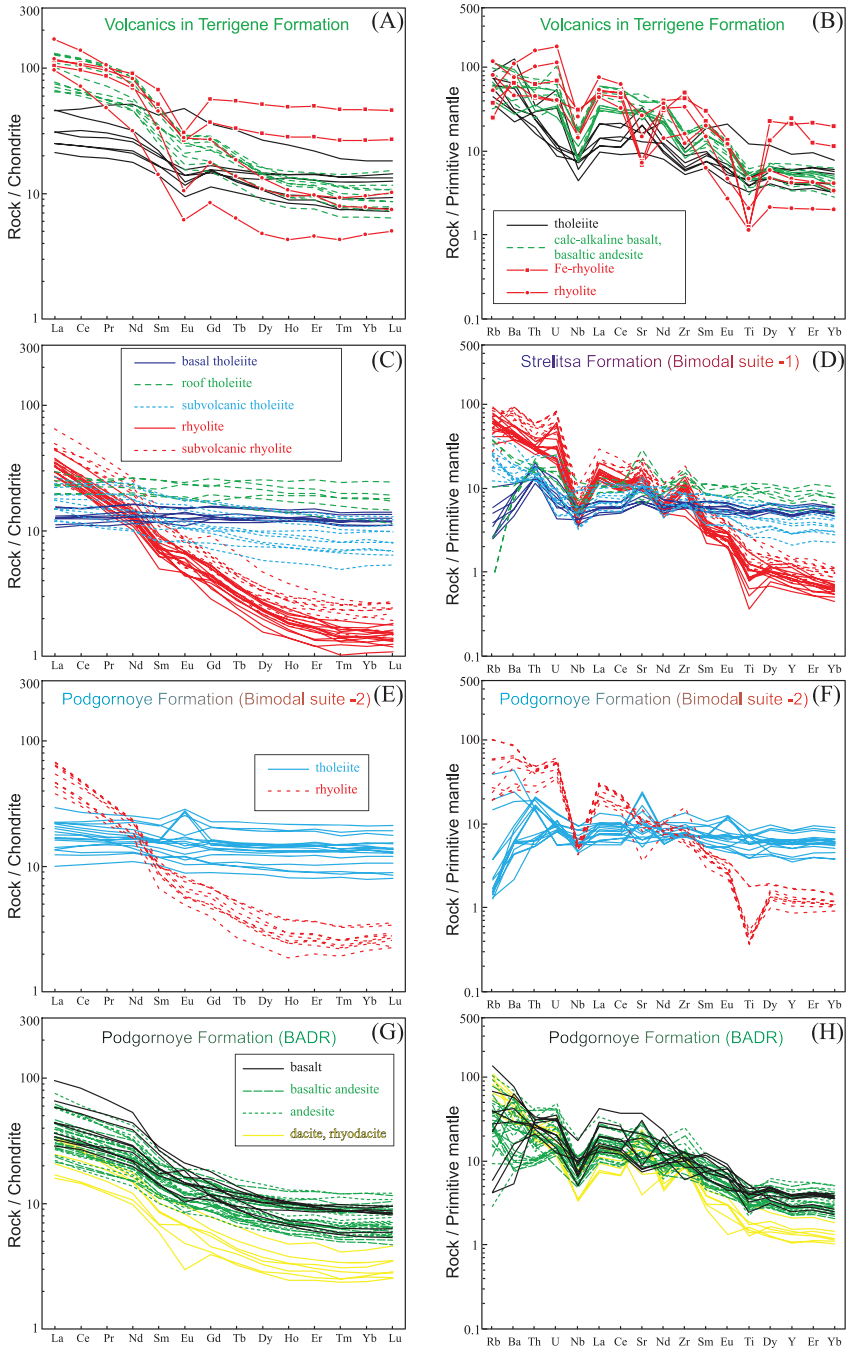

Fig. 9. (A), (C), (E) and (G) Chondrite normalized REE distributions for the volcanic rocks of the Losevo terrain. (B), (D), (F) and (H) Primitive mantle normalized spidergram of the Losevo terain volcanic rocks. Chondrite and primitive mantle-normalize values are from Sun and McDonough (1989).

TABLE 4

Sm–Nd isotopic data on the volcanic rocks of the Losevo terrain

Formation	Rock type	Drillhole No	Depth, m	Sm ppm	Nd ppm	$^{147}Sm/^{144}Nd$	$^{143}Nd/^{144}Nd$	T*, Ma	$\varepsilon_{Nd}(T)$	T_{Nd}-(DM)**
Terrigene	tholeiite	0181	242.0	3.807	15.16	0.1518	0.512136	2165	+2.7	2488
	Fe-rhyolite	0181	439.5	9.94	40.87	0.14739	0.512068	2165	+2.6	2479
	rhyolite	0181	578.8	3.01	18.57	0.09818	0.511209	2165	-0.5	2550
	microgabbro	0181	625.5	7.24	34.30	0.13093	0.511835	2165	+2.6	2413
Strelitsa	tholeiite	7782	546.0	2.640	8.232	0.1939	0.512784	2140	+3.6	
	tholeiite	7782	237.9	2.891	8.849	0.1976	0.512803	2140	+3.0	
	rhyolite***	7782	189.0	0.82	4.54	0.10911	0.511551	2140	+2.9	2322
	rhyolite***	7782	414.0	1.08	5.75	0.11403	0.511607	2140	+2.6	2351
	rhyolite***	0150	437.7	2.84	15.18	0.11318	0.511552	2140	+1.8	2414
Podgornoye	tholeiite	0182	806.0	3.543	11.39	0.18810	0.512707	2120	+3.7	2634
	rhyolite	0160	537.0	1.53	8.58	0.10800	0.511508	2120	+2.1	2359
	dacite	0160	653.0	1.99	10.77	0.11191	0.511586	2120	+2.6	2334
	basaltic andesite	0182	1149.2	2.422	11.37	0.12870	0.511874	2120	+3.6	2281

Assumed error in $^{147}Sm/^{144}Nd$ is no greater than 0.2%.
* – Age according to U–Pb dating (see text).
** – Model age (Ma) according to (Goldstein and Jacobsen, 1988).
*** – Primary data are from (Shchipansky and others 2007).

Sm-Nd Isotopic Data

The Sm-Nd isotopic data of the LT volcanic rocks are given in table 4. The initial isotopic values are calculated for the age of 2120, 2140 and 2165 Ma as based on the results of zircon U-Pb dating. Tholeiites of the Strelitsa and Podgornoye Fms. display uniform Sm–Nd isotopic compositions with $^{143}Nd/^{144}Nd$ varying from 0.512136 to 0.512874 and $\varepsilon Nd(t)$ values ranging from +2.7 to +3.6 and the rhyolite samples have $^{143}Nd/^{144}Nd$ varying from 0.511508 to 0.511607 and have enriched $\varepsilon Nd(t)$ values ranging from +1.8 to +2.9. In contrast, the BADR mafic rocks of the Podgornoye Fm. and the BBA of the Terrigene Fm. have $^{143}Nd/^{144}Nd$ 0.511874 and 0.511835 and $\varepsilon Nd(t)$ values +3.6 and +2.6, respectively. The felsic dikes of the Terrigene Fm. show varying Sm–Nd isotopic components ($^{143}Nd/^{144}Nd = 0.512068$ and 0.511209; $\varepsilon Nd(t) =$ +2.6 and −0.5) (table 4 and fig. 10), suggesting that these rocks originated from different magmatic source regions. The Podgornoye and Strelitsa Fms. volcanic rocks are characterized by similar Nd model ages in the range of 2281 to 2334 and 2332 to 2414 Ma, respectively. The Terrigene Fm. samples display higher Nd model ages between 2413 and 2550 Ma.

DISCUSSION

Timing of the Volcanism and Its Significance

As mentioned earlier, the LT volcanic rocks have been subdivided into the lower, middle and upper sequences, namely the Terrigene, Strelitsa and Podgornoye Fms., respectively. The Terrigene Fm. is composed of interlayered calc-alkaline (BBA) and tholeiitic basalts and felsic dikes (FR+R), whereas the Strelitsa Fm. contains bimodal suite 1 (BS-1). The Podgornoye Fm. is represented by BADR and bimodal suite 2 (BS-2). A pegmatoid gabbro of the Rozhdestvenskoe complex (with $^{207}Pb/^{206}Pb$ zircon age of 2128±21 Ma, Terentiev, 2014) is structurally lower than the Podgornoye Fm. and is coeval with the Strelitsa tholeiites. The contact between the Podgornoye volcanic rocks and the gabbro passes through an intensely crushed zone indicating tectonic contact. The metamorphic grade increases from the young Podgornoye Fm. to the old Terrigene Fm. The stratigraphic subdivisions of the LT volcanic sequences are supported by new SHRIMP U-Pb zircon data obtained in this study. The Strelitsa

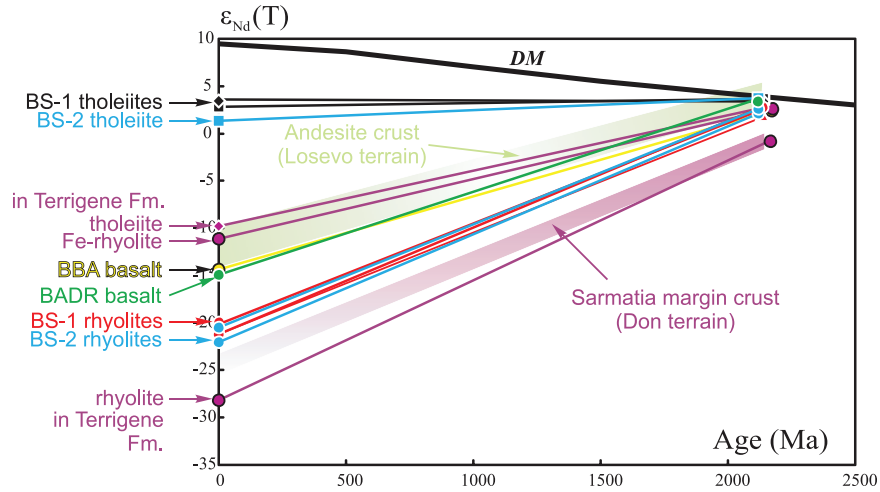

Fig. 10. Plot of εNd(T) values versus formation ages for volcanic rocks from the Losevo terrain. The Sarmatia margin crust (Don terrain) data are from (Shchipansky and others, 2007); field of andesite crust (Losevo terrain) from the core of the LT meta-graywacke are from our unpublished data.

rhyolite yielded the presence of detrital zircons, as evidenced by the dispersion of the $^{207}Pb/^{206}Pb$ ages from 2163±15 to 2229±22 Ma (fig. 11) and one Archean grain with distinct zircon chemistry (fig. 7). Detrital nature of the zircons is also confirmed by rounding grains, the difference in morphology and internal structure of crystals. The

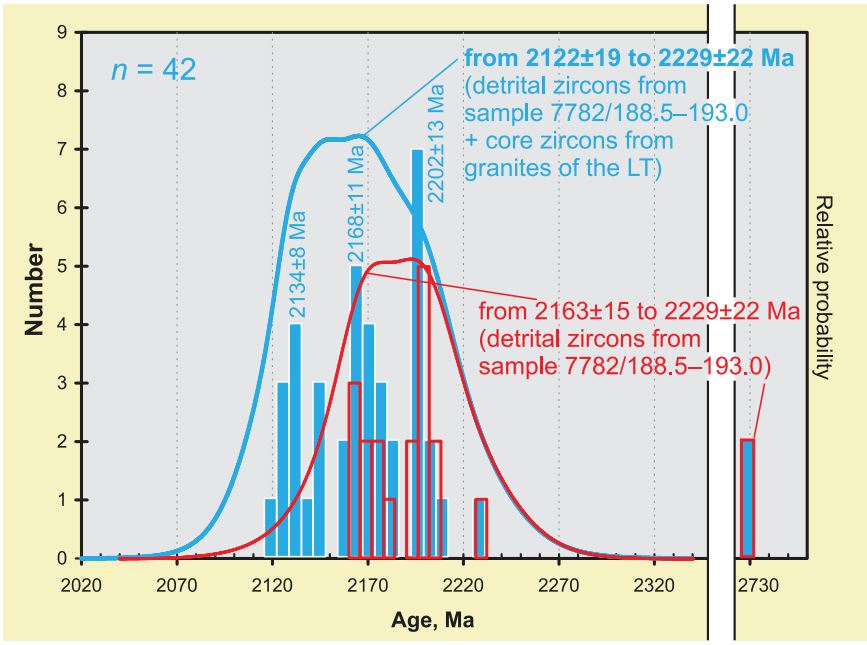

Fig. 11. Relative probability plot of ages of detrital zircons from the LT. Peak ages are identified for reference. Forty two concordant U-Pb zircon analyses were included in this plot.

grains overgrowth rims also display ages not older than 2140 Ma. Age of the oldest detrital grains (2.7 Ga) correlates with ages of Archean granitoids of Sarmatia (Artemenko, 1995). Geochemical data (Terentiev, 2013) indicate that the Terrigene Fm. was derived from magmatic protoliths, predominantly of mafic composition, but the genetic relationship with bimodal volcanism of the Strelitsa Fm. has been not identified. Also, part of the clastic sediments are products of recycling. The ages of the Paleoproterozoic detrital zircon coincide with the age intervals obtained by zircon cores from granites and migmatites in the western part of the LT (fig. 11) (Terentiev and others, 2016). These features, as well as a decrease in the age of zircon cores from the LT granite from west to east indicates that (1) the maximum sedimentation age limit of Terrigene Fm. is about 2163 to 2168 Ma, that is older than the Strelitsa Fm. and (2) average age of the volcanic-sedimentary strata (Podgornoye and Strelitsa Fms.) in the central and eastern parts of the LT is between 2134 Ma and 2122 Ma. The crystallization age of BS-1 rhyolite is about 2140 Ma as confirmed by the weighted mean $^{207}Pb/^{206}Pb$ age of 2140±9.5 Ma (fig. 5) of the oscillatory zoned magmatic zircons of the Strelitsa Fm. subvolcanic rhyolites. Similarly, our new data show that the Strelitsa Fm. is older than the Podgornoye Fm., where the age of volcanism is 2122±7 Ma as indicated by the weighted mean $^{207}Pb/^{206}Pb$ age of a rhyolite sample (fig. 6). All of these data demonstrate that the scheme of stratigraphic subdivisions of the LT volcanic sequences as shown in figure 2 is viable. They also indicate that the duration of volcanism in the LT formations is between 2168±11 Ma and 2122±7 Ma suggesting possibly multiple pulses of volcanism.

The Nature of Magma Source

Crustal contamination.—The enrichment of in K_2O, Ba, Th, U and LREE in the tholeiitic and, to a greater extent in the calc-alkaline basalts of Losevo terrain, together with the near constant contents of Ta, Nb, Ti, with negative anomalies (fig. 9) suggest continental crust contamination or melting in subduction–related settings (Rollinson,1993; Turner and others, 1997; Rudnick and Gao, 2003; Niu and O'Hara, 2009; Zheng, 2012). Nb, Th, Ta, U are relatively incompatible during basaltic magmatism (Niu and O'Hara, 2009), and therefore the Nb/Th and Ta/U ratios remain constant during magmatism and their variation would be inherited from the source rocks. The Nb/Th and Ta/U would decrease with increasing SiO_2, if mafic magmas were contaminated by the average composition of crust (Niu and O'Hara, 2009; Hu and others, 2016). However, Nb/Th versus SiO_2 plots show negative correlations for the BADR and to a lesser degree for the BBA. The BADR also display Ta/U minor correlation with SiO_2 (figs. 12A, 12C and 12D). The negative Zr anomalies observed in the spider diagrams for the Terrigene Fm. mafic rocks support an interpretation that only little or no crustal contamination occurred. Weak positive Zr anomalies in the roof and subvolcanic tholeiites of Strelitsa Fm., and especially in the BADR-series of Podgornoye Fm. indicate slightly higher degrees of crustal contamination or mixing parent mafic melts and felsic ones. Another crustal contamination indicator is Th. Low and constant Th, low Th/Yb and high Nb/Th ratios in the BS-2 tholeiites, low to moderate Th/Yb and moderate Nb/Th ratios in the BS-1 tholeiites, high and variable Th, high Th/Yb and low Nb/Th ratios in the tholeiitic basalts and BBA of the Terrigene Fm., and moderate Th/Yb and variable Nb/Th ratios in the BADR mafic rocks (figs. 13A and 13B) suggesting that the degree of crustal contamination increases: (1) from tholeiitic to calc-alkaline rocks and (2) from younger tholeiites to older ones of the Losevo terrain. The Nb/U values (9–53, average of 25) are typical for mantle origin melts (Sun and others, 2008). Furthermore, the relatively low concentrations of Th, and the lack of correlation of the La/Sm versus Nb/Th ratios confirm the minor role of contamination of magma in the genesis of LT tholeiites. Variations of Nb/Th with constant La/Sm ratios in tholeiites of the Podgornoye Fm. and basal

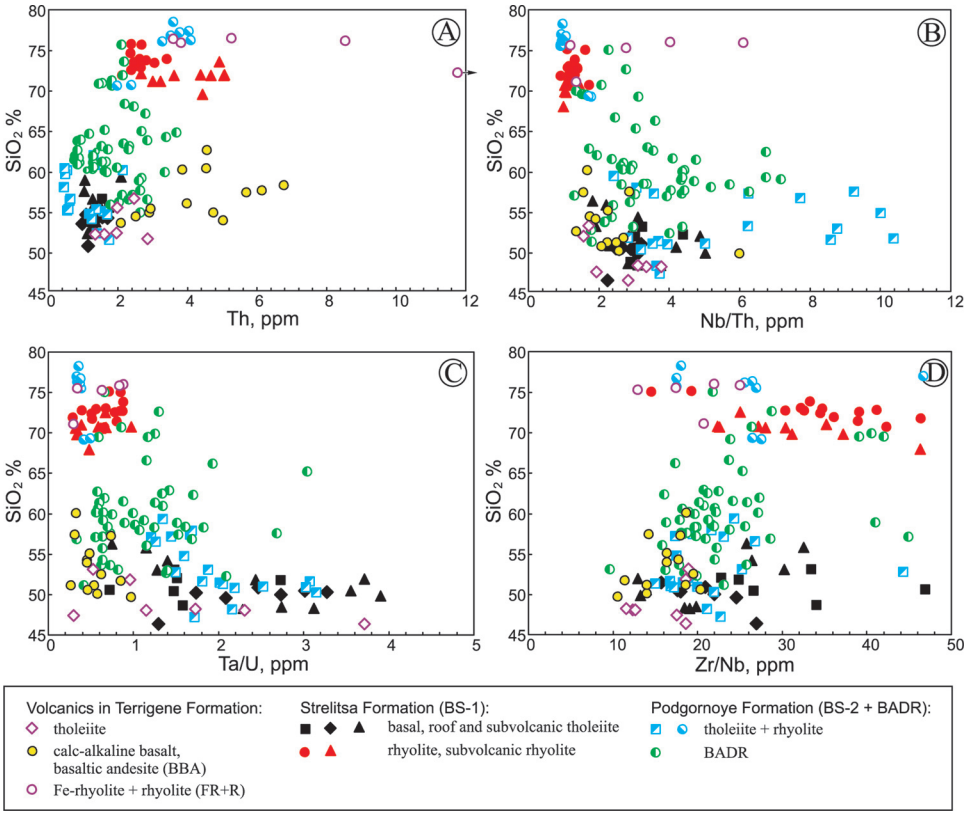

Fig. 12. Plots of SiO_2 vs. Th, Nb/Th, Ta/U, Zr/Nb for the LT volcanic rocks.

tholeiites of the Strelitsa Fm. are likely an attribute of magmatic source modification (metasomatism). Conversely, lower values of Nb/U (5–25, average of 12), relatively high concentrations of Th and weak correlation La/Sm versus Nb/Th ratios confirm crustal contamination in the genesis of LT calc-alkaline volcanic rocks. Thus, the effect of continental crustal contamination/magma mixing should be considered when discussing the petrogenesis and sources of the melts parental to the LT volcanic rocks.

Source of the mafic rocks.—The LT tholeiites are characterized by low to moderate Mg# (34–55) in the Strelitsa Fm. roof, moderate Mg# (48–55) in the base and high Mg# (up to 67) in the subvolcanic rocks of BS-1, mafic rocks of BS-2 and volcanic rocks alternating with the Terrigene Fm. The Cr, Ni and Co abundance also increases in the same succession, suggesting that the mantle parental melts of tholeiites within each of several stratigraphic units underwent fractional crystallization of olivine and clinopyroxene. Moreover, the impact of fractional crystallization is more significant for the tholeiitic magmas of Strelitsa Fm. roof and tholeiitic magmas of Podgornoye Fm., compared with the basal tholeiites of Strelitsa Fm. and tholeiites in Terrigene Fm. Plagioclase fractionation, consistent with negative Eu anomalies (fig. 9) and negative correlation of SiO_2 versus Al_2O_3 (not shown) (Wilson, 1989) are displayed by the tholeiites and BBA in the Terrigene Fm., BADR and to a lesser extent by the tholeiitic basalts of BS-2 of the Podgornoye Fm.

Most basalts are derived from asthenosphere-derived or lithospheric primitive magmas. The asthenosphere is either depleted or enriched in incompatible elements

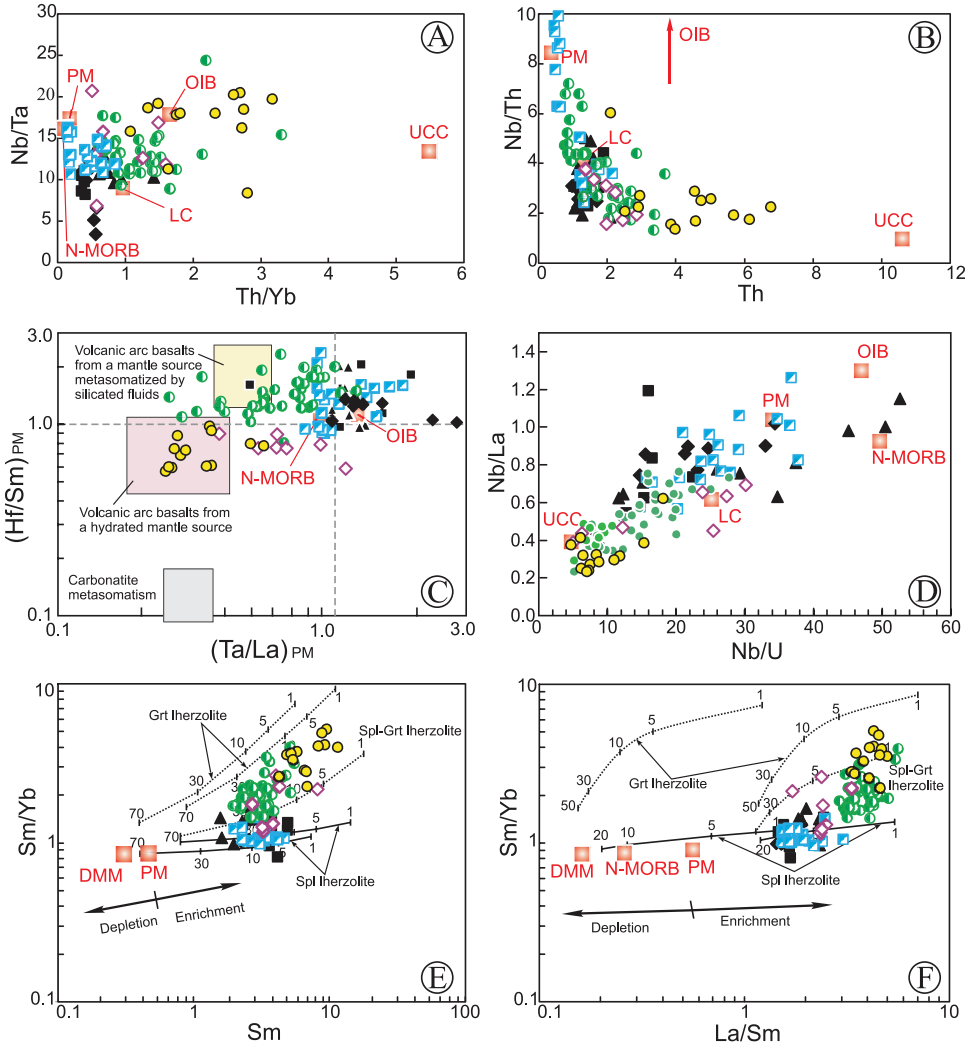

Fig. 13. Plots of Nb/Ta vs. Th/Yb (A), Nb/Th vs. Th (B), $(Hf/Sm)_{PM}$ vs. $(Ta/La)_{PM}$ (after LaFlèche and others, 1998) (C), Nb/La vs. Nb/U (D); Sm/Yb vs. Sm (E) and Sm/Yb vs. La/Sm (F) for the LT volcanic rocks. Values of OIB and primitive mantle are from Sun and McDonough (1989). Values for the upper and lower crust are from Rudnick and Gao (2003). Melting curves for spinel lherzolite (Ol53 + Opx27 + Cpx17 + Sp11) and garnet peridotite (Ol60 + Opx20 + Cpx10 +Gt10) with both DMM and PM compositions are after Aldanmaz and others (2000). Numbers along lines represent the degree of the partial melting.

with a varying degree of heterogeneity. Magmas from the asthenosphere components are characterized by a high εNd (Saunders and others, 1992; Hoffman, 1997). Lithospheric mantle as opposed to asthenosphere, is isotopically enriched (relatively low Nd), enriched in LILE, LREE and depleted in Nb, Ti, compared with OIB and N-MORB sources (for example, Fitton and others, 1991; Saunders and others, 1992). Significant enrichment in LILE, HFSE and negative Nb and Ti anomalies of basalts are generally explained by derivation from either an ancient enriched lithospheric source or metasomatized mantle (for example, Stolz and others, 1990; Turner and others, 1992; Plank and Languir, 1998; Gertisser and Keller, 2003; Donnelly and others, 2004;

Niu and O'Hara, 2009). Similar geochemical signatures are typical for all the LT calc-alkaline basalts, the tholeiites among the Terrigene Fm. and to a lesser extent for the Strelitsa Fm. roof tholeiites and subvolcanic rocks and the Podgornoye Fm. tholeiites. The Nd isotope composition of the BADR basalts shows that the mantle source was depleted with a relatively young model age of 2281 Ma. In contrast, the tholeiite basalts and BBA of the Terrigene Fm. have lower εNd values and more ancient model ages of 2413 to 2488 Ma. We therefore exclude an ancient lithospheric magma source for the BADR and infer a younger metasomatized lithospheric source. This conclusion is supported by the low Th concentrations of the BADR basalts against high Th of the basalts of the Terrigene Fm. (fig. 13B), and is consistent with the interpretation of high-Th concentrations in the high-K mafic rocks derived from enriched lithospheric source (for example, Zhang and others, 2011; Zhu and others, 2012). The TiO_2 content in the BADR basalts is ≤ 1 percent, which is characteristic for island arc basalts generated by partial melting of metasomatized mantle wedge (Perfit and others, 1980). However, the Nd, high Nb/U, Nb/La, Ta/La, Hf/Sm ratio (figs. 13C and 13D), and depletion in LILE and LREE indicate the generation of BS-1 tholeiites from asthenosphere source similar in composition to N-MORB source. The Nd isotopic composition of the BS-1 and BS-2 tholeiites also confirms that the mantle source was depleted and corresponded to MORB source. Very similar Zr/Nb (fig. 12D), Zr/Ti, Ti/Yb of all LT tholeiites are evidence of the same mantle component type (Pearce, 2008). However, other geochemical features indicate some modification of the tholeiitic mantle source. Recent studies indicate that Paleoproterozoic MORB source is characterized by lower radiogenic Nd in comparison with modern MORB (for example, Zimmer and others, 1995; Zhao and Zhou, 2007). The Nb anomalies in the rest of the LT tholeiites in conjunction with their age data, suggest that they were influenced by mantle metasomatism or by melt interaction with the lithospheric mantle. As the Strelitsa Formation roof tholeiites are interbedded with rhyolites, that is their eruption was contemporaneous, we do not exclude a mixture of tholeiitic and felsic magmas. However, mass balance calculations (20% of rhyolite + 80% of basal tholeiite) explain the sharp decrease in MgO of the roof tholeiites compared to the basal tholeiites, the decreasing CaO, increase in Na_2O and some other geochemical characteristics, but it does not explain the higher TiO_2, REE enrichment. Therefore, mixing of magmas with contrasting composition is not favored. A more realistic model is contamination of tholeiitic melts by metasomatized lithospheric mantle, and contamination of calc-alkaline magmas by continental crust.

Thus, we conclude that the LT magmas were derived from or were involved with components of metasomatized lithospheric mantle. It is generally accepted that metasomatism is typical for the mantle wedge above a subduction zone. The metasomatizing components include fluids and/or melts derived from newly-formed subducting slab (for example, Hawkesworth and others, 1993, 1997; Peacock and others, 1994; Stern and Kilian, 1996; Elliott and others, 1997; Turner and others, 1997; Tatsumi, 2006). The tholeiites and BBA of the Terrigene Fm. and the BADR of the Podgornoye Fm. display arc-like geochemical signature. Positive, but lower εNd values, together with primitive mantle normalized Ta/La, Hf/Sm ratios that plot along a trajectory between those of N-MORB and basalts from a hydrated mantle source and also between N-MORB and basalts from a mantle source metasomatized by silicated fluids (fig. 13C) are all consistent with mantle metasomatism.

The depth of origin and degree of partial melting of melts are defined using the REE contents and their ratios (figs. 13E and 13F). The tholeiites of the BS-1 and BS-2 are characterized by low Sm/Yb falling along spinel lherzolite melting curve. Because crustal contamination is minimal or absent, the magma source depth is estimated to be not more than 60 km and the degree of melting between 5 and 10 percent. Crustal

contamination can increase their Sm/Yb and La/Sm ratios, indicating that the compositions of parental melts in this case is not far deviated from the melting curves of spinel-garnet lherzolite. Thus, the depth of magma source depth of the contaminated rocks was at 70 to 80 km, with approximately 10 percent partial melting for the BADR and tholeiites of the Terrigene Fm. whereas it was less than 5 percent for the BBA in the Terrigene Fm. Thus, the LT basalts derived from different source composition and depths that have undergone low degree partial melting.

Source of the felsic rocks.—The origin of felsic rocks, especially rhyolite of bimodal volcanic suite, is controversial. Among the various models are: (1) Single-stage extensive fractional crystallization of mantle-derived basaltic melts or partial melting of contemporaneous mafic source; multiple-stage processes involving fractional crystallization and magma mixing occasionally accompanied with crustal contamination (Grove and Donnelly-Nolan, 1986; McCulloch and others, 1994; Pin and Paquette, 1997; Shinjo and Kato, 2000; Ayalew and Yirgu, 2003; Peccerillo and others, 2003; Bonin, 2004, among others), with basalts and rhyolites in most cases showing similar isotopic and geochemical features. (2) Melting of continental crust as a result of underplating of mantle magmas (Atherton and Petford, 1993; Guffanti and others, 1996; Sage and others, 1996; Tura and others, 1998; Pamić and others, 2000; Wareham and others, 2001; Brewer and others, 2004; Lacasse and others, 2007; Zhu and others, 2012, among others), with basalts and rhyolites predominantly display contrasting isotopic and geochemical features. Rhyolites from distinct tectonic settings may form through partial melting of young mafic crust or ancient intermediate crust. (3) An apart group is felsic parental melts of mantle origin (for example, Barbarin, 1999; Takagi and others, 1999). For example, coexisting mafic and felsic magmas may form independently of each other from the same mantle source (Bonin, 2004). In addition, there is a version that adakite felsic rocks are formed by mantle wedge melting (Macpherson and others, 2006).

Mafic rocks and felsic dikes of the Terrigene Fm. are unlikely to be related by fractional crystallization. Major element oxides do not show the expected trends in variation diagrams; also rocks of intermediate composition such as rhyodacites and dacite are absent. However, bimodal volcanic series is often attributed to an extreme differentiation of basaltic melts (for example, Turner and others, 1992; Streck and Gunder, 2008). The felsic dikes have highly incompatible trace element ratios which are comparable to those of the basalts. For example, the rhyolite and Fe-rhyolite are characterized by Nb/Ta around 12 and 16, Zr/Hf = 40–42 and 35–40, Nb/Th = around 1.2 and 4, and Ta/U = around 0.3 and 0.9, respectively; whereas the calc-alkaline mafic rocks and tholeiites have Nb/Ta = 11–21, Zr/Hf = 34–45, Nb/Th = 1.6–3.8 and Ta/U = 0.3–2.3. Fe-rhyolites ($^{143}Nd/^{144}Nd$ = 0.512068, $\varepsilon Nd(t)$ = +2.6, model age 2479 Ma) are similar to tholeiites ($^{143}Nd/^{144}Nd$ = 0.512136, $\varepsilon Nd(t)$ = +2.7, model age 2488 Ma) based on the Sm-Nd systematics, and both the rhyolites and mafic rocks have subparallel REE spectra (fig. 9). These characteristics suggest that the rhyolites could be generated by fractional crystallization or melting of basaltic magmas (for example, Shinjo and Kato, 2000; Peccerillo and others, 2003; Tian and others, 2010). Nevertheless, distinct isotopic compositions of the calc-alkaline mafic and low-Fe felsic rocks with $^{143}Nd/^{144}Nd$ = 0.511209, $\varepsilon Nd(t)$ = −0.5, model age 2550 Ma preclude their genetic link through simple fractional crystallization. However, the geochemical signature of the rhyolites indicates a significant contribution of ancient continental crust in their petrogenesis (crustal anatexis and mixing with mantle magma or crustal contamination of highly differentiated mafic magmas). Their Sm-Nd characteristics, similarity of tholeiitic and Fe-rhyolite, plus low MgO and CaO, strongly negative Eu anomalies, low Ba and Sr, and high Zr, Nb and Y are features of A-type granites (Frost and others, 2001), which are products of (Frost

and Frost, 2011): (1) partial melting of crustal rocks; (2) differentiation of tholeiitic magma; (3) differentiation of basaltic magmas assimilate crustal rocks. The Fe-rhyolites and tholeiites of the Terrigene Fm. are geochemically similar and therefore the former could have formed by differentiation or melting of the tholeiites. Low content of Sr, high Zr (>400 ppm) and slightly peraluminous nature of the Fe-rhyolites are evidence of continental crust contamination (Frost and Frost, 2011). Involvement of tholeiitic magma in genesis of the Fe-rhyolite is also confirmed by the high temperatures (Frost and others, 2016) as calculated by the equations of Watson and Harrison (1983). For comparison the BS-1, BS-2, and BADR rhyolites yield temperature 759±9 °C, 734±13 °C, and 764±30 °C, respectively, while the Fe-rhyolites yield temperature up to 907 °C. High abundances of Nb and REE are also characteristic of hot Si-rich magmas (Frost and others, 2016) associated with the differentiation or melting of tholeiitic basalts (Frost and Frost, 2011).

The BS-1 and BS-2 rhyolites have positive values εNd (from +1.8 to +2.9) like their associated basalts, but differ from the basalts by Nd and Sm isotopic ratio, REE and other elements distribution (fig. 9). On the one hand, their geochemical data do not favor the interpretation that the basalt and rhyolite are genetically related by extreme fractional crystallization. The adakitic geochemical signatures together with high concentrations of $Cr_{average}$ (55 and 24 ppm) and $Ni_{average}$ (35 and 56 ppm), dominantly high-Mg (Mg # up to 0.54 and up to 0.46) of the BS-1 and BS-2 rhyolites, and radiogenic composition of Nd contradicts the probability of crustal anatexis associated with mantle magma underplating. Some of the geochemical characteristics of the BS-1 and BS-2 rhyolites are comparable with the data for high-Al TTG (tonalite–granodiorite–trondhjemite) and adakites. The TTG and adakites are contrastingly different from island arc andesite, dacite and rhyolite (Drummond and Defant, 1990; Martin and others, 2005) in their high contents of Al_2O_3, Na_2O/K_2O, strongly fractionated REE patterns with low HREE contents and lack of significant Eu anomalies, high Sr and low Y, and thus a high Sr/Y ratio (fig. 14). The BS-1 and BS-2 rhyolites compare with these features of adakites (at the same time the BS-2 rhyolites has reduced Sr and are not really adakite, but adakite-like rocks) whereas the other LT volcanic rocks are characterized by low Sr/Y and high Y concentrations. Unusual geochemical characteristics of high-SiO_2 adakites and TTG are correlated with deep melting of subducted slab (see synthesis, Martin and others, 2005; Moyen, 2009). Thus, the higher the Al_2O_3, Na_2O, Sr, Sr/Y, the deeper is the adakite source. If we follow this logic, then basalt source of the BS-1 subvolcanic rhyolite coincides with high pressures (more than 20 kbar), suggesting garnet in the restite, which is also confirmed by the high ratio of $(Gd/Yb)_N = 3.9$. Alternatively, the BS-2 rhyolite melts were generated at relatively low pressures (about 10 kbar), with a minimum content of restite garnet or amphibole control, as evidenced by the reduced Sr/Y ratio (fig. 14B) and $(Gd/Yb)_N = 2.1$, at high $(La/Yb)_N$ (fig. 14A). Inversion of the high-pressure rhyolites by low-pressure ones is also confirmed by the REE distribution in zircon (fig. 7), which show flat spectra in the case where zircon crystallized in the presence of garnet and, conversely, steep pattern for garnet-free paragenesis (Hoskin and Schaltegger, 2003; Rubatto and Hermann, 2003). Relationship of U/Yb and Y in zircon help to diagnose the tectonic setting of their formation (Grimes and others, 2007), and the coincidence of inherited zircons from the BS-1 rhyolite (DH 7782) with the compositions of oceanic zircons indirectly confirm our inference of melting of oceanic crust (fig. 15). From this brief overview, the felsic melts of the LT bimodal suites are inferred to have formed at greater depths than the associated basalts. The felsic melts with adakitic characteristics can be related to potential metasomatic processes and the conversion of the overlying mantle and, accordingly, on the geochemical features of the contemporaneous basaltic parental magmas and their derivates. A similar scenario has been

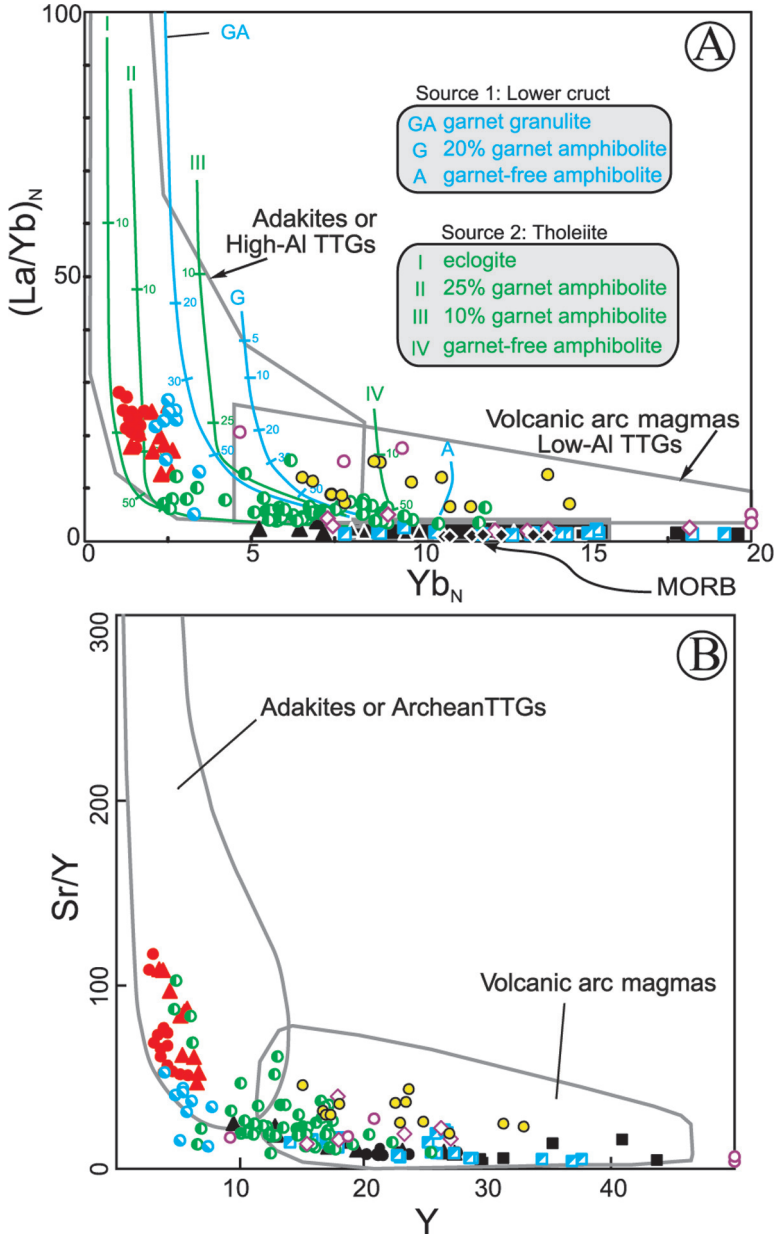

Fig. 14. (A) Plot of $(La/Yb)_N$ vs Yb_N normalized to chondritic values (Sun and McDonough,1989) considering a tholeiite crust the source of the parental magmas of the LT rhyolites. Archean TTG (trondhjemite–tonalite–granodiorite) and Volcanic arc magmas fields are from Drummond and Defant (1990). Partial melting (PM) curves were calculated using the batch melting equation of Shaw (1970) and the partition coefficients compiled by Martin (1987), Rollinson (1993) and Nielsen (2006). (B) Plot of Sr/Y vs Y for the same datasets and model curves. The adakite, Archean TTG and Volcanic arc magma fields are from Defant and others (1991). Labelled tick marks indicate degrees of partial melting percent.

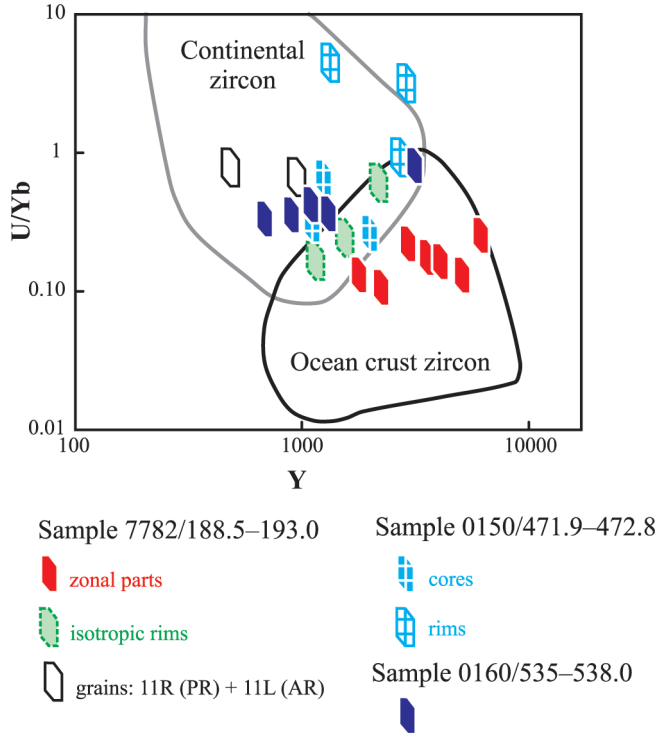

Fig. 15. U/Yb versus Y plots showing the trace element signatures of zircons from the Losevo terrain rhyolites. Fields of the continental and ocean crust zircons are from Grimes and others (2007).

proposed to explain the petrogenesis of adakitic magmas and Nb-rich basalts of Pliocene-Pleistocene age in the Philippines, Japan and Kamchatka (Kepezhinskas and others, 1996; Sajona and others, 1996; Ayabe and others, 2012). The role of felsic fluids in the metasomatism of the upper mantle and in the change of mafic rock compositions of the roof components of the Strelitsa and Podgornoye Fms. is also justified by the high ratio $(Hf/Sm)_{PM}$ (fig. 13C) and increase of island geochemical signatures in the basalts over time.

With regard to the andesites and dacites of the Podgornoye BADR, with only subordinate dacites compared, their high $Cr_{average}$ (63 ppm) and $Ni_{average}$ (26 ppm), dominantly elevated Mg ($Mg\#_{average}$ = 0.34), and moderate to low potassium contents argue against the possibility of their generation by melting of continental crust of felsic and intermediate composition. Instead, the presence of basalt to dacite suites (rarely rhyolite tuffs) with the prevalence of basaltic andesites, negative correlation of silica content with most incompatible elements such as Cr and Ni, and subparallel REE patterns (fig. 9G) indicate that the andesites and dacites were formed by fractional crystallization of basaltic magmas and form a classic BADR rock series. As we noted above, the Podgornoye Fm. BADR have undergone crustal contamination, as evidenced by strongly varying Mg # of the volcanic rocks in various paleoflows and tuffs. The intermediate volcanic rocks show Mg# = 0.57 (up to 0.77) typical of high-Mg andesites (Kelemen, 1995; Stern and Kilian, 1996; Shimoda and others, 1998; Tatsumi, 2006; Wood and Turner, 2009). The high magnesium content of the BADR rocks suggests that the parental melts were in equilibrium with upper mantle lithologies, and their island arc geochemical signatures indicate generation from the mantle wedge

(for example, Kelemen, 1995). Evidence of contamination of BADR series is similar to those established in other regions (Gill, 1981; Graham and Cole, 1991; Tiepolo and others, 2011). Weak LILE and REE enrichment in the BADR, and the characteristic decrease in REE from basalt to dacite were likely caused by contamination of juvenile mafic crust depleted in these elements.

Tectonic Implications

The tectonic settings of the bimodal volcanic suites were diverse and ranged from intraplate (oceanic and continental) through post-collisional to divergent, to subduction-related environments (table 5 and Pin and Paquette, 1997; Wang and others, 2000; Ayalew and Ishiwatari, 2011). From table 5, it is evident that the bimodal volcanic rocks are mostly associated with lithospheric extension. Exceptions include island arcs, where oceanic plate subducts beneath continent. However, bimodal volcanic rocks (following the classification of Draut and Clift, 2012; Ingersoll, 2012) occurring in intra-arc basins are associated with local extension.

According to the major features listed in table 5, the LT formations are characterized by the predominance of mafic rocks, tholeiitic chemistry, and the mafic and felsic rocks have low and/or moderate potassic and other geochemical features. These features exclude within-plate and transitional tectonic environments, as well as active continental margins (magmatic arcs). The model of a Cordillera-type active margin (Shchipansky and others, 2007) cannot explain many of the geochemical characteristics of the LT volcanics and the evolution of the belt. First, voluminous felsic and subordinate mafic rocks are typical of a bimodal association of this type of margin, as distinct from the BS-1 and BS-2. Other differences between active margins without opening back-arc basins are calc-alkaline chemistry, moderate- and high-K, enriched LILE *et cetera* (see table 5). Secondly, Shchipansky and others suggested a Cordillera-type tectonic setting that relied on the belief that Vorontsovka sediments were the products of the destruction of the Losevo belt and therefore represent an accretionary prism on the Sarmatia margin. However, recent data (Savko and others, 2011; Terentiev and Santosh, 2016) prove that this is not the case as the Vorontsovka sediments are related to the Volgo-Uralia margin and lack any connection with the LT protolith. Thirdly, a Cordilleran active margin has a specific association of adakites and Nb-enriched tholeiites (Aguillon-Robles and others, 2001) and, on the contrary, lack typical island-BADR. These strongly expected associations contradict our data on the geochemistry of LT volcanics. Finally, a forearc basin in a Cordilleran system has relatively shallow marine sediments. However, the Strelitsa Fm. have meta-sediments and tholeiites with signs of deep-water (see below), which is more typical for a back-arc basin. Moreover, the geochemical signature of the LT volcanics contradict generation of these melts on an active continental margin. The majority of LT mafic rocks show (fig. 9) LILE enrichment, HFSE depletion, and the LT calc-alkaline basalts and andesites are characterized by HREE depletion, all of which suggest their generation in a subduction zone (Wilson, 1989; Arculus, 1994; Condie, 1997; Stern, 2002). On the Y–La–Nb diagram after Cabanis and Lecolle (1989) the LT tholeiites plot in the field of back-arc basin and arc tholeiites, whereas the LT calc-alkaline basalts straddle the arc calc-alkaline basalt and the continental basalt fields (fig. 16A). On the other binary and ternary plots (figs. 16B and 16C) the LT tholeiites demonstrate similarity to the MORB and arc tholeiitic compositions. From these features, two tectonic settings can be inferred - a back-arc basin and an island arc. The Cr, Ti, V, FeO^*/TiO_2 (figs. 16D, 16E and 16F) of the BS-1 tholeiites are consistent with back-arc basin basalts (BABB), whereas those of the BS-2 tholeiites are similar with the compositions of island arc tholeiites (IAT). The contaminated tholeiites of the Terrigene Fm. show considerable variation in composition and carry the features of both and BABB, and IAT. In the Th/Yb–T/Yb diagram after Pearce (1982) (fig. 16G) it can be clearly seen that the

TABLE 5

Salient aspects of the tectonic settings of bimodal volcanic associations

	Tectonic settings	Mafic / felsic ratio	Geochemistry of mafic rocks	Geochemistry of felsic rocks	References
Within-plate environments	Continental rifts	locally abundant felsic and minor or dominant mafic rocks	alkali- to transitional tholeiitic affinities: high-K, enriched LREE, fractionated HREE, positive Nb-anomaly, obvious enrichment in LILE and HFSE; variable εNd	calc-alkaline to (per-)alkaline (trachytes and rhyolites): high-K, slight to strong LREE-enriched, negative Eu anomalies, enriched in LILE, depleted in Nb, Ta, and Ti; variable negative εNd	Bonnichsen and Kauffman, 1987; Martin and Piwinski 1972; Pin and Marini, 1993; Pin and Paquette, 1997; Seyler 1986; Turner and others, 1992; Vervoort and others, 2007
	Large Igneous Provinces	varies greatly from one province to another LIP	continental flood basalt OIB-like affinities: high or/and low Ti, LREE- and Th enriched, no Eu anomalies, enrichment in LILE, slight or no Nb, Ta and Ti anomalies; around 0 or negative εNd, variable Sr_i	calc-alkaline dacites to rhyolites (two coeval groups high-K): (1) high-Ti, P, Zr, Nb, Ta, Hf, enriched LREE, no Eu anomalies, enrichment in LILE, slight Nb, Ta anomalies; (2) low-Ti, P, Zr, Nb, Ta, Hf, slightly enriched LREE, negative Eu anomalies, enrichment in LILE, negative Nb, Ta anomalies; negative εNd and variable Sr_i	Ayalew and Yirgu, 2003; Duncan and others, 1984; Garland and others, 1995; Hooper, 1997; Shellnutt and others, 2012; Tian and others, 2010
	Oceanic islands	abundant mafic and minor felsic rocks	tholeiitic OIB-like affinities:	Fe-dacite to Fe-rhyolite:	Geist and others, 1995
			similar geochemical characteristics: medium-K to high-K and an obvious enrichment in LILE and HFSE, enriched LREE; positive εNd		
Transitional	Post-collisional extension	dominant felsic rocks, subordinate basalt	relatively low-alkali tholeiites to alkaline basalts: slightly enriched LREE, no or small negative Eu anomalies, enrichment in LILE, negative Nb, Ta and Ti anomalies; variable εNd and Sr_i	calc-alkaline sometimes A-type affinity: high-K, variable LREE-enriched, strongly negative Eu anomalies, enriched in LILE, depleted in Ba, Sr, Nb, Ta, P and Ti; variable εNd and Sr_i	Bonin, 2004; Chen and others, 2011; Hu and others, 2016; Zhang and others, 2008
Plate margin environments	Island arcs	voluminous mafic and subordinate felsic rocks	island arc tholeiites: low-K, depleted or/and slight enrichment in LILE, depleted in HFSE, flat or light-depleted REE, very low Nb and Th; high εNd and low Sr_i	dacites, rhyolites: low-K to medium-K, high-Na, enrichment in LILE, depleted in HFSE, depleted or slightly enriched LREE, no or slight negative Eu-anomaly, very low Nb; moderate εNd and low Sr_i	Donnelly and Rogers 1980; Graham and others, 1995; Ikeda and Yuasa, 1989; Notsu and others 1987; Ohki and others, 1994; Wilson and others, 1995
	Active continental margins	voluminous felsic and subordinate mafic rocks	calc-alkaline basalts to andesites: medium -K to high-K, enrichment in LILE, depleted in HFSE, enreached LREE, negative Nb anomalies; low εNd and medium Sr_i	rhyolites: medium -K to high-K, enrichment in LILE, depleted in HFSE, enriched LREE, negative Eu-anomaly, negative Nb anomalies; low εNd and high Sr_i	Christiansen and McCurry, 2008; Frey and others, 1984; Zhu and others, 2012
	Backarc basins	different ratio: mainly predominance of mafic rocks*	tholeiitic BABB-like affinities, rare calc-alkaline: mainly low-K, depleted to enriched LREE, no Eu anomalies, moderate enrichment in LILE, no or slight negative Nb, Ta and Ti anomalies; high εNd and low Sr_i	rhyolite-dacite: low-K, rare medium-K to high-K, slight to strongly enriched LREE, small or no Eu anomalies, enriched LILE, Th, negative Nb, Ta, Ti anomaly; mainly moderate εNd and low to moderate Sr_i	Clift and others, 1994; Fryer and others, 1990; Hochstaedter and others, 1990; Ikeda and Yuasa, 1989; Meng and others, 2011; Pin and Paquette, 1997; Shinjo and Kato, 2000; Shuto and others, 2006; Takagi and others, 1999; Xie and others, 2011

* Ancient (Precambrian) back-arc basins have approximately equal mafic/felsic ratio (Li and others, 2013; Kerrich and others, 2008; Manikyamba and others, 2016; Morris and Witt, 1997; Tomlinson and others, 2002).

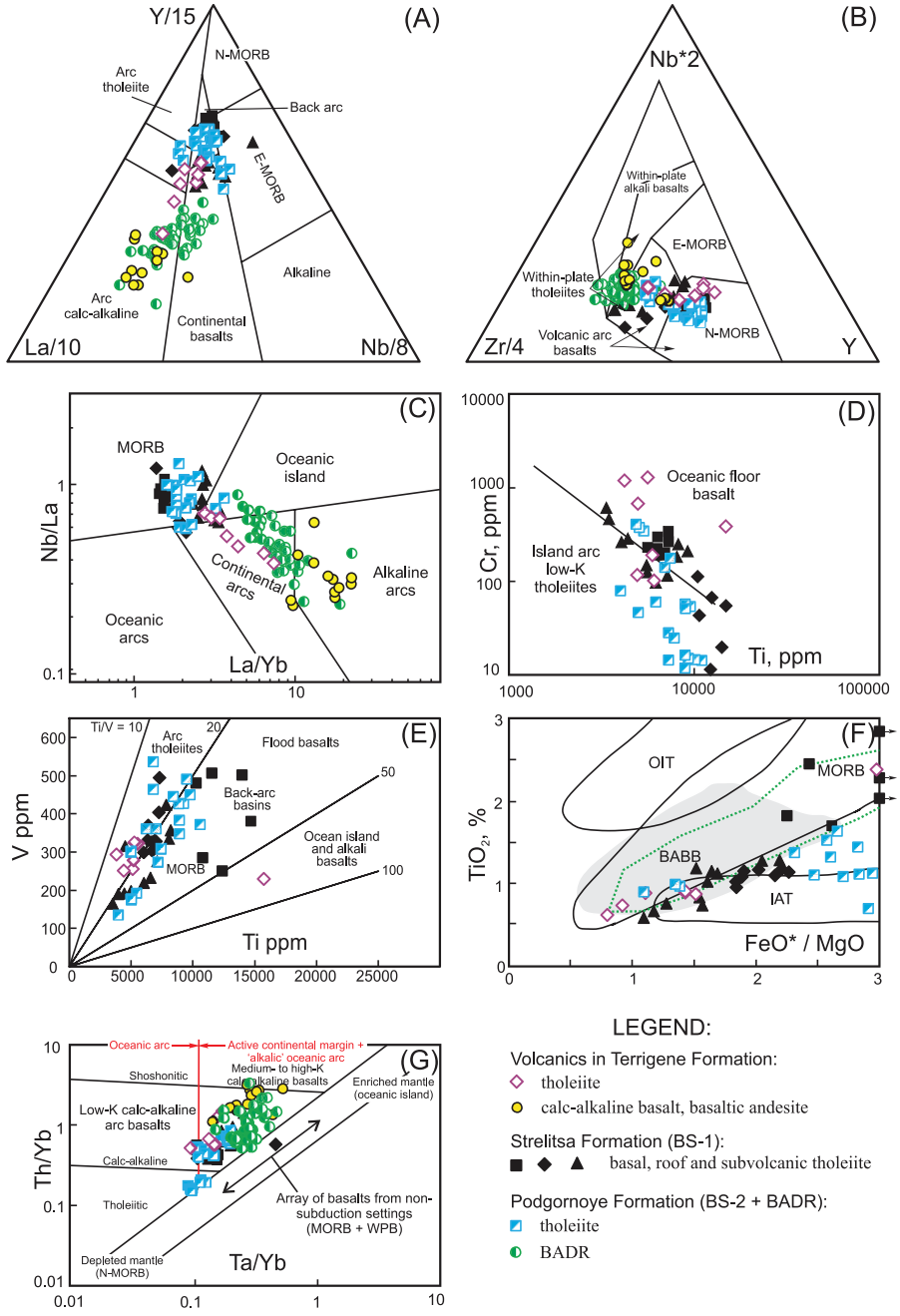

Fig. 16. Discrimination diagram for the LT mafic rocks. (A) – (Cabanis and Lecolle, 1989); (B) – (Meschede, 1986); (C) – (Hollocher and others, 2012); (D) – (Pearce, 1975); (E) – (Shervias, 1982); (F) – (Shuto and others, 2006); (G) – (Pearce, 1982).

compositions of the studied mafic rocks do not coincide with the trend of basalts from non-subduction environments. This confirms once again an arc–back-arc system for the LT volcanics. Moreover the decrease in Th/Yb and Ta/Yb ratios from older to

younger basalt suites suggest mantle source depletion with time, as well as the maturation of arc–back-arc system (shift from immature continental type to mature intra-ocean type, Saunders and Tarney, 1984). The shift in the geochemical characteristics of the basalts occurs both in time and in space. For example, geochemical indicators of incipient back-arc rifting are highly variable along the axis of modern back-arc basins (for example, Hawkins, 1995; Pearce and Stern, 2006). The basalts of early stage that formed on continental crust through back-arc spreading generally exhibit island-signatures, whereas the later stage basalts show similarities with MORB (for example, Hickey-Vargas and others, 1995; Gribble and others, 1998; Pearce and Stern, 2006).

The BBA of the Terrigene Fm. are enriched in LILE (K, Ba, Rb) and LREE, possess Nb anomaly, high ratios $(La/Yb)_N > 6$, $Th/Yb > 1$, low Nb/Ta, Nb/U, $(Ta/La)_{PM}$ and $(Hf/Sm)_{PM}$, high contents of Th > 2 ppm, and relatively low $^{143}Nd/^{144}Nd$ isotopic ratio. These features may have resulted from contamination of continental crust, and also through the interaction of enriched fluids released by subducted slab and lithospheric mantle. The eruption of calc-alkaline mafic magmas is well correlated with an island-arc paleotectonic setting (fig. 17A). A nascent island arc that developed adjacent to the continental crust at about 2170 to 2150 Ma is proposed. The tholeiites associated with meta-graywackes are enriched in LILE (K, Ba, Rb and Sr) and LREE, possess Nb anomaly, with $(La/Yb)_N \geq 2$, $Th/Yb > 0.5$, low $(Ta/La)_{PM}$ and $(Hf/Sm)_{PM}$, and relatively low $^{143}Nd/^{144}Nd$ isotopic ratio that are also consistent with the island arc environment. The geochemical characteristics indicating transition between BABB and IAT, as well as the spatial relationships with felsic dikes of A-type indicate an extensional setting, probably in the intra-arc basin, which could later have evolved into a back-arc basin.

In the subsequent stage dated as *ca.* 2140 Ma (fig. 17B), the initial eruption of tholeiites occurred, represented by BS-1 rocks that are depleted in comparison with other LT basalts. They also show other characteristics such as weak depletion in LILE (K, Ba, Rb) and LREE, the absence of a Nb anomaly, low $(La/Yb)_N \sim 1$, $Th/Yb \sim 0.5$, moderate Nb/Ta, and Nb/U, high $(Ta/La)_{PM}$ and $(Hf/Sm)_{PM}$, and low Th of < 2 ppm. These features along with the discrimination diagrams (fig. 16) indicate tholeiite parental melts with MORB sources, and suggest the ascent of asthenosphere mantle initiated the back-arc extension. Eruption of the Strelitsa Fm. roof tholeiites, rhyolite and subvolcanic analogues are related to this time interval. The assumption of mantle metasomatism caused by high-pressure adakite melts are also in good agreement with the roof tholeiites and their subvolcanic analogues showing enrichment in LILE and LREE ($(La/Yb)_N$ up to 3.8) and the appearance of Nb anomaly. The asthenosphere source is confirmed from the high contents of Ti, low $Th/Yb \sim 0.5$, high Nb/Ta, Nb/U, $(Ta/La)_{PM}$ and $(Hf/Sm)_{PM}$, in the BS-1 basalts. Features of the greenschist metamorphosed tholeiites of BS-1 such as the small amount of pyroclastic rocks at the base and the lack of relict amygdaloidal textures (primary porosity) (Terentiev, 2014) confirm the subaqueous eruption in the early stages of back-arc paleobasin development below the pressure compensation level (PCL). The PCL (Fisher, 1984) for basic magmas is at least 500 m (McBirney, 1963), and for silicic magmas, it may exceed 1000 m (Moore, 1970; Fisher and Schminckle, 1984).

Conversely, the amygdaloidal textures and extensive development of metamorphosed pyroclastics (Terentiev, 2014) among volcanic rocks of the next stage (2140–2120 Ma, fig. 17C), indicate the subaerial-to-subaqueous type of eruption, which occurred in an island arc setting. Typical IAT associations (Podgornoye Fm.) are represented with characteristic variations of depletion to enrichment in LILE and LREE, weak Nb anomaly, reduced $(La/Yb)_N \sim 1.4$, very low Th/Yb down to 0.15, high Nb/Ta, Nb/U, $(Ta\ La)_{PM}$ and $(Hf/Sm)_{PM}$ and low content of Th < 2 ppm. The

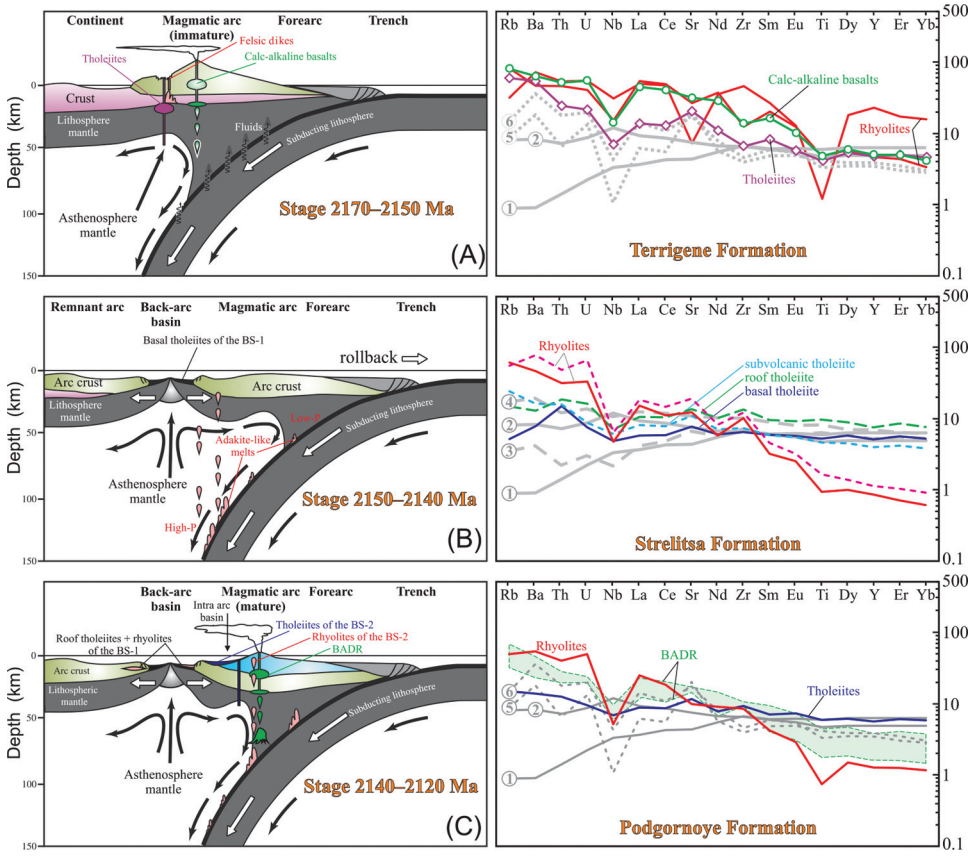

Fig. 17. Cartoon model for the evolution of the Losevo terrain during *ca.* 2170–2120 Ma. Sketch of schematic section through subduction zone is from Stern (2002). The right panel shows primitive mantle normalized trace element distributions for the average volcanic rock types of the Losevo terrain. Primitive mantle-normalize values are from Sun and McDonough (1989). Numbers in circles: 1 and 2 – normal and enriched midocean ridge basalts (N-MORB, E-MORB); 3 and 4 – data for depleted and enriched back-arc basin basalts (Pearce and Stern, 2006) are from Fretzdorff and others (2002), Leat and others (2000), Pearce and others (1995), Peate and others (1997); 5 and 6 – Arc Tholeiite and Back Arc Basin Basalt are from Stern (2002).

eruption of relatively low pressure adakite-like magmas (BS-2 rhyolite), is marked by the BADR-series with attributes of juvenile crust contamination and island-signature, suggesting that the melts of the Podgornoye Fm. volcanic rocks formed from metasomatized mantle wedge with crust characterized by oceanic lithosphere plus a layer of juvenile andesite in the island-arc setting.

Implications for the Reconstruction of the Columbia Supercontinent

Interpretation of the LT as a Western Pacific type margin of the Precambrian microcontinent provides important constraints for the reconstruction of the Paleoproterozoic Columbia supercontinent (Rogers and Santosh, 2002; Zhao and others, 2002; Meert, 2014; Nance and others, 2014). Firstly, this conclusion contradicts the speculation (Chernyshov and others, 1997; Mints and others, 2015) that the Losevo terrain is a record of intra- or marginal continental rift. In contrast, the evolution of the LT volcanic eruptions in basins formed on continental crust to mature intraoceanic basins

indicates that the interval 2170 to 2120 Ma is not a period of destruction of an integrated continent that existed before Columbia, and marks the starting of amalgamation period of the Paleoproterozoic supercontinent. It is believed that collision between the two crustal segments of Sarmatia and Volgo–Uralia occurred around 2100 Ma ago (Bibikova and others, 2009; Bogdanova and others, 2016). This conclusion is consistent with our data on the early orogenic stage before 2120 Ma, with the upper age limit of sedimentation in the adjacent Vorontsovka terrain constrained as ~ 2100 Ma (Terentiev and Santosh, 2016). The ages of post-collisional granitoids in the Losevo and Vorontsovka terrains are also not older than ~ 2085 Ma (Savko and others, 2014; Terentiev and others, 2016).

Secondly, the initiation of volcano-sedimentary basins during the later stages of the LT evolution on oceanic lithosphere, as well as the interpretation of the adjacent Vorontsovka terrain as an accretionary prism on the Volgo-Uralia microcontinent margin (Savko and others, 2011; Terentiev and Santosh, 2016) suggest the presence of an oceanic realm between the Volgo-Uralia and Sarmatia at the pre-collision time of 2170 to 2120 Ma, and possibly even earlier of > 2200 Ma.

In conclusion, we note that Sarmatia and Volga-Uralia collided at about 2100 Ma to form the ESO, which is about the same time that the Amazonia, San Francisco Cratons, West African and Congo Cratons collided along the Transamazonian and Eburnean Orogens, respectively (for example, Swapp and Onstott, 1989; Bertrand and Jardim de Sá, 1990; Feybesse and Milesi, 1994; Zhao and others, 2004), and the Yilgarn and Pilbara Cratons collided along the Capricorn Orogen (for example, Myers, 1990; Pirajno and others, 1998; Cawood and Tyler, 2004; Zhao and others, 2004). These microcontinents were at the periphery of the supercontinent configuration (Rogers and Santosh, 2002; Zhao and others, 2002; Zhao and others, 2004), and all other cratons collided later at *ca.* 1900 Ma and are located at the core of the supercontinent (see Zhao and others, 2004) in a centripetal style.

CONCLUSION

1. SIMS (SHRIMP) zircon analyses, combined with cathodeluminescence (CL) images and zircon geochemistry, have enabled the identification of xenocrystic and magmatic zircons that provide important age constrains on the Losevo terrain (LT) volcanic rocks. Our data indicate that the stratigraphic subdivision of the lower (Terrigene Fm.), middle (Strelitsa Fm.) and upper (Podgornoye Fm.) sequences of the LT (Terentiev, 2013, 2014) is viable and that most of the LT rocks formed at 2170 to 2120 Ma.

2. The basalts from the Terrigene Fm. have slightly positive $\varepsilon Nd(t)$ values (+2.6) and exhibit tholeiitic and calc-alkaline affinity, significant enrichment in LILE and LREE and strong depletion in HFSE, similar to arc-like volcanics. These geochemical and isotopic signatures suggest that the basalts were derived from a slightly depleted lithospheric mantle and asthenosphere sources metasomatized by fluids released from a newly subducted slab with a low degree of mantle melting and crustal contamination. The felsic dikes show A-type affinity, with typical enrichment in Zr, Nb, Y, and depletion in Sr and Ti, and fractionated REE patterns with very strong negative Eu anomalies. Combined with their variable εNd (t) values (-0.5–+2.6), a significant contribution of the continental crust source is inferred.

3. The volcanic rocks of the Strelitsa Fm. are bimodal in nature in which the basalts can be divided into two groups based on their εNd values and geochemistry. One group at the base of the Formation shows higher εNd values (+3.6) and slight depletion in REE and multi-element patterns that are similar to those of the transitional MORB in contrast to the units at the roof of the Formation showing slightly lower εNd values (+3.0), and slight enrichment of LILE and depletion of Nb. Both basalt types are most likely derived from partial melting of a depleted asthenospheric

mantle that was metasomatized by melts. The felsic volcanic rocks are characterized by high LREE/HREE (for example, $[La/Yb]_N$ of 13.1–28.0), high Sr/Y (46–116), lack of Eu anomaly, strong depletion in Nb and Ti, and moderate εNd values (+1.8 – +2.9) resembling slab derived high-pressure adakites.

4. The volcanic rocks of the Podgornoye Fm. are bimodal and unimodal (BADR) in nature. The bimodal suite consists of tholeiites with positive εNd values (+3.7) and exhibit no enrichment in LILE and LREE and slight depletion in HFSE. The bimodal suite felsic volcanic rocks are characterized by high LREE/HREE (for example, $[La/Yb]_N$ of 13.0–26.5), moderate Sr/Y (15–52) with no Eu anomaly, strong depletion in Nb and Ti, and moderate εNd values (+2.1 – +2.6) resembling slab-derived relatively low-pressure adakite-like melts. The BADR basalts have positive εNd values (+3.6) and exhibit significant enrichment in LILE and LREE and strong depletion in HFSE, similar to arc-like volcanics. The tholeiites are most likely derived from partial melting of depleted mantle that was metasomatized by fluids, but the BADR basalts are most likely derived from partial melting of a mantle wedge that was metasomatized by melts. Crustal contamination in the genesis of LT calc-alkaline volcanic rocks was confirmed as well.

5. Geochronological and geochemical data indicate that the LT volcanic rocks were formed during the early (Terrigene Fm.) stage of intra-continental arc with a continental basement whereas the Strelitsa bimodal volcanic rocks were formed during the middle stage of back-arc extension. The Podgornoye bimodal volcanic rocks plus BADR were formed during a later stage of intra-oceanic arc. The identification of a 2170 to 2120 Ma back-arc basin in the East Sarmatian Orogen together with broadly coeval arcs indicate that the eastern margin of Sarmatia was an active margin within an arc–back-arc environment.

6. Relying on the model isotopic age of whole-rock sampling, we conclude that the earliest volcanism stage has experienced some contribution of the ancient lithospheric mantle source and continental crust. The subsequent volcanic activity is associated with mantle metasomatism during the early Paleoproterozoic. And the slab melting during the arc–back-arc system development has given growth to a young mafic crust of the orogen.

7. The major mechanisms for the formation of felsic rocks in bimodal suites include (1) partial melting of crust via mafic magma underplating and (2) fractional crystallization of mantle basalts. However our new data, together with those reported in recent studies lead to the inference that the initial melts in bimodal suites were adakitic felsic magmas derived by slab melting, followed by mantle metasomatism and generation of basaltic magmas with island arc signature.

8. Similar-aged volcanic belts have also been found in the Transamazonian and Eburnean Orogens (the Amazonia, San Francisco Cratons, West African and Congo Cratons), the Capricorn Orogen (the Yilgarn and Pilbara Cratons), which are considered to represent the initial (2.1–2.0 Ga), subduction-related growth at the periphery of the Paleoproterozoic Columbia supercontinent.

ACKNOWLEDGMENTS

We thank Dr. Peter Cawood, Associate Editor, American Journal of Science, referees Svetlana Bogdanova and Hugh Smithies for their critical and generous comments on this paper. We are grateful to A. N. Larionov, S. G. Simakin, and Y. V. Potapov are appreciated for their help with the SIMS (SHRIMP) zircon, REE and other elements in zircons analyses. We thank mineralogists of Institute of Geology of Ore Deposits, Petrography, Mineralogy, and Geochemistry (IGEM), Russian Academy of Sciences for separation of zircon monofractions. This research was supported by the program of strategic development of the Voronezh State University. M. Santosh is

supported by Foreign Expert funding from China University of Geosciences Beijing, China and Professorial position at the Univerity of Adelaide, Australia.

REFERENCES

Aguillón-Robles, A., Calmus, Ò., Benoit, M., Bellon, H., Maury, R. C., Cotton, J., Bourgois, J., and Michaud F., 2001, Late Miocene adakites and Nb-enriched basalts from Vizcaino Peninsula, Mexico: Indicators of East Pacific Rise subduction below southern Baja California?: Geology, v. 29, n. 6, p. 531–534, https://doi.org/10.1130/0091-7613(2001)029<0531:LMAANE>2.0.CO;2

Aldanmaz, E., Pearce, J. A., Thirlwall, M. F., and Mitchell, J. G., 2000, Petrogenetic evolution of late Cenozoic, post-collision volcanism in western Anatolia, Turkey: Journal of Volcanology and Geothermal Research, v. 102, n. 1–2, p. 67–95, https://doi.org/10.1016/S0377-0273(00)00182-7

Arculus, R. J., 1994, Aspects of magma genesis in arcs: Lithos, v. 33, n. 1–3, p. 189–208, https://doi.org/10.1016/0024-4937(94)90060-4

Artemenko, G. V., 1995, Geochronological correlation of volcanic and granitoid magmatism in the southeastern Ukrainian Shield and the Kursk magnetic anomaly: Geochemistry and Ore Forming (Kiev), v. 21, p. 129–154 (in Russian).

Atherton, M. P., and Petford, N., 1993, Generation of sodium-rich magmas from newly underplated basaltic crust: Nature, v. 362, p. 144–146, https://doi.org/10.1038/362144a0

Ayabe, M., Takanashi, K., Shuto, K., Ishimoto, H., and Kawabata, H., 2012, Petrology and geochemistry of adakitic dacites and high-MgO andesites, and related calc-alkaline dacites from the Miocene Okoppe Volcanic Field, N Hokkaido, Japan: Journal of Petrology, v. 53, n. 3, p. 547–588, https://doi.org/10.1093/petrology/egr071

Ayalew, D., and Ishiwatari, A., 2011, Comparison of rhyolites from continental rift, continental arc and oceanic island arc: Implication for the mechanism of silicic magma generation: Island Arc, v. 20, n. 1, p. 78–93, https://doi.org/10.1111/j.1440-1738.2010.00746.x

Ayalew, D., and Yirgu, G., 2003, Crustal contribution to the genesis of Ethiopian plateau rhyolitic ignimbrites: Basalt and rhyolite geochemical provinciality: Journal of the Geological Society, London, v. 160, p. 47–56, https://doi.org/10.1144/0016-764901-169

Barbarin, B., 1999, A review of the relationships between granitoid types, their origins and their geodynamic environments: Lithos, v. 46, n. 3, p. 605–626, https://doi.org/10.1016/S0024-4937(98)00085-1

Bertrand, J. M., and Jardim de Sá, E. F., 1990, Where are the Eburnean–Transamazonian collisional belts?: Canadian Journal of Earth Sciences, v. 27, n. 10, p. 1382–1393, https://doi.org/10.1139/e90-148

Bibikova, E. V., Bogdanova, S. V., Postnikov, A. V., Popova, L. P., Kirnozova, T. I., Fugzan, M. M., and Glushchenko, V. V., 2009, Sarmatia-Volgo-Uralia junction zone: isotopic-geochronologic characteristic of supracrustal rocks and granitoids: Stratigraphy and Geological Correlation, v. 17, n. 6, p. 561–573, https://doi.org/10.1134/S086959380906001X

Bienvenu, P., Bougault, H., Joron, J. L., Treuil, M., and Dmitriev, L., 1990, MORB alteration: Rare-earth element/non-rare-earth hygromagmaphile element fractionation: Chemical Geology, v. 82, p. 1–14, https://doi.org/10.1016/0009-2541(90)90070-N

Black, L. P., Kamo, S. L., Allen, C. M., Aleinikoff, J. N., Davis, D. W., Korsch, R. J., and Foudoulis, C., 2003, TEMORA 1: A New Zircon standard for Phanerozoic U-Pb Geochronology: Chemical Geology, v. 200, n. 1–2, p. 155–170, https://doi.org/10.1016/S0009-2541(03)00165-7

Bogdanova, S. V., 1993, Segments of the East European Craton, *in* Gee, D. G., and Beckholmen, M., editors, EUROPROBE in Jablonna 1991: Warszawa, Poland, Institute of Geophysics, Polish Academy of Sciences - European Science Foundation, p. 33–38.

Bogdanova, S. V., Gorbatschev, R., and Garetsky, R. G., 2016, EUROPE|East European Craton, *in* Scott, E., editor, Reference Module in Earth Systems and Environmental Sciences: Amsterdam, Elsevier, Geology of Europe, https://doi.org/10.1016/B978-0-12-409548-9.10020-X

Bonin, B., 2004, Do coeval mafic and felsic magmas in post-collisional to within-plate regimes necessarily imply two contrasting, mantle and crustal, sources? A review: Lithos, v. 78, n. 1–2, p. 1–24, https://doi.org/10.1016/j.lithos.2004.04.042

Bonnichsen, B., and Kauffman, D. F., 1987, Physical features of rhyolite lava flows in the Snake River Plain volcanic province, southwestern Idaho, *in* Fink, J. H., editor, The emplacement of silicic domes and lava flows: Geological Society of America Special Papers, v. 212, p. 119–145, https://doi.org/10.1130/SPE212-p119

Brewer, T. S., Ahäll, K.-I., Menuge, J. F., Storey, C. D., and Parrish, R. R., 2004, Mesoproterozoic bimodal volcanism in SW Norway, evidence for recurring pre-Sveconorwegian continental margin tectonism: Precambrian Research, v. 134, n. 3–4, p. 249–273, https://doi.org/10.1016/j.precamres.2004.06.003

Cabanis, B., and Lecolle, M., 1989, Le diagramme La/10-Y/15-Nb/8: un outil pour la discrimination des séries volcaniques et la mise en évidence des processus de mélange et/ou de contamination crustale: Comptes Rendus de l'Academie des Sciences, Paris, Series 2, v. 313, p. 2023–2029.

Cawood, P. A., and Tyler, I. M., 2004, Assembling and reactivating the Proterozoic Capricorn Orogen: Lithotectonic elements, orogenies, and significance: Precambrian Research, v. 128, n. 3–4, p. 201–218, https://doi.org/10.1016/j.precamres.2003.09.001

Chen, X., Shu, L., and Santosh, M., 2011, Late Paleozoic post-collisional magmatism in the Eastern Tianshan Belt, Northwest China: New insights from geochemistry, geochronology and petrology of bimodal volcanic rocks: Lithos, v. 127, n. 3–4, p. 581–598, https://doi.org/10.1016/j.lithos.2011.06.008

Chernyshov, N. M., Nenakhov, V. M., Lebedev, I. P., Strik, and Yu. N., 1997, A Model of Geodynamic History of the Voronezh Massif in the Early Precambrian: Geotektoniks, v. 31, n. 3, p. 186–194.

Clift, P. D., and ODP Leg 135 Scientific Party, 1994, Volcanism and sedimentation in a rifting island-arc terrain: An example from Tonga, SW Pacific: Geological Society, London, Special Publications, v. 81, p. 29–51, https://doi.org/10.1144/GSL.SP.1994.081.01.03

Condie, K. C., 1997, Plate Tectonics and Crustal Evolution: Amsterdam, Elsevier, Fourth edition, 283 p.

Christiansen, E. H., and McCurry, M., 2008, Contrasting origins of Cenozoic silicic volcanic rocks from the western Cordillera of the United States: Bulletin of Volcanology, v. 70, n. 3, p. 251–267, https://doi.org/10.1007/s00445-007-0138-1

Defant, M. J., Richerson, P. M., de Boer, J. Z., Stewart, R. H., Maury, R. C., Bellon, H., Drummond, M. S., Feigenson, M. D., and Jackson, T. E., 1991, Dacite genesis via both slab melting and differentiation: Petrogenesis of La Yeguada Volcanic Complex, Panama: Journal of Petrology, v. 32, n. 6, p. 1101–1142, https://doi.org/10.1093/petrology/32.6.1101

Donnelly, K. E., Goldstein, S. L., Langmuir, C. H., and Spiegelman, M., 2004, Origin of enriched ocean ridge basalts and implications for mantle dynamics: Earth and Planetary Science Letters, v. 226, n. 3–4, p. 347–366, https://doi.org/10.1016/j.epsl.2004.07.019

Donnelly, T. W., and Rogers, J. J. W., 1980, Igneous series in island arcs: The northeastern Caribbean compared with worldwide island-arc assemblages: Bulletin of Volcanology, v. 43, n. 2, p. 347–382, https://doi.org/10.1007/BF02598038

Draut, A. E., and Clift, P. D., 2012, Basins in ARC-continent collisions, *in* Busby, C., and Azor Pérez, A., editors, Tectonics of Sedimentary Basins: Recent Advances, First Edition: Chichester, United Kingdom, John Wiley & Sons, Ltd., p. 347–368, https://doi.org/10.1002/9781444347166.ch17

Drummond, M. S., and Defant, M. J., 1990, A model from trondhjemite–tonalite–dacite genesis and crustal growth via slab melting: Archaean to modern comparisons: Journal of Geophysical Research-Solid Earth, v. 95, n. B13, p. 21503–21521, https://doi.org/10.1029/JB095iB13p21503

Duncan, A. R., Erlank, A. J., and Marsh, J., 1984, Regional geochemistry of the Karoo igneous province, *in* Erlank, A. J., editor, Petrogenesis of the volcanic rocks of the Karoo Province: Special Publication Geological Society of Africa, v. 13, p. 355–388.

Elliott, T., Plank, T., Zindler, A., White, W., and Bourdon, B., 1997, Element transport from slab to volcanic front at the Mariana arc: Journal of Geophysical Research-Solid Earth, v. 102, n. B7, p. 14991–15019, https://doi.org/10.1029/97JB00788

Ewart, A., 1982, The mineralogy and petrology of Tertiary-Recent orogenic volcanic rocks: With special reference to the andesitic-basaltic compositional range, *in* Thorpe, R. S., editor, Andesites: Orogenic Andesites and Related Rocks: New York, John Wiley & Sons, p. 25–95.

Ferry, J. M., and Watson, E. B., 2007, New thermodynamic models and revised calibrations for the Ti-in-zircon and Zr-in-rutile thermometers: Contributions to Mineralogy and Petrology, v. 154, n. 4, p. 429–437, https://doi.org/10.1007/s00410-007-0201-0

Feybesse, J. L., and Milési, J. P., 1994, The Archean/Proterozoic contact zone in West Africa: A mountain belt of décollement thrusting and folding on a continental margin related to 2.1 Ga convergence of Archean cratons?: Precambrian Research, v. 69, p. 199– 227, https://doi.org/10.1016/0301-9268(94)90087-6

Fisher, R. V., 1984, Submarine volcaniclastic rocks, *in* Kokelaar, B. P., and Howells, M. F., editors, Marginal basin geology: Volcanic and associated sedimentary and tectonic processes in modern and ancient marginal basins: Geological Society, London, Special Publications, v. 16, p. 5–27, https://doi.org/10.1144/gsl.sp.1984.016.01.02

Fisher, R. V., and Schminckle, H.-U., 1984, Pyroclastic Rocks: Heidelberg, Springer, 472 p.

Fitton, J. G., James, D., and Leeman, W. P., 1991, Basic magmatism associated with Late Cenozoic extension in the western United States: Compositional variations in space and time: Journal of Geophysical Research-Solid Earth, v. 96, n. B8, p. 13693–13711, https://doi.org/10.1029/91JB00372

Fretzdorff, S., Livermore, R. A., Devey, C. W., Leat, P. T., and Stoffers, P., 2002, Petrogenesis of the back-arc East Scotia Ridge, South Atlantic Ocean: Journal of Petrology, v. 43, n. 8, p. 1435–1467, https://doi.org/10.1093/petrology/43.8.1435

Frey, F. A., Gerlach, D. C., Hickey, R. L., Lopez-Escobar, L., and Munizaga-Villavicencio, F., 1984, Petrogenesis of the Laguna el Maule volcanic complex, Chile (36° S): Contributions to Mineralogy and Petrology, v. 88, n. 1, p. 133–149, https://doi.org/10.1007/BF00371418

Frost, B. R., Barnes, C. G., Collins, W. J., Arculus, R. J., Ellis, D. J., and Frost, C. D., 2001, A geochemical classification for granitic rocks: Journal of Petrology, v. 42, n. 11, p. 2033–2048, https://doi.org/10.1093/petrology/42.11.2033

Frost, C. D., and Frost, B. R., 2011, On ferroan (A-type) granitoids: Their compositional variability and modes of origin: Journal of Petrology, v. 52, n. 1, p. 39–53, https://doi.org/10.1093/petrology/egq070

Frost, C. D., Frost, B. R., and Beard, J. S., 2016, On silica-rich granitoids and their eruptive equivalents: American Mineralogist, v. 101, n. 6, p. 1268–1284, https://doi.org/10.2138/am-2016-5307

Fryer P., Taylor B., Langmuir, C. H., and Hochstaedter, A. G., 1990, Petrology and geochemistry of lavas from the Sumisu and Torishima backarc rift: Earth and Planetary Science Letters, v. 100, n. 1–3, p. 161–178, https://doi.org/10.1016/0012-821X(90)90183-X

Garland, F., Hawkesworth, C. J., and Mantovani, M. S. M., 1995, Description and petrogenesis of the Paraná rhyolites, southern Brazil: Journal of Petrology, v. 36, n. 5, p. 1193–1227, https://doi.org/10.1093/petrology/36.5.1193

Geist, D., Howard, K. A., and Larson, P., 1995, The generation of oceanic rhyolites by crystal fractionation: The basalt-rhyolite association at Volcán Alcedo, Galápagos Archipelago: Journal of Petrology, v. 36, n. 4, p. 965–982, https://doi.org/10.1093/petrology/36.4.965

Gertisser, R., and Keller, J., 2003, Trace element and Sr, Nd, Pb and O isotope variations in medium-K and high-K volcanic rocks from Merapi volcano, central Java, Indonesia: Evidence for the involvement of subducted sediments in Sunda arc magma genesis: Journal of Petrology, v. 44, n. 3, p. 457–489, https://doi.org/10.1093/petrology/44.3.457

Gill, J. B., 1981, Orogenic Andesites and Plate Tectonics: Berlin, New York, Springer-Verlag, 390 p.
Goldstein, S. J., and Jacobsen, S. B., 1988, Nd and Sr isotopic systematics of river water suspended material: Implications for crustal evolution: Earth and Planetary Science Letters, v. 87, n. 3, p. 249–265, https://doi.org/10.1016/0012-821X(88)90013-1
Graham, I. J., and Cole, J. W., 1991, Petrogenesis of andesites and dacites of White Island volcano, Bay of Plenty, New Zealand, in the light of new geochemical and isotopic data: New Zealand Journal of Geology and Geophysics, v. 34, n. 3, p. 303–315, https://doi.org/10.1080/00288306.1991.9514468
Graham, I. J., Cole, J. W., Briggs, R. M., Gamble, J. A., and Smith, I. E. M., 1995, Petrology and petrogenesis of volcanic rocks from the Taupo Volcanic Zone: A review: Journal of Volcanology and Geothermal Research, v. 68, n. 1–3, p. 59–87, https://doi.org/10.1016/0377-0273(95)00008-I
Gribble, R. F., Stern, R. J., Newman, S., Bloomer, S. H., and O'Hearn, T., 1998, Chemical and isotopic composition of lavas from the Northern Mariana Trough: Implications for magmagenesis in back-arc-arc basins: Journal of Petrology, v. 39, n. 1, p. 125–154, https://doi.org/10.1093/petroj/39.1.125
Grimes, C. B., John, B. E., Kelemen, P. B., Mazdab, F. K., Wooden, J. L., Cheadle, M. J., Hanghoj, K., and Schwartz, J. J., 2007, Trace element chemistry of zircons from oceanic crust: A method for distinguishing detrital zircon provenance: Geology, v. 35, n. 7, p. 643–646, https://doi.org/10.1130/G23603A.1
Grove, T. L., and Donnelly-Nolan, J. M., 1986, The evolution of young silicic lavas at Medicine Lake Volcano, California: Implications for the origin of compositional gaps in calcalkaline series lavas: Contributions to Mineralogy and Petrology, v. 92, n. 3, p. 281–302, https://doi.org/10.1007/BF00572157
Guffanti, M., Clynne, M. A., and Muffler, L. J. P., 1996, Thermal and mass implications of magmatic evolution in the Lassen volcanic region, California, and minimum constraints on basalt influx to the lower crust: Journal of Geophysical Research-Solid Earth, v. 101, n. B2, p. 3001–3013, https://doi.org/10.1029/95JB03463
Hart, S. R., 1969, K, Rb, Cs contents and K/Rb, K/Cs ratios of fresh and altered submarine basalts: Earth and Planetary Science Letters, v. 6, n. 4, p. 295–303, https://doi.org/10.1016/0012-821X(69)90171-X
Hawkesworth, C. J., Gallagher, K., Hergt, J. M., and McDermott, F., 1993, Mantle and slab contributions in arc magmas: Annual Review of Earth and Planetary Sciences, v. 21, p. 175–204, https://doi.org/10.1146/annurev.ea.21.050193.001135
Hawkesworth, C. J., Turner, S. P., McDermott, F., Peate, D. W., and van Calsteren, P., 1997, U–Th isotopes in arc magmas: Implications for element transfer from the subducted crust: Science, v. 276, n. 5312, p. 551–555, https://doi.org/10.1126/science.276.5312.551
Hawkins, J. W., Jr., 1995, The geology of the Lau Basin, *in* Taylor, B., editor, Backarc Basins: Tectonics and Magmatism: New York, Plenum Press, p. 63–138, https://doi.org/10.1007/978-1-4615-1843-3_3
Hickey-Vargas, R., Hergt, J. M., and Spadea, P., 1995, The Indian Ocean-type isotopic signature in western Pacific marginal basins: Origin and signifcance, *in* Taylor, B., and Natland, J., editors, Active Margins and Marginal Basins of the Western Pacific: American Geophysical Union, Geophysical Monograph Series, v. 88, p. 175–197, https://doi.org/10.1029/GM088p0175
Hochstaedter, A. G., Gill, J. B., Kusakabe, M., Newman, S., Prinle, M., Taylor, B., and Fryer, P., 1990, Volcanism in the Sumisu Rift I: Major element, volatile and stable geochemistry: Earth and Planetary Science Letters, v. 100, n. 1–3, p. 179–194, https://doi.org/10.1016/0012-821X(90)90184-Y
Hoffman, A., 1997, Mantle geochemistry: The message from oceanic volcanism: Nature, v. 389, p. 219–229, https://doi.org/10.1038/385219a0
Holland, T., and Blundy, J., 1994, Non-ideal interactions in calcic amphiboles and their bearing on amphibole-plagioclase thermometry: Contributions to Mineralogy and Petrology, v. 116, n. 4, p. 433–447, https://doi.org/10.1007/BF00310910
Hollocher, K., Robinson, P., Walsh, E., and Roberts, D., 2012, Geochemistry of amphibolite-facies volcanics and gabbros of the Støren Nappe in extensions west and southwest of Trondheim, Western Gneiss Region, Norway: A key to correlations and paleotectonic settings: American Journal of Science, v. 312, n. 4, p. 357–416, https://doi.org/10.2475/04.2012.01
Hooper, P. R., 1997, The Columbia River flood basalt province: Current status, *in* Mahoney, J. J., and Coffin M. F., editors, Large Igneous Provinces: Continental, oceanic, and planetary flood volcanism: American Geophysical Union Monograph, Washington, v. 100, p. 1–28, https://doi.org/10.1029/GM100p0001
Hoskin, P. W. O., and Schaltegger, U., 2003, The composition of zircon and igneous and metamorphic petrogenesis: Reviews in Mineralogy and Geochemistry, v. 53, p. 27–62, https://doi.org/10.2113/0530027
Hu, Y., Niu, Y., Li, J., Ye, L., Kong, J., Chen, S., Zhang, Y., and Zhang, G., 2016, Petrogenesis and tectonic significance of the late Triassic mafic dikes and felsic volcanic rocks in the East Kunlun Orogenic Belt, Northern Tibet Plateau: Lithos, v. 245, p. 205–222, https://doi.org/10.1016/j.lithos.2015.05.004
Ikeda, Y., and Yuasa, M., 1989, Volcanism in nascent backarc basins behind the Schichito Ridge and adjacent areas in the Izu-Ogasawara arc, NW Pacific: Evidence for mixing between E-type MORB and island arc magmas at the initiation of bac-karc rifing: Contributions to Mineralogy and Petrology, v. 101, n. 4, p. 377–393, https://doi.org/10.1007/BF00372212
Ingersoll, R. V., 2012, Tectonics of sedimentary basins, with revised nomenclature, *in* Busby, C., and Azor, A., editors, Tectonics of Sedimentary Basins: Recent Advances, First Edition: Chichester, United Kingdom, John Wiley and Sons, p. 3–43, https://doi.org/10.1002/9781444347166.ch1
Irvine, T. N., and Baragar, W. R. A., 1971, A guide to the chemical classification of the common volcanic rocks: Canadian Journal of Earth Sciences, v. 8, n. 5, p. 523–548, https://doi.org/10.1139/e71-055
Karandashev, V. K., Turanov, A. N., Orlova, T. A., Lezhnev, A. E., Nosenko, S. V., Zolotareva, N. I., and Moskvitina, I. R., 2008, Use of the inductively coupled plasma mass spectrometry for element analysis of environmental objects: Inorganic Material, v. 44, n. 14, p. 1491–1500, https://doi.org/10.1134/S0020168508140045

Kelemen, P. B., 1995, Genesis of high Mg# andesites and the continental crust: Contributions to Mineralogy and Petrology, v. 120, n. 1, p. 1–19, https://doi.org/10.1007/BF00311004
Kepezhinskas, P., Defant, M. J., and Drummond, M. S., 1996, Progressive enrichment of island arc mantle by melt–periodotite interaction inferred from Kamchatcka xenoliths: Geochimica et Cosmochimica Acta, v. 60, n. 7, p. 1217–1229, https://doi.org/10.1016/0016-7037(96)00001-4
Kerrich, R., Polat, A., and Xie, Q., 2008, Geochemical systematics of 2.7 Ga Kinojevis Group (Abitibi), and Manitouwadge and Winston Lake (Wawa) Fe-rich basalt–rhyolite associations: Backarc rift oceanic crust?: Lithos, v. 101, n. 1–2, p. 1–23, https://doi.org/10.1016/j.lithos.2007.07.009
La Flèche, M. R., Camiré, G., and Jenner, G. A., 1998, Geochemistry of post-Acadian, Carboniferous continental intraplate basalts from the Maritimes Basin, Magdalen islands, Quebec, Canada: Chemical Geology, v. 148, n. 3–4, p. 115–136, https://doi.org/10.1016/S0009-2541(98)00002-3
Lacasse, C., Sigurdsson, H., Carey, S. N., Jóhannesson, H., Thomas, L. E., and Rogers, N. W., 2007, Bimodal volcanism at the Katla subglacial caldera, Iceland: Insight into the geochemistry and petrogenesis of rhyolitic magmas: Bulletin of Volcanology, v. 69, p. 373–399, https://doi.org/10.1007/s00445-006-0082-5
Larionov, A. N., Andreichev, V. A., and Gee, D. G., 2004, The Vendian alkaline igneous suite Northern Timan: zircon ages of gabbros and syenites, *in* Gee, D. G., and Pease, V., editors, The Neoproterozoic Timanide Orogen of Eastern Baltica: Geological Society, London, Memoirs, v. 30, p. 69–74, https://doi.org/1144/GSL.MEM.2004.030.01.07
Leat, P. T., Livenmore, R. A., Millar, I. L., and Pearce, J. A., 2000, Magma supply in back-arc spreading centre Segment E2, East Scotia Ridge: Journal of Petrology, v. 41, n. 6, p. 845–866, https://doi.org/10.1093/petrology/41.6.845
Li, L., Lin, S., Xing, G., Davis, D. W., Davis, W. J., Xiao, W., and Yin, C., 2013, Geochronology and geochemistry of volcanic rocks from the Shaojiwa Formation and Xingzi Group, Lushan area, SE China: Implications for Neoproterozoic back-arc basin in the Yangtze Block: Precambrian Research, v. 238, p. 1–17, https://doi.org/10.1016/j.precamres.2013.09.016
Ludwig, K. R., 2008, Isoplot/Ex ver. 3.6: Berkeley, California, Berkeley Geochronology CenterSpecial Publications, No 4, 77 p.
Ludden, J. N., and Thompson, G., 1978, Behavior of rare earth elements during submarine weathering of tholeiitic basalt: Nature, v. 274, p. 147–149, https://doi.org/10.1038/274147a0
MacLean, W. H., and Barrett, T. J., 1993, Lithogeochemical techniques using immobile elements: Journal of Geochemical Exploration, v. 48, n. 2, p. 109–133, https://doi.org/10.1016/0375-6742(93)90002-4
Macpherson, C.G., Dreher, S. T., and Thirlwall, M. F., 2006, Adakites without slab melting: High pressure differentiation of island arc magma, Mindanao, the Philippines: Earth and Planetary Science Letters, v. 243, n. 3–4, p. 581–593, https://doi.org/10.1016/j.epsl.2005.12.034
Manikyamba, C., Santosh, M., Kumar, B. C., Rambabu, S., Tang, L., Saha, A., Khelen, A. C., Ganguly, S., Singh, Th. D., and Subba Rao, D. V., 2016, Zircon U-Pb geochronology, Lu-Hf isotope systematics, and geochemistry of bimodal volcanic rocks and associated granitoids from Kotri Belt, Central India: Implications for Neoarchean-Paleoproterozoic crustal growth: Gondwana Research, v. 38, p. 313–333, https://doi.org/10.1016/j.gr.2015.12.008
Martin, H., 1987, Petrogenesis of Archean trondhjemites, tonalites and granodiorites from eastern Finland: Major and trace element geochemistry: Journal of Petrology, v. 28, n. 5, p. 921–953, https://doi.org/10.1093/petrology/28.5.921
Martin, H., Smithies, R. H., Rapp, R., Moyen, J.-F., and Champion, D., 2005, An overview of adakite, tonalite–trondhjemite–granodiorite (TTG), and sanukitoid: Relationships and some implications for crustal evolution: Lithos, v. 79, n. 1–2, p. 1–24, https://doi.org/10.1016/j.lithos.2004.04.048
Martin, R F., and Piwinskii, A. J., 1972, Magmatism and tectonic settings: Journal of Geophysical Research, v. 77, n. 26, p. 4966–4975, https://doi.org/10.1029/JB077i026p04966
McBirney, A. R., 1963, Factors governing the nature of submarine volcanism: Bulletin of Volcanology, v. 26, n. 1, p. 455–469, https://doi.org/10.1007/BF02597304
McCulloch, M. T., Kyser, T. K., Woodhead, J. D., and Kinsley, L., 1994, Pb–Sr–Nd–O isotopic constraints on the origin of rhyolites from the Taupo Volcanic Zone of New Zealand: Evidence for assimilation followed by fractionation from basalt: Contributions to Mineralogy and Petrology, v. 115, n. 3, p. 303–312, https://doi.org/10.1007/BF00310769
Meert, J. G., 2014, Strange attractors, spiritual interlopers and lonely wanderers: The search for pre-Pangean supercontinents: Geoscience Frontiers, v. 5, n. 2, p. 155–166, https://doi.org/10.1016/j.gsf.2013.12.001
Meng, E., Xu, W.-L., Pei, F.-P., Yang, D.-B., Wang, F., and Zhang, X.-Z., 2011, Permian bimodal volcanism in the Zhangguangcai Range of eastern Heilongjiang Province, NE China: Zircon U–Pb–Hf isotopes and geochemical evidence: Journal of Asian Earth Sciences, v. 41, n. 2, p. 119–132, https://doi.org/10.1016/j.jseaes.2011.01.005
Meschede, M., 1986, A method of discriminating between different types of mid-ocean ridge basalts and continental tholeiites with the Nb-Zr-Y diagram: Chemical Geology, v. 56, n. 3–4, p. 207–218, https://doi.org/10.1016/0009-2541(86)90004-5
Mints, M. V., Dokukina, K. A., Konilov, A. N., Philippova, I. B., Zlobin, V. L., Babayants, P. S., Belousova, E. A., Blokh, Y. I., Bogina, M. M., Bush, W. A., Dokukin, P. A., Kaulina, T. V., Natapov, L. M., Piip, V. B., Stupak, V. M., Suleimanov, A. K., Trusov, A. A., Van, K. V., and Zamozhniaya, N. G., 2015, East European Craton: Early Precambrian History and 3D Models of Deep Crustal Structure: Geological Society of America Special Papers, v. 510, 433 p.
Moore, J. G., 1970, Water content of basalt erupted on the ocean floor: Contributions to Mineralogy and Petrology, v. 28, n. 4, p. 272–279, https://doi.org/10.1007/BF00388949
Morris, P. A., and Witt, W. K., 1997, Geochemistry and tectonic settings of two contrasting Archaean felsic

volcanic associations in Eastern Goldfields, Western Australia: Precambrian Research, v. 83, n. 1–3, p. 83–107, https://doi.org/10.1016/S0301-9268(97)00006-5
Moyen, J.-F., 2009, High Sr/Y and La/Yb ratios: the meaning of the "adakitic signature": Lithos, v. 112, n. 3–4, p. 556–574, https://doi.org/10.1016/j.lithos.2009.04.001
Myers, J. S., 1990, Capricorn Orogen: Geological Survey of Western Australia, v. 3, p. 197–198.
Nance, R. D., Murphy, J. B., and Santosh, M., 2014, The supercontinent cycle: A retrospective essay: Gondwana Research, v. 25, n. 1, p. 4–29, https://doi.org/10.1016/j.gr.2012.12.026
Nielsen, R., 2006, Geochemical Earth Reference Model (GERM) partition coefficient (Kd) database: Available at http://www.geo.oregonstate.edu/people/faculty/nielsenr.htm
Niu, Y. L., and O'Hara, M. J., 2009, MORB mantle hosts the missing Eu (Sr, Nb, Ta and Ti) in the continental crust: New perspectives on crustal growth, crust–mantle differentiation and chemical structure of oceanic upper mantle: Lithos, v. 112, n. 1–2, p. 1–17, https://doi.org/10.1016/j.lithos.2008.12.009
Nosova, A. A., Sazonova, L. V., Narkisova, V. V., and Simakin, S. G., 2002, Minor elements in clinopyroxene from Paleozoic volcanics of the Tagil island arc in the Central Urals: Geochemistry International, v. 40, n. 3, p. 219–232.
Notsu, K., Ono, K., and Soya, T., 1987, Strontium isotopic relations of bimodal volcanic rocks at Kikai volcano in the Ryūkyū arc, Japan: Geology, v. 15, n. 4, p. 345–348, https://doi.org/10.1130/0091-7613(1987)15<345:SIROBV>2.0.CO;2
Ohki, J., Shuto, K., and Kagami, H., 1994, Middle Miocene bimodal volcanism by asthenospheric upwelling: Sr and Nd isotopic evidence from the back-arc region of the Northeast Japan arc: Geochemical Journal, v. 28, n. 6, p. 473–487, https://doi.org/10.2343/geochemj.28.473
Pamić, J., Belak, M., Bullen, T. D., Lanphere, M. A., and McKee, E. H., 2000, Geochemistry and geodynamics of a Late Cretaceous bimodal volcanic association from the southern part of the Pannonian Basin in Slavonija (Northern Croatia): Mineralogy and Petrology, v. 68, n. 4, p. 271–296, https://doi.org/10.1007/s007100050013
Peacock, S. M., Rushmer, T., and Thompson, A. B., 1994, Partial melting of subducting oceanic crust: Earth and Planetary Science Letters, v. 121, n. 1–2, p. 227–244, https://doi.org/10.1016/0012-821X(94)90042-6
Pearce, J. A., 1975, Basalt geochemistry used to investigate past tectonic environments on Cyprus: Tectonophysics, v. 25, n. 1–2, p. 41–67, https://doi.org/10.1016/0040-1951(75)90010-4
——— 1982, Trace element characteristics of lavas from destructive plate boundaries, *in* Thorp, R.S., editor, Andesites: Orogenic Andesites and Related Rocks: New York, John Wiley and Sons, p. 525–548.
——— 2008, Geochemical fingerprinting of oceanic basalts with applications to ophiolite classification and the search for Archean oceanic crust: Lithos, v. 100, n. 1–4, p. 14–48, https://doi.org/10.1016/j.lithos.2007.06.016
Pearce, J. A., and Stern, R. J., 2006, Origin of Back-Arc Basin Magmas: Trace Element and Isotope Perspectives, *in* Christie, D. M., Fisher, C. R., Lee, S. M., and Givens, S., editors, Back-Arc Spreading Systems: Geological, Biological, Chemical, and Physical Interactions: Geophysical Monograph Series, v. 166, p. 63–86, https://doi.org/10.1029/166gm06
Pearce, J. A., Ernewein, M., Bloomer, S. H., Parson, L. M., Murton, B. J., and Johnson, L. E., 1995, Geochemistry of Lau Basin volcanic rocks: Influence of ridge segmentation and arc proximity: Geological Society, London, Special Publications, v. 81, p. 53–75, https://doi.org/10.1144/GSL.SP.1994.081.01.04
Peate, D. W., Pearce, J. A., Hawkesworth, C. J., Colley, H., Edwards, C. M. H., and Hirose K., 1997, Geochemical variations in Vanuatu arc lavas: the role of subducted material and a variable mantle wedge composition: Journal of Petrology, v. 38, n. 10, p. 1331–1358, https://doi.org/10.1093/petroj/38.10.1331
Peccerillo, A., Barberio, M. R., Yirgu, G., Ayalew, D., Barbieri, M., and Wu, T. W., 2003, Relationships between mafic and peralkaline silicic magmatism in continental rift settings: A petrological, geochemical and isotopic study of the Gedemsa Volcano, Central Ethiopian Rift: Journal of Petrology, v. 44, n. 11, p. 2003–2032, https://doi.org/10.1093/petrology/egg068
Perfit, M. R., Gust, D. A., Bence, A. E., Arculus, R. J., and Taylor, S. R., 1980, Chemical characteristics of island-arc basalts: Implications for mantle sources: Chemical Geology, v. 30, n. 3, p. 227–256, https://doi.org/10.1016/0009-2541(80)90107-2
Pin, C., and Marini, F., 1993, Early Ordovician continental break-up on Variscan Europe: Nd–Sr isotope and trace element evidence for bimodal igneous associations of the southern Massif Central, France: Lithos, v. 29, n. 3–4, p. 177–196, https://doi.org/10.1016/0024-4937(93)90016-6
Pin, C., and Paquette, J. L., 1997, A mantle-derived bimodal suite in the Hercynian belt: Nd isotope and trace element evidence for a subduction-related rift origin of the late Devonian Brévenne metavolcanics, Massif Central (France): Contributions to Mineralogy and Petrology, v. 129, n. 2, p. 222–238, https://doi.org/10.1007/s004100050334
Pirajno, F., Occhipinti, S. A., and Swager, C. P., 1998, Geology and tectonic evolution of the Paleoproterozoic Bryah, Padbury and Yerrida Basins (formerly Glengarry Basin), Western Australia: Implications for the history of the south-central Capricorn Orogen: Precambrian Research, v. 90, n. 3–4, p. 119–140, https://doi.org/10.1016/S0301-9268(98)00045-X
Plank, T., and Langmuir, C. H., 1998, The geochemical compositions of subducting sediment and its consequences for the crust and mantle: Chemical Geology, v. 145, n. 3–4, p. 325–394, https://doi.org/10.1016/S0009-2541(97)00150-2
Polat, A., Kerrich, R., and Wyman, D. A., 1999, Geochemical diversity in oceanic komatiites and basalts from the late Archean Wawa greenstone belt, Superior Province, Canada: Trace element and Nd isotope evidence for a heterogeneous mantle: Precambrian Research, v. 94, n. 3–4, p. 139–173, https://doi.org/10.1016/S0301-9268(98)00110-7

Rogers, J. J. W., and Santosh, M., 2002, Configuration of Columbia, a Mesoproterozoic Supercontinent: Gondwana Research, v. 5, n. 1, p. 5–22, https://doi.org/10.1016/S1342-937X(05)70883-2
Rollinson, H. R., 1993, Using Geochemical Data: Evaluation, Presentation, Interpretation: London, Longman Geochemistry Society, 352 p.
Roser, B. P., and Nathan, S., 1997, An evaluation of elemental mobility during metamorphism of a turbidite sequence (Greenland Group, New Zealand): Geological Magazine, v. 134, n. 2, p. 219–234, https://doi.org/10.1017/S0016756897006638
Rubatto, D., and Hermann, J., 2003, Zircon formation during fluid circulation in eclogites (Monviso, Western Alps): Implications for Zr and Hf budget in subduction zones: Geochimica et Cosmochimica Acta, v. 67, n. 12, p. 2173–2187, https://doi.org/10.1016/S0016-7037(02)01321-2
Rudnick, R., and Gao, S., 2003, Composition of the Continental Crust, *in* Rudnick, R. L. editor, The Crust: Oxford, Elsevier-Pergamon, Treatise on Geochemistry, v. 3, p. 1–64, http://dx.doi.org/10.1016/B0-08-043751-6/03016-4
Sage, R. P., Lightfoot, P. C., and Doherty, W., 1996, Bimodal cyclical Archean basalts and rhyolites from the Michipicoten (Wawa) greenstone belt, Ontario: Geochemical evidence for magma contributions from the asthenospheric mantle and ancient continental lithosphere near the southern margin of the Superior Province: Precambrian Research, v. 76, n. 2–3, p. 119–153, https://doi.org/10.1016/0301-9268(95)00020-8
Sajona, F. G., Maury, R. C., Bellon, H., Cotten, J., and Defant, M., 1996, High field strength element enrichment of Pliocene–Pleistocene island arc basalts, Zamboanga Peninsula, Western Mindanao Philippines: Journal of Petrology, v. 37, n. 3, p. 693–726, https://doi.org/10.1093/petrology/37.3.693
Santosh, M., 2010, Assembling North China Craton within the Columbia supercontinent: The role of double-sided subduction: Precambrian Research, v. 178, n. 1–4, p. 149–167, https://doi.org/10.1016/j.precamres.2010.02.003
Savko, K. A., and Gerasimov, V. Yu., 2002, Petrology and Geospidometry of Metamorphic Rocks in the Eastern Voronezh Crystalline Massif: Voronezh, Voronezh State University, 131 p. (in Russian).
Savko, K. A., Samsonov, A. V., and Bazikov, N. S., 2011, Metaterrigenous rocks of Vorontsovka series of the Voronezh Crystalline Massif: geochemistry, formation features and provenance: Proceedings of Voronezh State University, Series: «GEOLOGY», No. 1, p. 98–115 (in Russian with English abstract).
Savko, K. A., Samsonov, A. V., Larionov, A. N., Larionova, Yu. O, and Bazikov, N. S., 2014, Paleoproterozoic A- and S-granites in the eastern Voronezh Crystalline Massif: Geochronology, petrogenesis, and tectonic setting of origin: Petrology, v. 22, n. 3, p. 205–233, https://doi.org/10.1134/S0869591114030059
Saunders, A. D., and Tarney, J., 1984, Geochemical characteristics of basaltic volcanism within back-arc basins, *in* Kokelaar, B. P., and Howells, M. F., editors, Marginal Basin Geology: volcanic and Associated Sedimentary and Tectonic Processes in Modern and Ancient arginal Basins: Geological Society, London, Special Publications, v. 16, p. 59–76, https://doi.org/10.1144/GSL.SP.1984.016.01.05
Saunders, A. D., Storey, M., Kent, R. W., and Norry, M. J., 1992, Consequences of plume–lithosphere interactions, *in* Storey, B. C., Alabaster, T., and Pankhurst, R. J., editors, Magmatism and the Causes of Continental Breakup: Geological Society, London, Special Publications, v. 68, p. 41–60, https://doi.org/10.1144/gsl.sp.1992.068.01.04
Seyler, M., 1986, Petrology and genesis of Hercynian alkaline orthogneisses from Provence, France: Journal of Petrology, v. 27, n. 5, p. 1229–1251, https://doi.org/10.1093/petrology/27.5.1229
Shaw, D. M., 1970, Trace element fractionation during anatexis: Geochimica at Cosmochimica Acta, v. 34, n. 2, p. 237–243, https://doi.org/10.1016/0016-7037(70)90009-8
Shchipansky, A. A., and Bogdanova, S. V., 1996, The Sarmatian crustal segment: Precambrian correlation between the Voronezh Massif and the Ukrainian Shield across the Dniepr-Donets Aulacoeen: Tectonophysics, v. 268, n. 1–4, p. 109–125, https://doi.org/10.1016/S0040-1951(96)00227-2
Shchipansky, A. A., Samsonov, A. V., Petrova, A. Yu., and Larionova, Yu. O., 2007, Geodynamics of the eastern margin of Sarmatia in the Paleoproterozoic: Geotectonics, v. 41, n. 1, p. 38–62, https://doi.org/10.1134/S0016852107010050
Shellnutt, J. G., Bhat, G. M., Wang, K.-L., Brookfield, M. E., Dostal, J., and Jahn, B.-M., 2012, Origin of the silicic volcanic rocks of the Early Permian Panjal Traps, Kashmir, India: Chemical Geology, v. 334, p. 154–170, https://doi.org/10.1016/j.chemgeo.2012.10.022
Shervias, J. W., 1982, Ti-V plots and the petrogenesis of modern and ophiolitic lavas: Earth and Planetary Science Letters, v. 59, n. 1, p. 101–118, https://doi.org/10.1016/0012-821X(82)90120-0
Shimoda, G., Tatsumi, Y., Nohda, S., Ishizaka, K., and Jahn, B. M., 1998, Setouchi high-Mg andesites revisited: Geochemical evidence for melting of subducting sediments: Earth and Planetary Science Letters, v. 160, n. 3–4, p. 479–492, https://doi.org/10.1016/S0012-821X(98)00105-8
Shinjo, R., and Kato, Y., 2000, Geochemical constraints on the origin of bimodal magmatism at the Okinawa Trough, an incipient back-arc basin: Lithos, v. 54, n. 3–4, p. 117–137, https://doi.org/10.1016/S0024-4937(00)00034-7
Shuto, K., Ishimoto, H., Hirahara, Y., Sato, M., Matsui, K., Fujibayashi, N., Takazawa, E., Yabuki, K., Sekine, M., Kato, M., and Rezanov, A. I., 2006, Geochemical secular variation of magma source during Early to Middle Miocene time in the Niigata area, NE Japan: Asthenospheric mantle upwelling during back-arc basin opening: Lithos, v. 86, n. 1–2, p. 1–33, https://doi.org/10.1016/j.lithos.2005.06.001
Stacey, J. S., and Kramers, J. D., 1975, Approximation of terrestrial lead isotope evolution by two-stage model: Earth and Planetary Science Letters, v. 26, n. 2, p. 207–221, https://doi.org/10.1016/0012-821X(75)90088-6
Steiger, R. H., and Jäger, E., 1977, Subcommission on Geochronology: Convention on the use of decay constants in geo- and cosmochronology: Earth and Planetary Science Letters, v. 36, n. 3, p. 359–362, https://doi.org/10.1016/0012-821X(77)90060-7
Stern, C. R., and Kilian, R., 1996, Role of the subducted slab, mantle wedge and continental crust in the

generation of adakites from the Andean Austral volcanic zone: Contributions to Mineralogy and Petrology, v. 123, n. 3, p. 263–281, https://doi.org/10.1007/s004100050155
Stern, R. J., 2002, Subduction Zones: Reviews of Geophysics, v. 40, n. 4, p. 3-1-3-38, https://doi.org/10.1029/2001RG000108
Stolz, A. J., Vame, R., Davies, G. R., Wheller, G. E., and Foden, J. D., 1990, Magma source components in an arc–continent collision zone: The Flores-Lembata sector, Sunda Arc, Indonesia: Contributions to Mineralogy and Petrology, v. 105, n. 5, p. 585–601, https://doi.org/10.1007/BF00302497
Streck, M. J., and Grunder, A. L., 2008, Phenocryst-poor rhyolites of bimodal, tholeiitic provinces: The Rattlesnake Tuff and implications for mush extraction models: Bulletin of Volcanology, v. 70, n. 3, p. 385–401, https://doi.org/10.1007/s00445-007-0144-3
Sun, S.-S., and McDonough, W. F., 1989, Chemical and Isotopic Systematics of Oceanic Basalts: Implications for Mantle Composition and Processes, *in* Saunders, A. D., and Norry, M. J., editors, Magmatism in the Ocean Basins: Journal of the Geological Society, London, Special Publications, v. 42, p. 313–345, https://doi.org/10.1144/GSL.SP.1989.042.01.19
Sun, W., Hu, Y., Kamenetsky, V. S., Eggins, S. M., Chen, M., and Arculus, R. J., 2008, Constancy of Nb/U in the mantle revisited: Geochimica et Cosmochimica Acta, v. 72, n. 14, p. 3542–3549, https://doi.org/10.1016/j.gca.2008.04.029
Swapp, S. M., and Onstott, T. C., 1989, *P–T*–time characterization of the Trans-Amazonian orogeny in the Imataca Complex, Venezuela: Precambrian Research, v. 42, n. 3–4, p. 293–314, https://doi.org/10.1016/0301-9268(89)90015-6
Takagi, T., Orihashi, Y., Naito, K., and Watanabe, Y., 1999, Petrology of a mantle-derived rhyolite, Hokkaido, Japan: Chemical Geology, v. 160, n. 4, p. 425–445, https://doi.org/10.1016/S0009-2541(99)00111-4
Tatsumi, Y., 2006, High-Mg andesites in the Setouchi volcanic belt, southwestern Japan: Analogy to Archean magmatism and continental crust formation?: Annual Review of Earth and Planetary Sciences, v. 34, p. 467–499, https://doi.org/10.1146/annurev.earth.34.031405.125014
Terentiev, R. A., 2002, Metavolcanics of the Losevo series and its formation belonging, Voronezh Crystalline massif: Proceedings of Voronezh State University, Series «GEOLOGY», No. 1, p. 140–150 (in Russian).
——— 2005, Paleoproterozoic paleobasin of the Losevo suture zone, Voronezh Crystalline Massif: Proceedings of Voronezh State University, Series: «GEOLOGY», No. 1, p. 81–93 (in Russian).
——— 2013, Geochemistry and stratigraphy of metaterrigenous cut rocks of Strelitsa thikness of the Losevo series of the Voronezh Crystalline Massif. Article II: geochemistry: Proceedings of Voronezh State University, Series: «GEOLOGY», No. 1, p. 127–138 (in Russian with English abstract).
——— 2014, Paleoproterozoic sequences and magmatic complexes of the Losevo suture zone of the Voronezh crystalline massif: Geological position, material composition, geochemistry, and paleogeodynamics: Stratigraphy and Geological Correlation, v. 22, n. 2, p. 123–146, https://doi.org/10.1134/S0869593814020087
Terentiev, R. A., and Chuvashina, G. A., 2003, About correlation of stratified rocks of the Losevo suture zone, Voronezh Crystalline massif: Proceedings of Voronezh State University, Series: «GEOLOGY», No. 2, p. 91–104 (in Russian).
Terentiev, R. A., and Santosh, M., 2016, Detrital zircon geochronology and geochemistry of metasediments from the Vorontsovka terrane: Implications for microcontinent tectonics: International Geology Review, v. 58, n. 9, p. 1108–1126, https://doi.org/10.1080/00206814.2016.1147386
Terentiev, R. A., and Skryabin, V. Yu., 2014, The Kalach post-collision structure of Voronezh Crystal Massif: Proceedings of Voronezh State University, Series: «GEOLOGY», No. 3, p. 14–34 (in Russian with English abstract).
Terentiev, R. A., Savko, K. A., Samsonov, A. V., and Larionov, A. N., 2014, Geochronology and geochemistry of acid metavolcanites, Losevo series, Voronezh crystalline massif: Doklady Earth Sciences, v. 454(2), p. 136–139.
Terentiev, R. A., Savko, K. A., Santosh, M., Korish, E. H., and Sarkisyan, L. S., 2016, Paleoproterozoic granitoids of the Losevo terrane, East European Craton: Age, magma source and tectonic implications: Precambrian Research, v. 287, p. 48–72, https://doi.org/10.1016/j.precamres.2016.10.015
Tian, W., Campbell, I. H., Allen, C. M., Guan, P., Pan, W., Chen, M., Yu, H., and Zhu, W., 2010, The Tarim picrite–basalt–rhyolite suite, a Permian flood basalt from northwest China with contrasting rhyolites produced by fractional crystallization and anatexis: Contributions to Mineralogy and Petrology, v. 160, n. 3, p. 407–425, https://doi.org/10.1007/s00410-009-0485-3
Tiepolo, M., Tribuzio, R., and Langone, A., 2011, High-Mg andesite petrogenesis by amphibole crystallization and ultramafic crust assimilation: Evidence from Adamello Hornblendites (Central Alps, Italy): Journal of Petrology, v. 52, n. 5, p. 1011–1045, https://doi.org/10.1093/petrology/egr016
Tomlinson, K. Y., Davis, D. W., Percival, J. A., Hughes, D. J., and Thurston, P. C., 2002, Mafic to felsic magmatism and crustal recycling in the Obonga Lake greenstone belt, western Superior Province: Evidence from geochemistry, Nd isotopes and U–Pb geochronology: Precambrian Research, v. 114, n. 3–4, p. 295–325, https://doi.org/10.1016/S0301-9268(01)00232-7
Tura, T., Deniel, C., and Mazzuoli, R., 1998, Crustal control in the genesis of Plio-Quaternary bimodal magmatism of the Main Ethiopian Rift (MER): Geochemical and isotopic (Sr, Nd, Pb) evidence: Chemical Geology, v. 155, n. 3–4, p. 201–231, https://doi.org/10.1016/S0009-2541(98)00174-0
Turner, S., Sandiford, M., and Foden, J., 1992, Some geodynamic and compositional constraints on "postorogenic" magmatism: Geology, v. 20, n. 10, p. 931–934, https://doi.org/10.1130/0091-7613(1992)020<0931:SGACCO>2.3.CO;2
Turner, S., Hawkesworth, C., Rogers, N., Bartlett, J., Worthington, T., Hergt, J., Pearce, J., and Smith, I., 1997, ^{238}U–^{230}Th disequilibria, magma petrogenesis, and flux rates beneath the depleted Tonga-Kermadec island arc: Geochimica et Cosmochimica Acta, v. 61, n. 22, p. 4855–4884, http://doi.org/10.1016/S0016-7037(97)00281-0

Vervoort, J. D., Wirth, K., Kennedy, B., Sandland, T., and Harpp, K. S., 2007, The magmatic evolution of the Midcontinent rift: New geochronologic and geochemical evidence from felsic magmatism: Precambrian Research, v. 157, n. 1–2, p. 235–268, https://doi.org/10.1016/j.precamres.2007.02.019

Wang, Y., Qian, Q., Liu, L., and Zhang, Q., 2000, Major geochemical characteristics of bimodal volcanic rocks in different geochemical environments (in Chinese with English abstract): Acta Petrologica Sinica, v. 16, p. 169–173.

Wareham, C. D., Stump, E., Storey, B. C., Millar, I. L., and Rile, T. R., 2001, Petrogenesis of the Cambrian Liv Group, a bimodal volcanic rock suite from the Ross orogen, Transantarctic Mountains: Geological Society of America Bulletin, v. 113, n. 3, p. 360–372, https://doi.org/10.1130/0016-7606(2001)113<0360:POTCLG>2.0.CO;2

Watson, E. B., and Harrison, T. M., 1983, Zircon saturation revisited: Temperature and composition effects in a variety of crustal magma types: Earth and Planetary Science Letters, v. 64, n. 2, p. 295–304, https://doi.org/10.1016/0012-821X(83)90211-X

Watson, E. B., Wark, D. A., and Thomas, J. B., 2006, Crystallization thermometers for zircon and rutile: Contributions to Mineralogy and Petrology, v. 151, p. 413–433, https://doi.org/10.1007/s00410-006-0068-5

Wiedenbeck, M., Allé, P., Corfu, F., Griffin, W. L., Meier, M., Oberli, F., von Quadt, A., Roddick, J. C., and Spiegel, W., 1995, Three natural zircon standards for U–Th–Pb, Lu–Hf, trace element and REE analyses: Geostandards Newsletter, v. 19, n. 1 p. 1–23, https://doi.org/10.1111/j.1751-908X.1995.tb00147.x

Wilson, C. J. N., Houghton, B. F., McWilliams, M. O., Lanphere, M. A., Weaver, S. D., and Briggs, R. M., 1995, Volcanic and structural evolution of Taupo Volcanic Zone, New Zealand: A review: Journal of Volcanology and Geothermal Research, v. 68, n. 1–3, p. 1–28, https://doi.org/10.1016/0377-0273(95)00006-G

Wilson, M., 1989, Igneous Petrogenesis-A Global Tectonic Approach: London, Unwin Hyman, 466 p.

Winchester, J. A., and Floyd, P. A., 1986, Geochemical magma type discrimination: Application to altered and metamorphosed igneous rock: Earth and Planetary Science Letters, v. 28, n. 3, p. 459–469, https://doi.org/10.1016/0012-821X(76)90207-7

Wood, B. J., and Turner, S. P., 2009, Origin of primitive high-Mg andesite: Constraints from natural examples and experiments: Earth and Planetary Science Letters, v. 283, n. 1–4, p. 59–66, https://doi.org/10.1016/j.epsl.2009.03.032

Xie, G., Mao, J., Xiongwei, L., Duan, C., and Yao, L., 2011, Late Mesozoic bimodal volcanic rocks in the Jinniu basin, Middle–Lower Yangtze River Belt (YRB), East China: Age, petrogenesis and tectonic implications: Lithos, v. 127, n. 1–2, p. 144–164, https://doi.org/10.1016/j.lithos.2011.08.012

Yang, Q. Y., and Santosh, M., 2015, Paleoproterozoic arc magmatism in the North China Craton: No Siderian global plate tectonic shutdown: Gondwana Research, v. 28, n. 1, p. 82–105, https://doi.org/10.1016/j.gr.2014.08.005

Zaytsev, Yu. S., 1966, The Michaelovo series of the Belgorod iron ore region and some problems of stratigraphy of the Voronezh anteclise Precambrian, *in* Proceedings of the Third meeting on the study of the Voronezh anteclise, 7–11 april 1964: Voronezh, Russia, p. 21–28 (in Russian).

Zaytsev, Yu. S., 1979, The Precambrian conglomerates of eastern part of the Voronezh Crystalline Massif: Izvestia AN USSR: Seria geologicheskaya, n. 11, p. 23–30 (in Russian).

Zhang, X., Zhang, H., Tang, Y., Wilde, S. A., and Hu, Z., 2008, Geochemistry of Permian bimodal volcanic rocks from central Inner Mongolia, North China: Implication for tectonic setting and Phanerozoic continental growth in Central Asian Orogenic Belt: Chemical Geology, v. 249, n. 3–4, p. 262–281, https://doi.org/10.1016/j.chemgeo.2008.01.005

Zhang, X. H., Mao, Q., Zhang, H. F., Zhai, M. G., Yang, Y. H., and Hu, Z. C., 2011, Mafic and felsic magma interaction during the construction of high-K calc-alkaline plutons within a metacratonic passive margin: The Early Permian Guyang batholith from the northern North China Craton: Lithos, v. 125, n. 1–2, p. 569–591, https://doi.org/10.1016/j.lithos.2011.03.008

Zhao, G. C., Cawood, P. A., Wilde, S. A., and Sun, M., 2002, Review of global 2.1–1.8 Ga orogens: Implications for a pre-Rodinia supercontinent: Earth Science Reviews, v. 59, n. 1–4, p. 125–162, https://doi.org/10.1016/S0012-8252(02)00073-9

Zhao, G., Sun, M., and Wilde, S. A., and Li, S., 2004, A Paleo-Mesoproterozoic supercontinent: Assembly, growth and breakup: Earth-Science Reviews, v. 67, n. 1–2, p. 91–123, https://doi.org/10.1016/j.earscirev.2004.02.003

Zhao, J.-H., and Zhou, M.-F., 2007, Geochemistry of Neoproterozoic mafic intrusions in the Panzhihua district (Sichuan Province, SW China): Implications for subduction related metasomatism in the upper mantle: Precambrian Research, v. 152, n. 1–2, p. 27–47, https://doi.org/10.1016/j.precamres.2006.09.002

Zheng, Y.-F., 2012, Metamorphic chemical geodynamics in continental subduction zones: Chemical Geology, v. 328, p. 5–48, https://doi.org/10.1016/j.chemgeo.2012.02.005

Zhu, D. C., Zhao, Z. D., Niu, Y., Dilek, Y., Wang, Q., Ji, W. H., Dong, G. C., Sui, Q. L., Liu, Y. S., Yuan, H. L., and Mo, X.-X, 2012, Cambrian bimodal volcanism in the Lhasa Terrane, southern Tibet: Record of an early Paleozoic Andean-type magmatic arc in the Australian proto-Tethyan margin: Chemical Geology, v. 328, p. 290–308, https://doi.org/10.1016/j.chemgeo.2011.12.024

Zimmer, M., Kröner, A., Jochum, K. P., Reischmann, T., and Todt, W., 1995, The Gabal Gerf complex: A Precambrian N-MORB ophiolite in the Nubian Shield, NE Africa: Chemical Geology, v. 123, n. 1–4, p. 29–51, https://doi.org/10.1016/0009-2541(95)00018-H